

Best Available Copy

①

CORROSION CONTROL THROUGH A BETTER UNDERSTANDING
OF THE METALLIC SUBSTRATE/ORGANIC COATING/INTERFACE

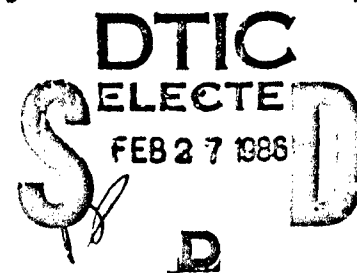
AD-A164 734

Agreement No. N00014-79-C-0731

Sixth Annual Report
Covering the Period

October 1, 1984 - September 30, 1985

Sponsor: Office of Naval Research
Washington, D.C.



Principal Investigator: Henry Leidheiser, Jr.

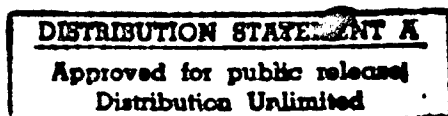
Co-Investigators: Eugene M. Allen
Frederick M. Fowkes
Richard D. Granata
Jack F. McIntyre
John A. Manson

20030121008

DTIC FILE COPY

Center for Surface and Coatings Research
LEHIGH UNIVERSITY
Bethlehem, PA 18015

January 31, 1986



86 2 10 050

TABLE OF CONTENTS

	<u>Page</u>
FOREWORD	1
SECTION #1 - Sensitive Test for Water under an Organic Coating	3
SECTION #2 - The Effect of Temperature and Alkali Metal Cation on the Cathodic Delamination of Polybutadiene from Steel	21
SECTION #3 - Acid-Base Effects in Glass/Bead Phenoxo Model Coating Systems	29
SECTION #4 - Surface Acidity of Ferric Oxides Studied by Flow Microcalorimetry	51
SECTION #5 - Inhibition of Iron Corrosion by Carboxylates in the Presence of Oxidants	73
SECTION #6 - Corrosion Behavior of Steel Pre-Treated with Silanes	95
SECTION #7 - Ionic Migration through Organic Coatings and Its Consequences to Corrosion	117
SECTION #8 - The Effect of Alkali Metal Hydroxides on the Dissolution Behavior of a Zinc Phosphate Conversion Coating on Steel and Pertinence to Cathodic Delamination	141
SECTION #9 - Corrosion beneath Polymeric Coatings on Thin Metal Films as Studied Using Concurrent AC Impedance and Parallel DC Resistance Measurements	151



NTIS CRA&I <input checked="" type="checkbox"/> DTIC TAB <input type="checkbox"/> Unannounced <input type="checkbox"/> Justification	
By <i>lta. on file</i> Distribution /	
Availability Codes	
Dist <div style="font-size: 1.5em; font-weight: bold;">A-1</div>	Avail and/or Special

FOREWORD

This report represents the sixth annual summary of research carried out under Office of Naval Research Contract No. N000014-79-C-0731. The objective of this research is to obtain a better understanding of the metallic substrate/organic coating/interface system so that improvements may be made in corrosion control of metals by painting. The activity during the period, October 1, 1984 - September 30, 1985 includes the research of a fewer number of senior staff than in previous years and the activity is being further reduced in the period, October 1, 1985 - September 30, 1986.

The report this year includes detailed summaries of 9 different thrusts. Two sections (#1 and #2) are concerned with the migration and detection of species diffusion through a coating; two sections (#3 and #4) are concerned with the acid/base properties of solid/solid interfaces; two sections (#5 and #6) are concerned with modifying a metal surface to improve its performance in an aggressive medium; two sections (#7 and #8) are concerned with principles involved in the cathodic delamination of an organic coating from a metal; and one section is concerned with a method of measuring the protective properties of a coating using a thin metallic film as a substrate. Three other studies concerned with (a) the effects of abrasion on the properties of metal/organic coating interfaces, (b) the wet adhesion of organic coatings to metals, and (c) the use of impedance measurements as a tool for studying the protective properties of organic coatings are not included in the present report because they have not reached the stage of completeness to write a detailed summary.

SECTION - #1

Sensitive Test for Water under an Organic Coating

Principal Investigator: Eugene Allen, Prof. of Chemistry

INTRODUCTION

A test for the first appearance of water in the interface between an organic coating and the underlying metal substrate would be of the utmost importance in the study of corrosion. Although uptake of water by the polymer is important, we restrict ourselves in this study to detection of water in the interfacial region.

A promising lead was obtained during the last reporting period, when we found that 2,2'-bipyridine (bipy) reacts with iron in a steel surface in the presence of water to yield a deeply-colored red complex, $\text{Fe}(\text{bipy})_3^{2+}$. Preliminary tests showed that this reaction did not occur in the absence of water. Both bipy and the ferrous complex have strong and characteristic Raman spectra. Furthermore, the spectrum of the ferrous complex is strongly enhanced by the resonance Raman effect, since it has a strong absorption band at the wavelength of the laser line used for excitation (514.5 nm). We therefore suggested that a solid layer of bipy be applied to a steel surface before the application of the coating. The presence of water would be detected by transition from the spectrum of bipy to that of the ferrous complex.

Figure 1 shows the Raman spectrum of bipy, and Figure 2 that of $\text{Fe}(\text{bipy})_3^{2+}$.

TESTS WITH BIPY UNDER KRYLON

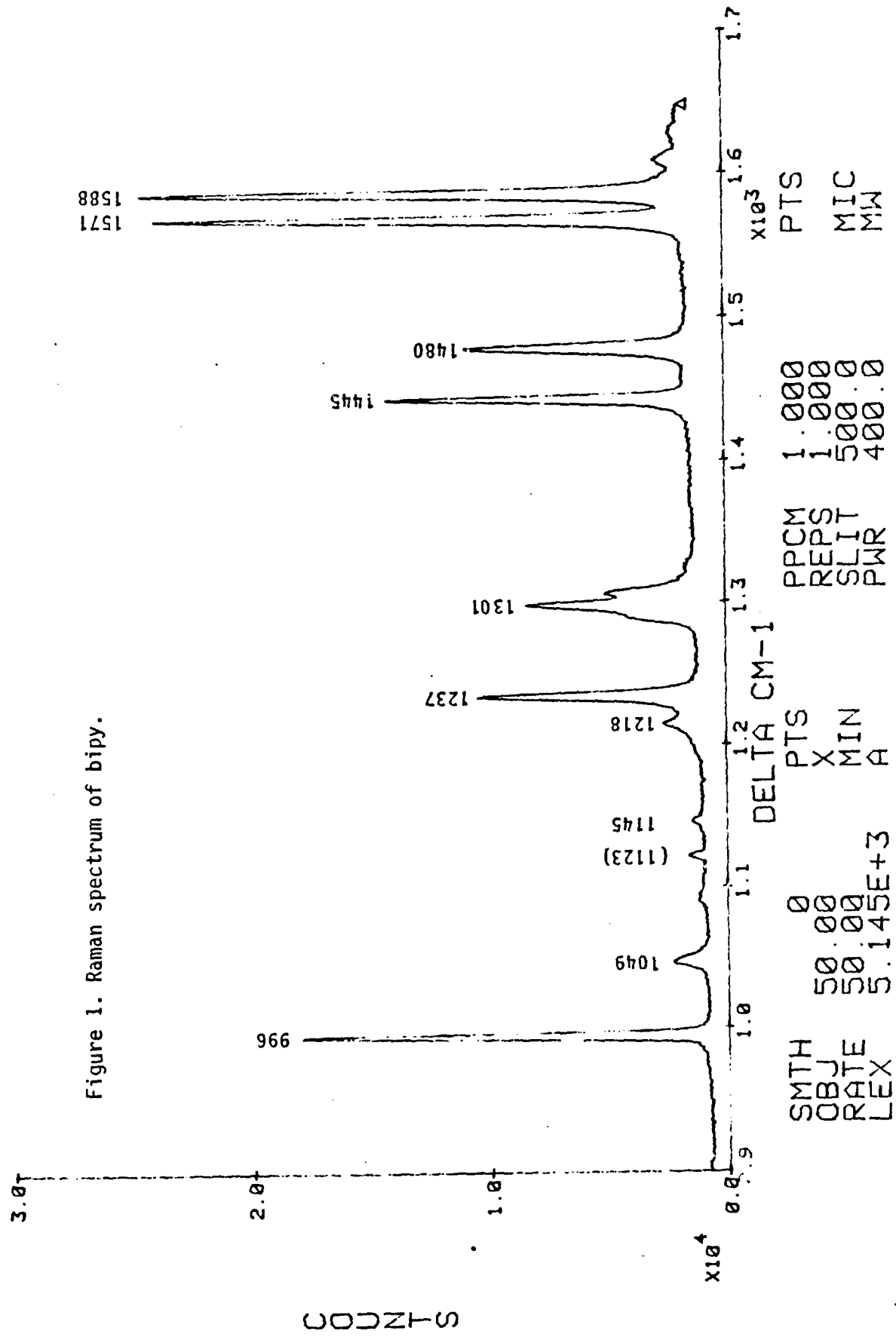
We wished to test the use of a layer of bipy as an indicator of water under a coating. We prepared the bipy layer by the technique described in the last progress report. We dropped 2 ml of a 1 mg/ml solution of bipy in absolute alcohol a little at a time on to a spot on a steel panel, allowing each increment of solution to evaporate before adding the next. This treatment left a thin layer of bipy crystals on the steel. We then sprayed a layer of Krylon®, a solvent based fixative used for art work, on to the panel. After the solvent had evaporated, we ran the portion of the spectrum between 1440 cm^{-1} and 1510 cm^{-1} . Reference to Figures 1 and 2 shows that bipy has two peaks in this region at 1445 cm^{-1} and 1480 cm^{-1} . The ferrous complex, on the other hand, has only one peak at 1487 cm^{-1} . The spectrum of the bipy under Krylon, shown in Figure 3, clearly shows the two bipy peaks and no ferrous complex peak.

Keeping the microscope of the MOLE aimed at the same spot, we then placed a drop of water on the panel so that it covered the area seen under the microscope, refocused the microscope, and ran periodic spectra. After

00:47:18

BIPY

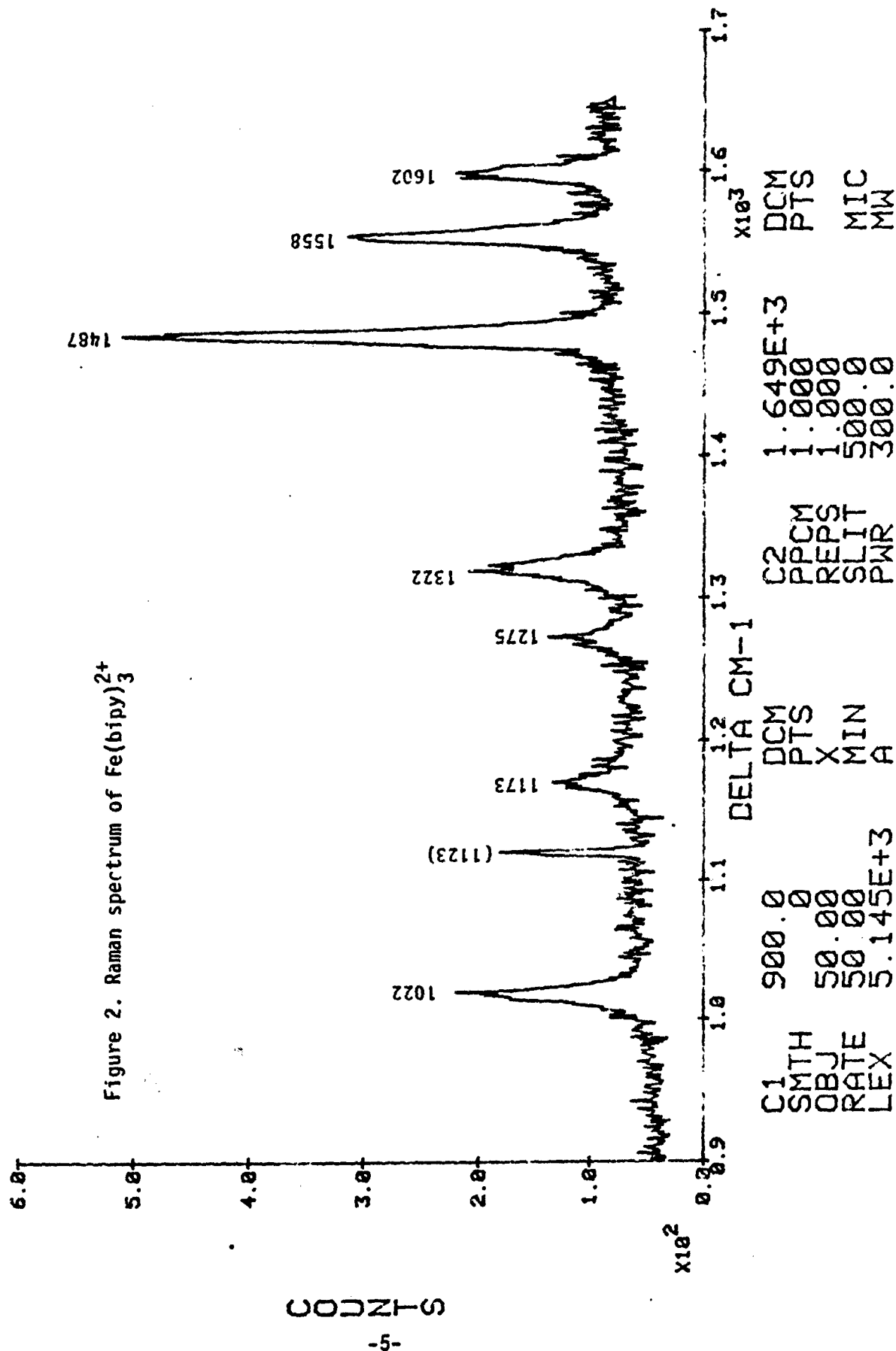
00/00/00



12/11/85

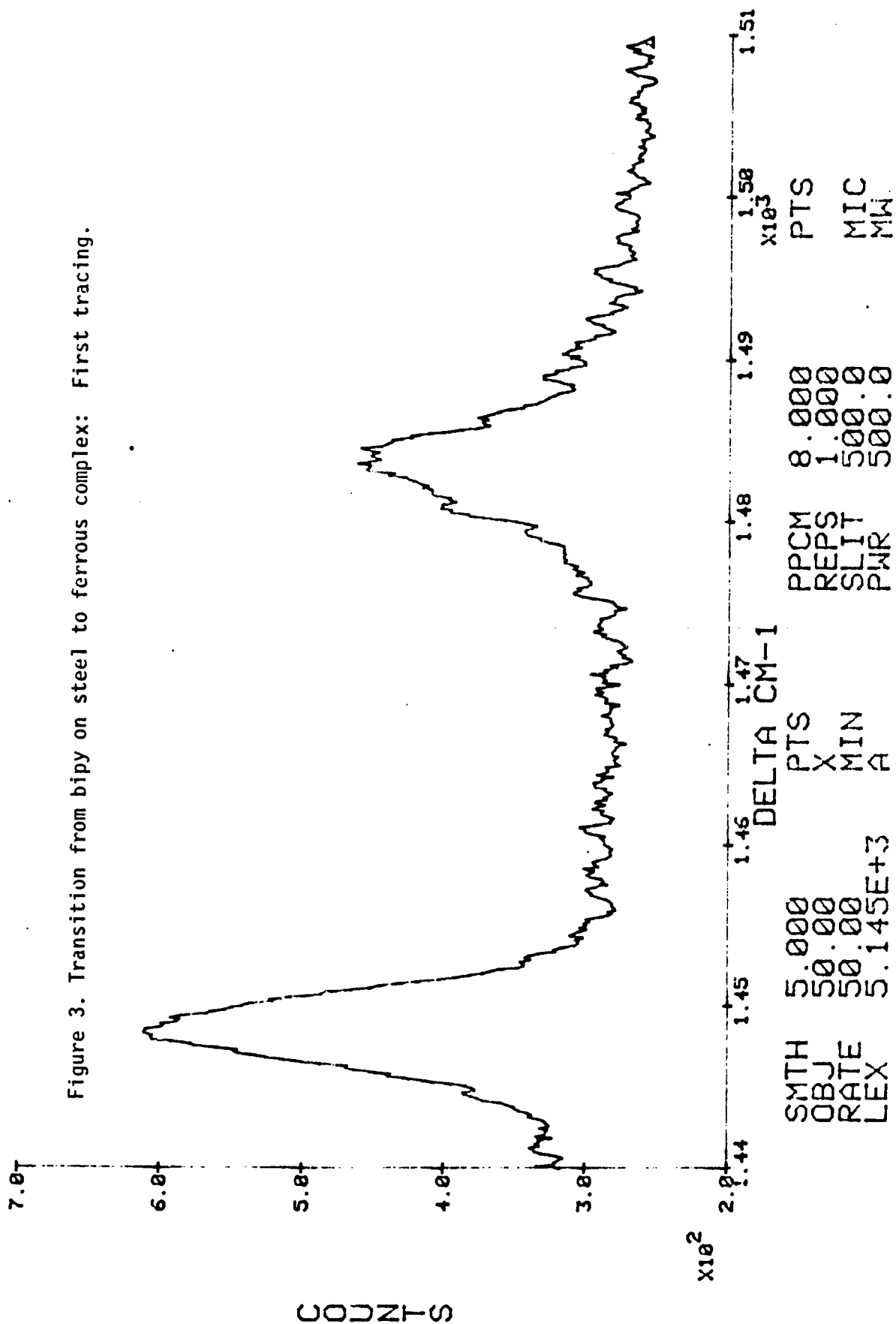
FE-BIPY COMPLEX

13:45:20



02/04/85

13:49:33



some practice and repetition of the entire technique from beginning to end, we obtained the remarkable series of curves shown in Figures 4-8. The time readings are shown at the upper right of each figure.

Figure 4, taken 45 minutes after the placement of the water drop, shows the beginning of broadening of the bipy 1480 cm^{-1} peak because of the appearance of the ferrous complex peak at 1487 cm^{-1} . In Figure 5, taken six minutes later, the ferrous complex peak is just about as strong as the bipy peak. Figures 6 and 7, taken at intervals of about five to six minutes, show further diminution of both bipy peaks and a strengthening of the ferrous complex peak. In Figure 8, taken 15 minutes later, the bipy peaks have virtually disappeared, and the $\text{Fe}(\text{bipy})^{2+}$ peak alone is seen. This series of curves shows that the appearance of water can be detected by this reaction.

TESTS WITH A MIXTURE OF FERROUS SULFATE AND BIPY

We originally thought that the 45-minute delay before the appearance of the ferrous complex was caused by the time of penetration of the water in the Krylon film. More recent work mentioned below, however, indicates that penetration of a Krylon film by water occurs within several seconds. We believe, therefore, that the delay was caused by the time of reaction of the aqueous bipy solution with the steel surface to liberate Fe_3^{2+} . This points up the fact that the test as conducted so far is not really a test for water but rather a test for corrosion caused by water.

We therefore decided to modify the test by using a mixture of dried ferrous sulfate (sold by Fisher Scientific in the dried powder form) and bipy. The stoichiometric weight ratio of bipy to ferrous sulfate is about 3:1, but we used equal weights of the two. We mixed 0.3 g of bipy and 0.3 g of dried ferrous sulfate and ground the mixture in a mortar. A pinkish powder resulted, the color probably coming from residual water in the powdered ferrous sulfate.

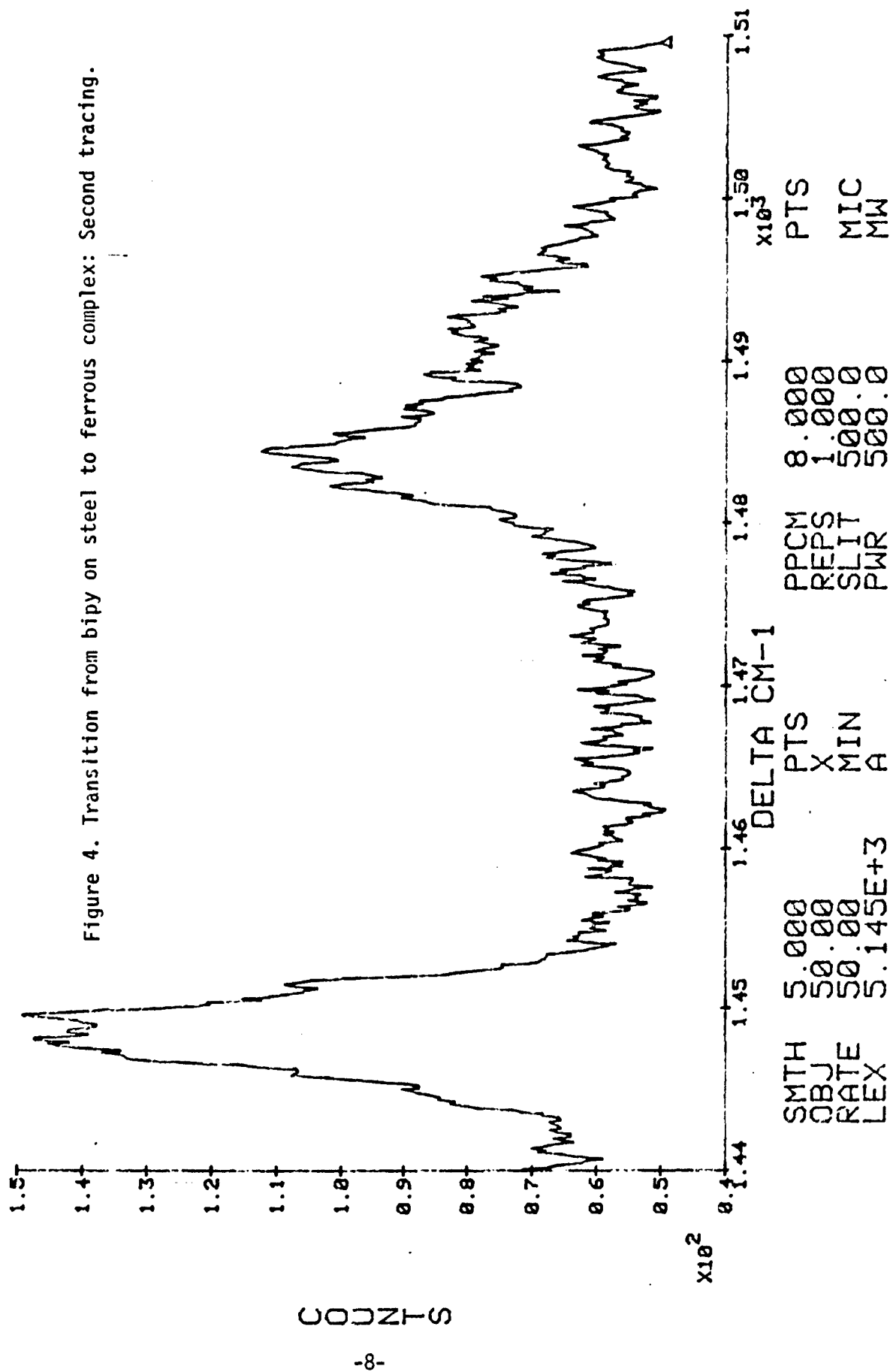
Addition of water to a small amount of this powder on a microscope slide produces a deep red color that is easily seen through the microscope as well as with the naked eye. Therefore, this system can possibly be used as a simple visual microscopic test.

To get some idea of the sensitivity of the Raman detection method, we placed a very small amount of the powder on a microscope slide and obtained a Raman tracing between 1440 cm^{-1} and 1510 cm^{-1} as explained above. See Figure 9. The two bipy peaks are clearly seen. We then left the slide in place on the microscope stage and breathed on the slide about five times. The tracing (Figure 10) showed unmistakable evidence of the formation of the ferrous complex: The left peak is reduced in comparison to the right peak, and the right peak has broadened and shows the incipient formation of the peak of the complex at the right of the bipy peak. Repetition of the breathing treatment produced Figure 11, in which we see that the left bipy peak has completely disappeared, whereas the right peak has changed into the peak of the ferrous complex (moved to the right). The qualitative indication is therefore that the test is extremely sensitive.

02/04/85

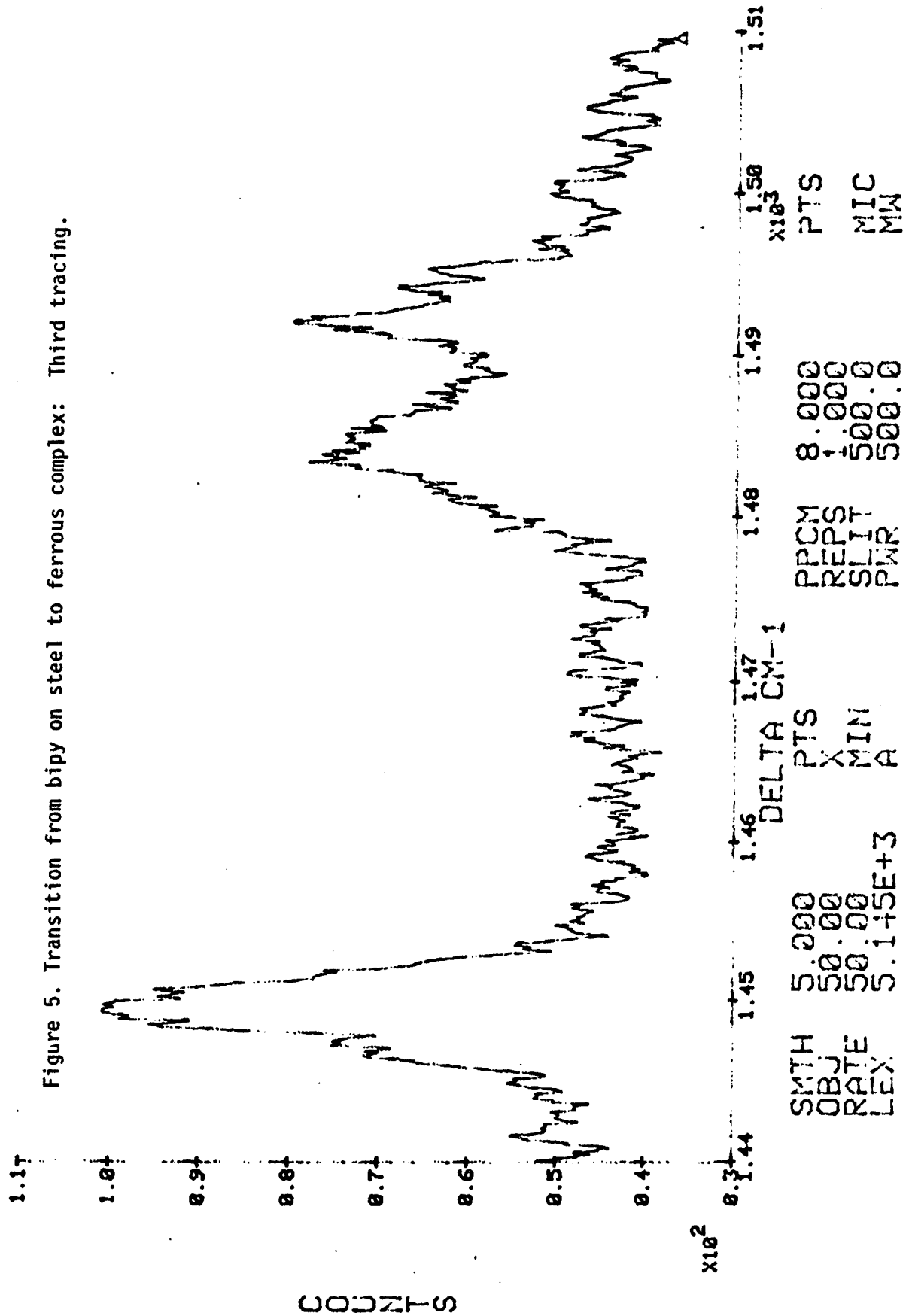
14:36:56

Figure 4. Transition from bipy on steel to ferrous complex: Second tracing.



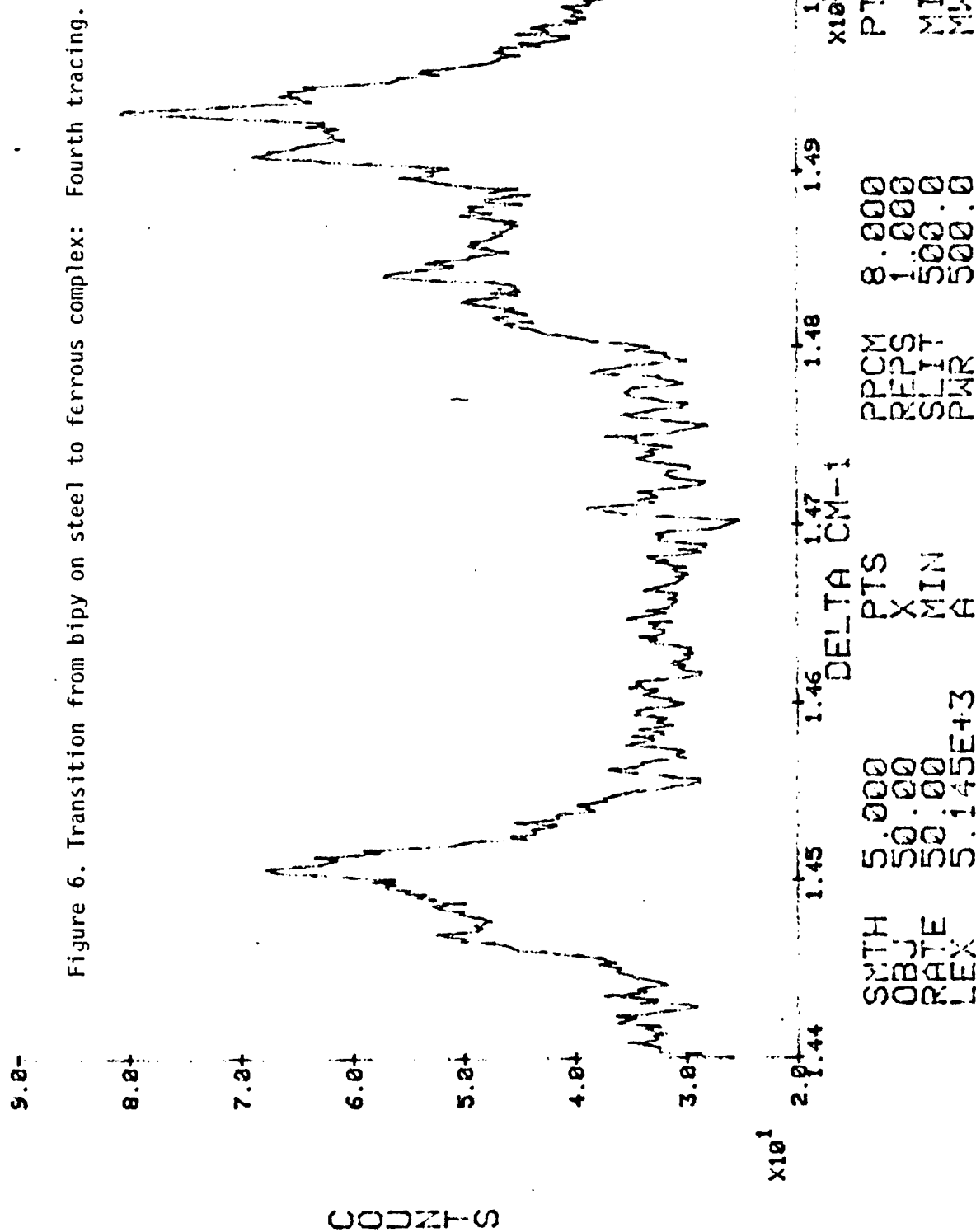
02/04/85

14:43:13



02/04/85

14:49:14



02/04/85

14:54:22

8.0+

7.0+

6.0+

5.0+

4.0+

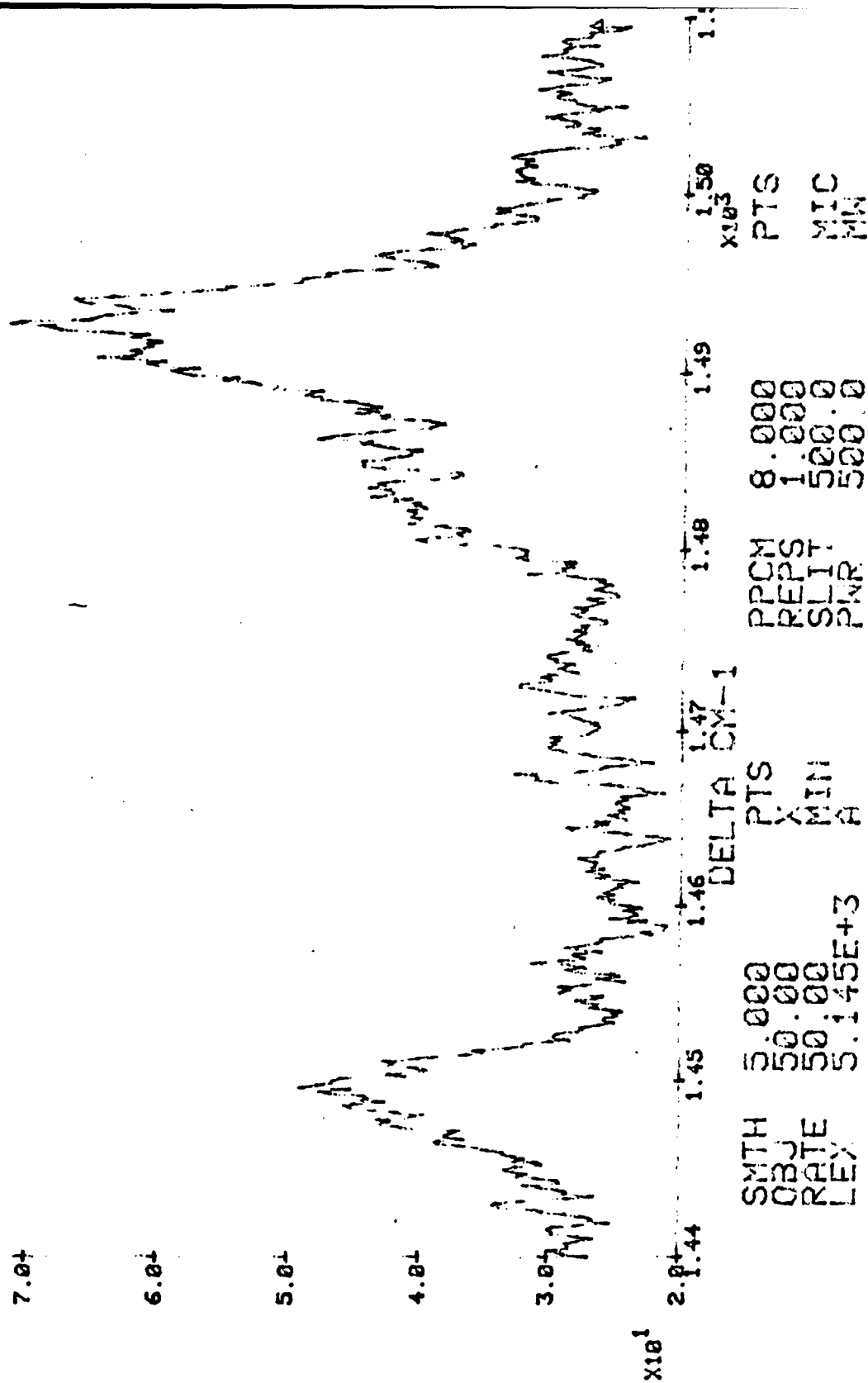
3.0+

$\times 10^1$

COUNTS

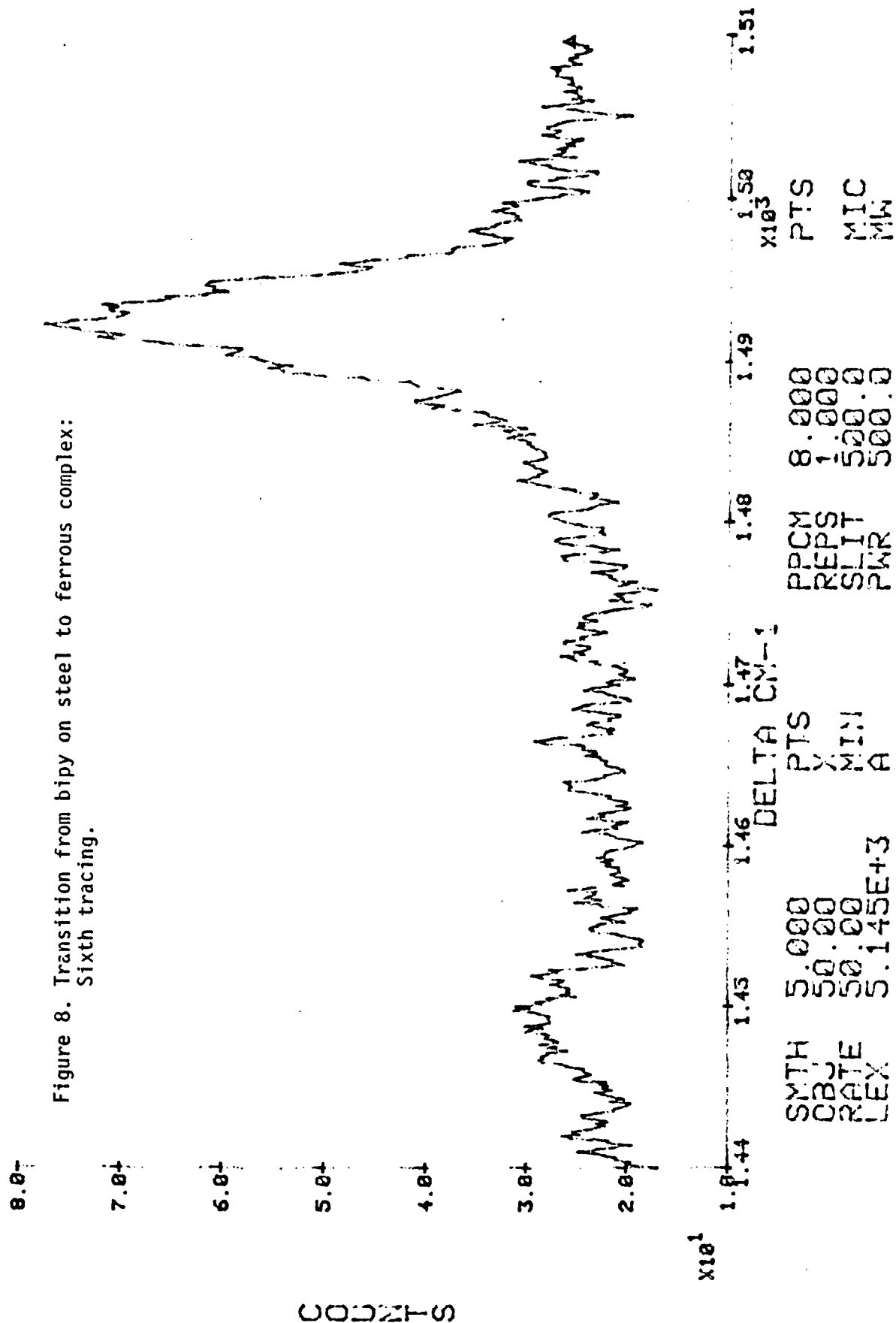
-11-

Figure 7. Transition from bipy on steel to ferrous complex: Fifth tracing.



02/04/85

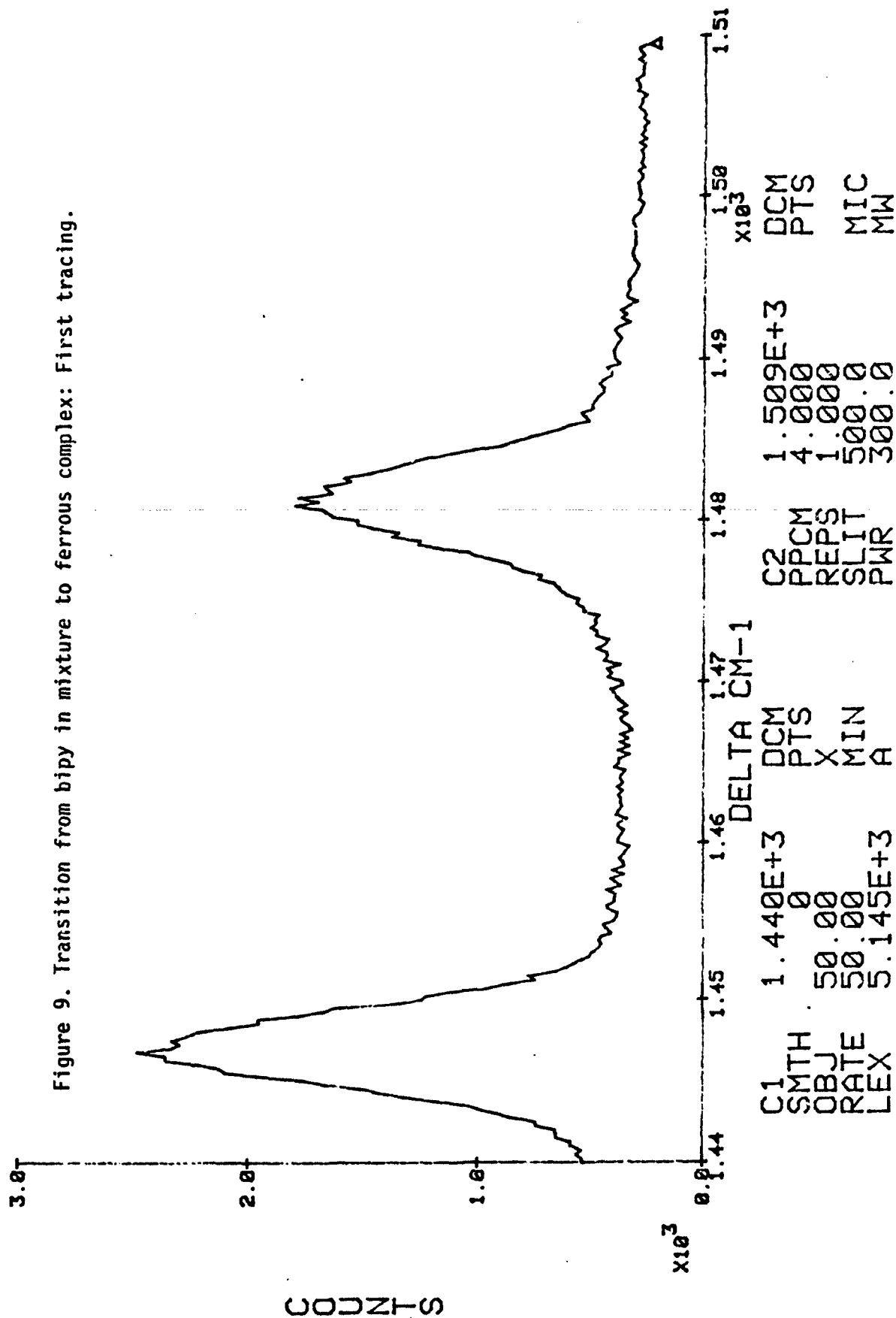
15:10:52



12/11/85

BIPY

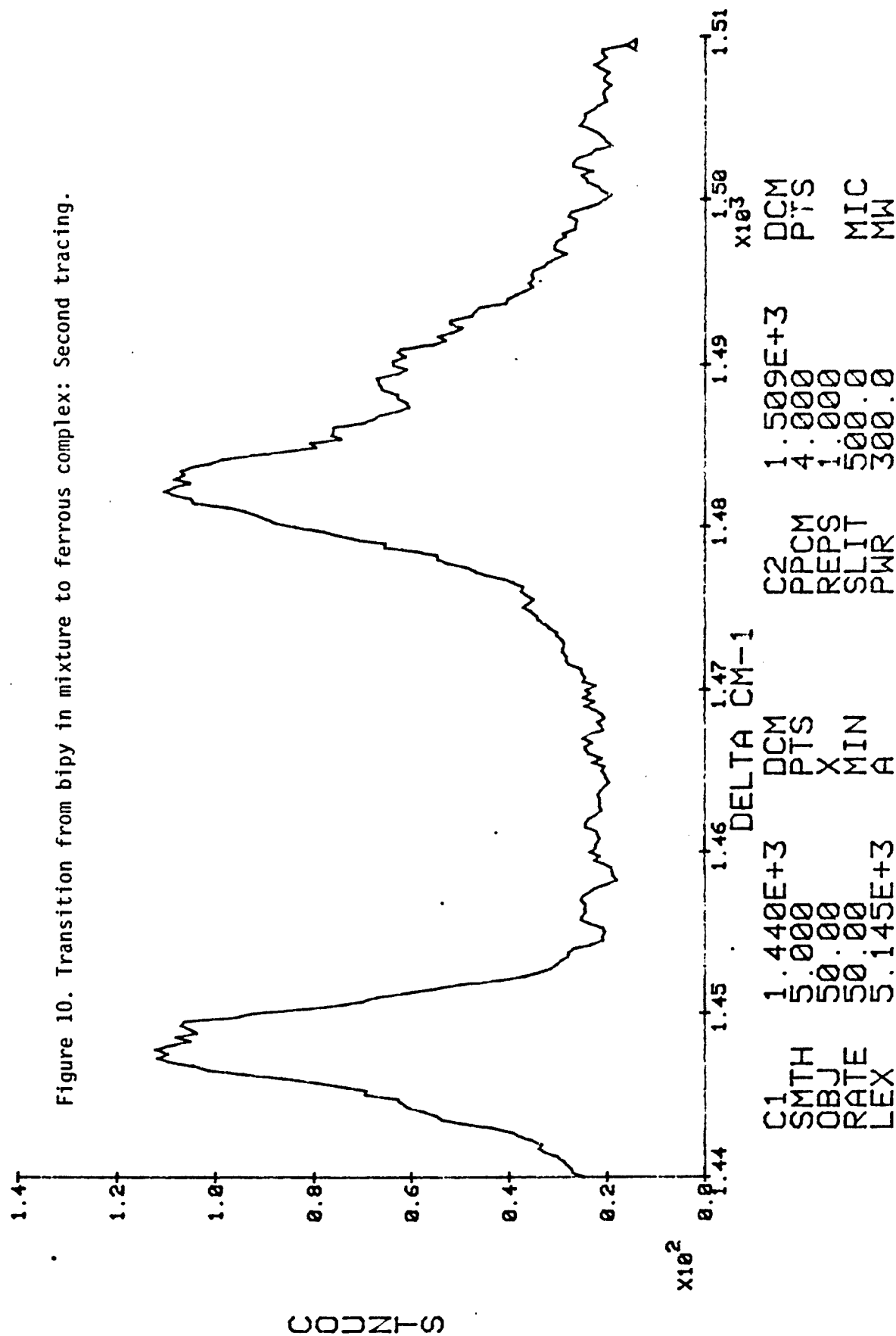
12:51:27



12/11/85

BIPY

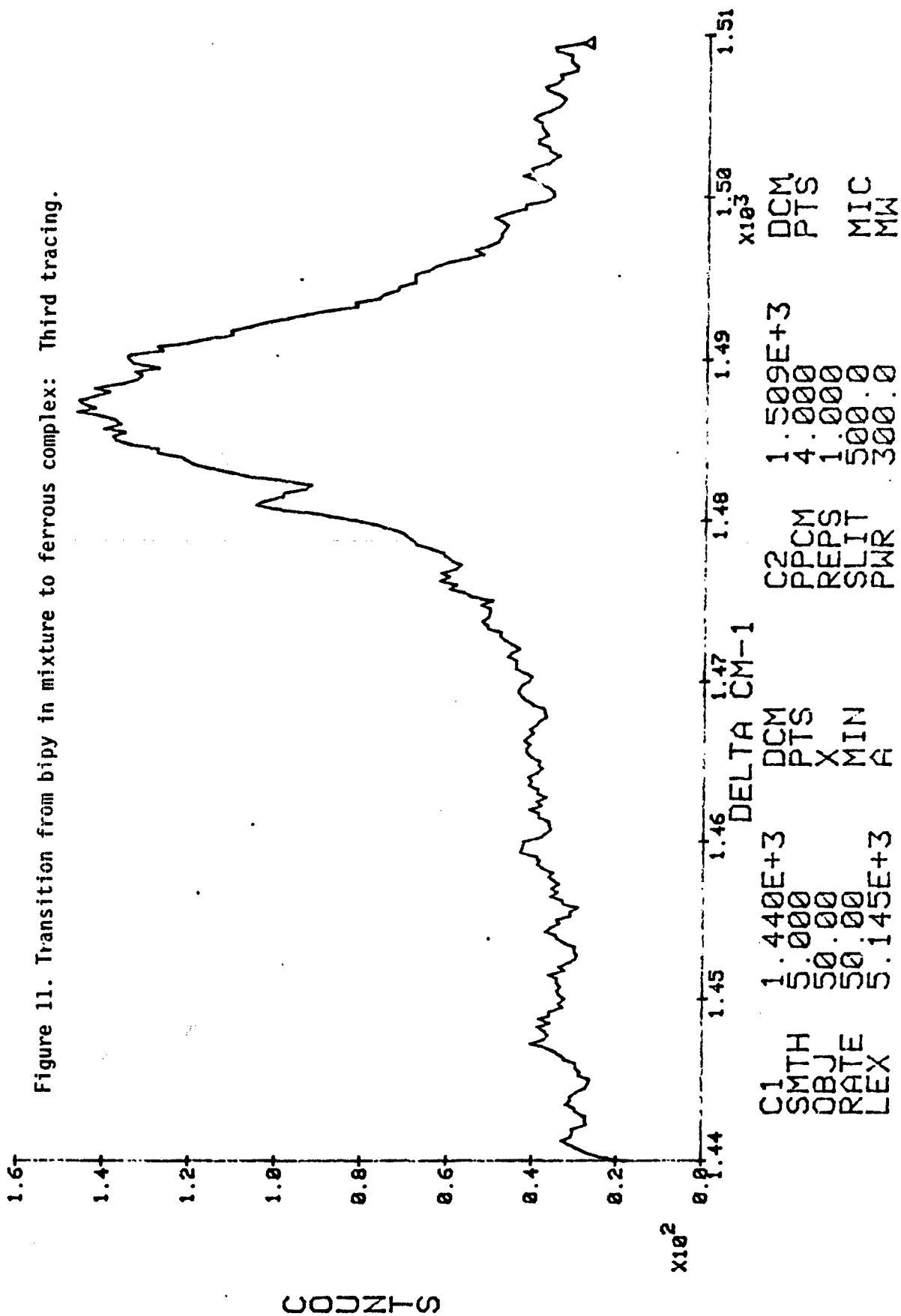
13:05:05



12/11/85

BIPY

13:11:12



TESTS WITH CUPRIC SULFATE

As an alternative technique, we tried using dried (130°C) cupric sulfate as an indicator for water, taking advantage of the fact that the dried form and the pentahydrate produce clearly different Raman spectra. The spectrum for the dried form is shown in Figure 12; that for the crystalline pentahydrate is shown in Figure 13. We hoped that the production of the intense pentahydrate peak at 983 cm^{-1} might serve as an indication of the presence of water.

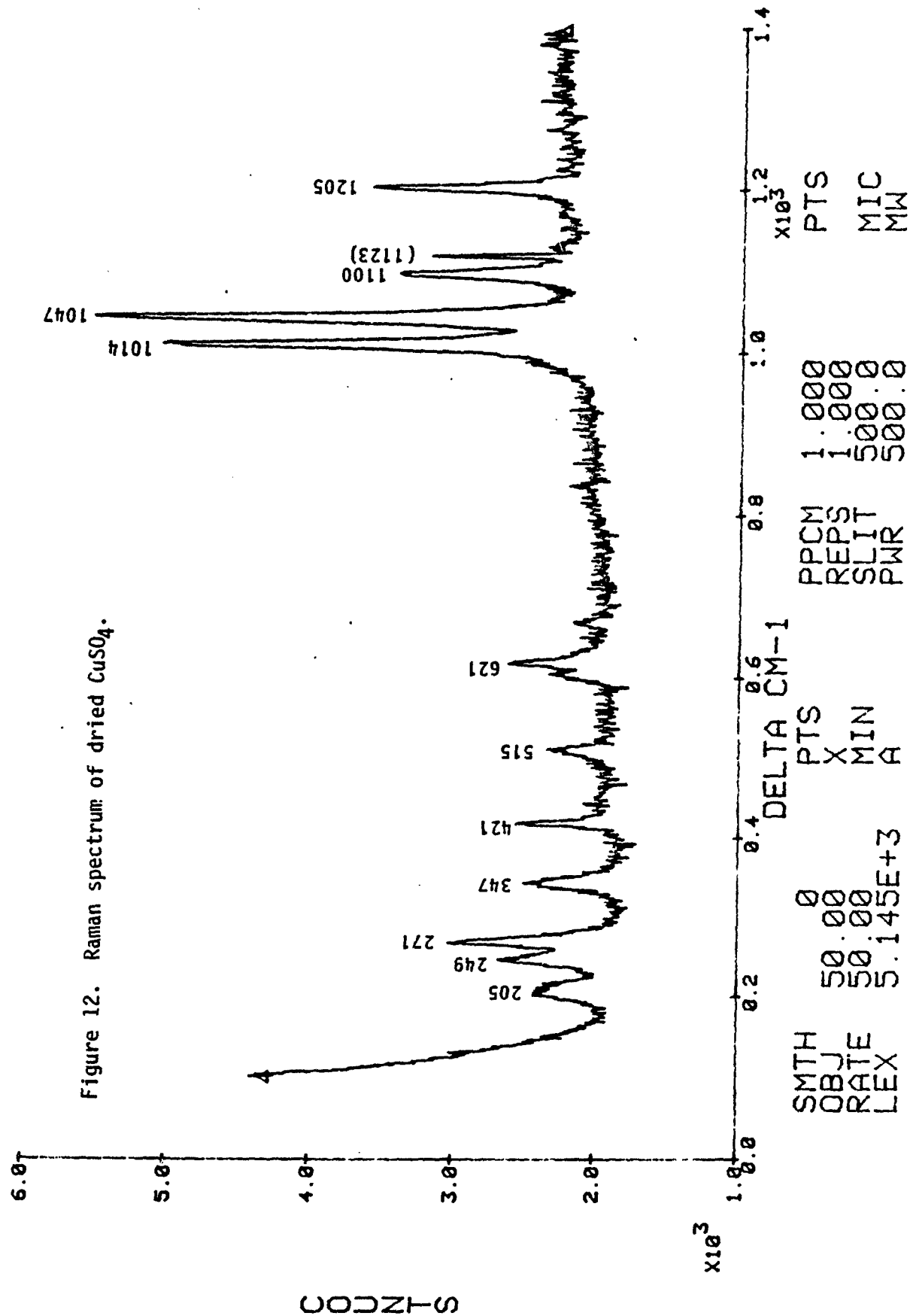
We tried the breathing experiment described above on the dried CuSO_4 powder. The resulting spectrum is shown in Figure 14. We see that practically all the peaks of the dried CuSO_4 spectrum are still present, but the 1014 cm^{-1} (now 1010 cm^{-1}) peak has maintained its intensity whereas all the other peaks have been reduced. There is no trace of the formation of the 983 cm^{-1} peak. These results were not consistent on repeated tests, but in no case did we observe the formation of the 983 cm^{-1} peak.

Cupric sulfate is known to exist in a number of different hydrated forms in addition to the pentahydrate. We believe that these complicate the picture.

12/09/85

CUS04 DRIED

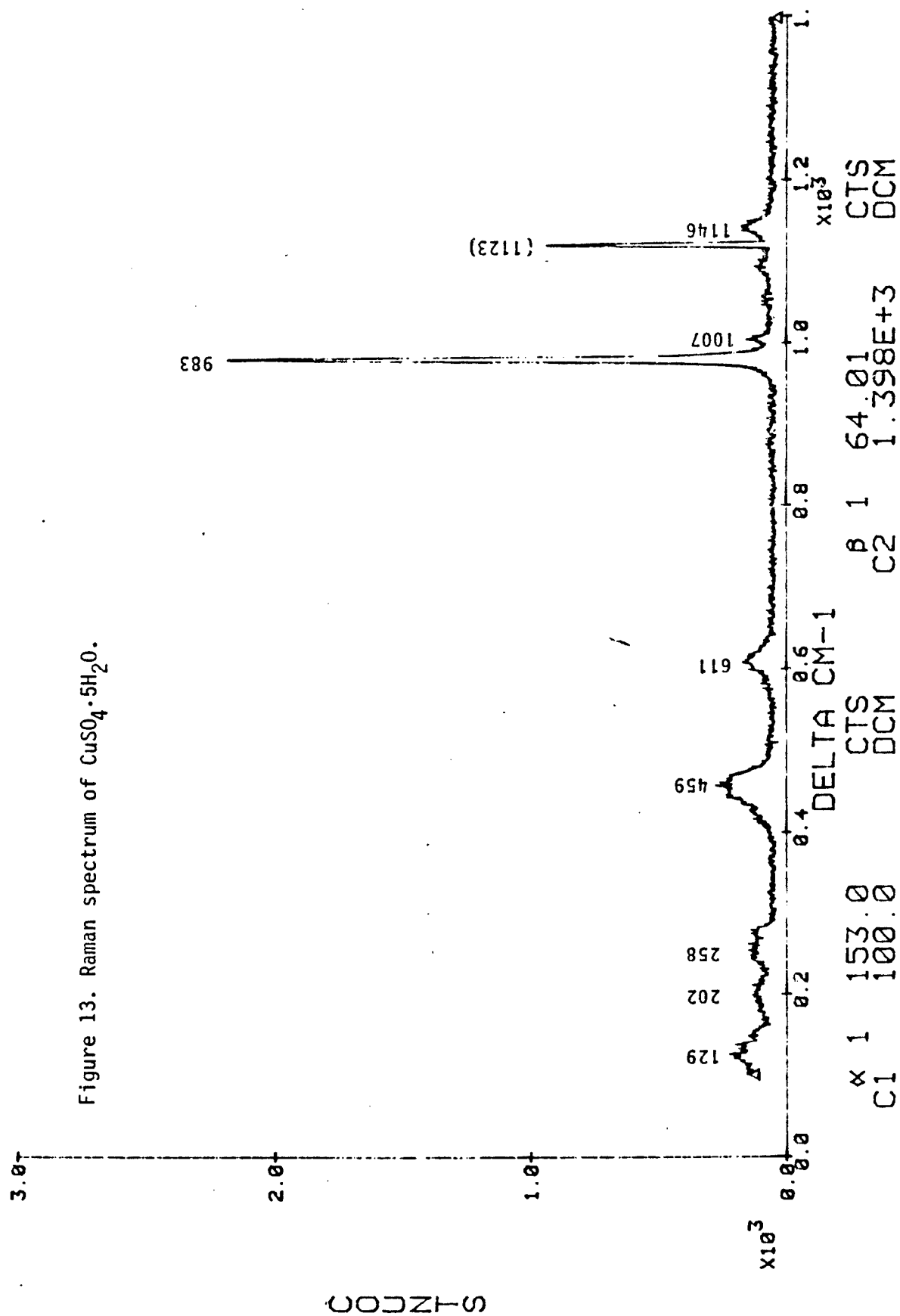
16:51:11



12/09/85

CUS04 5H20

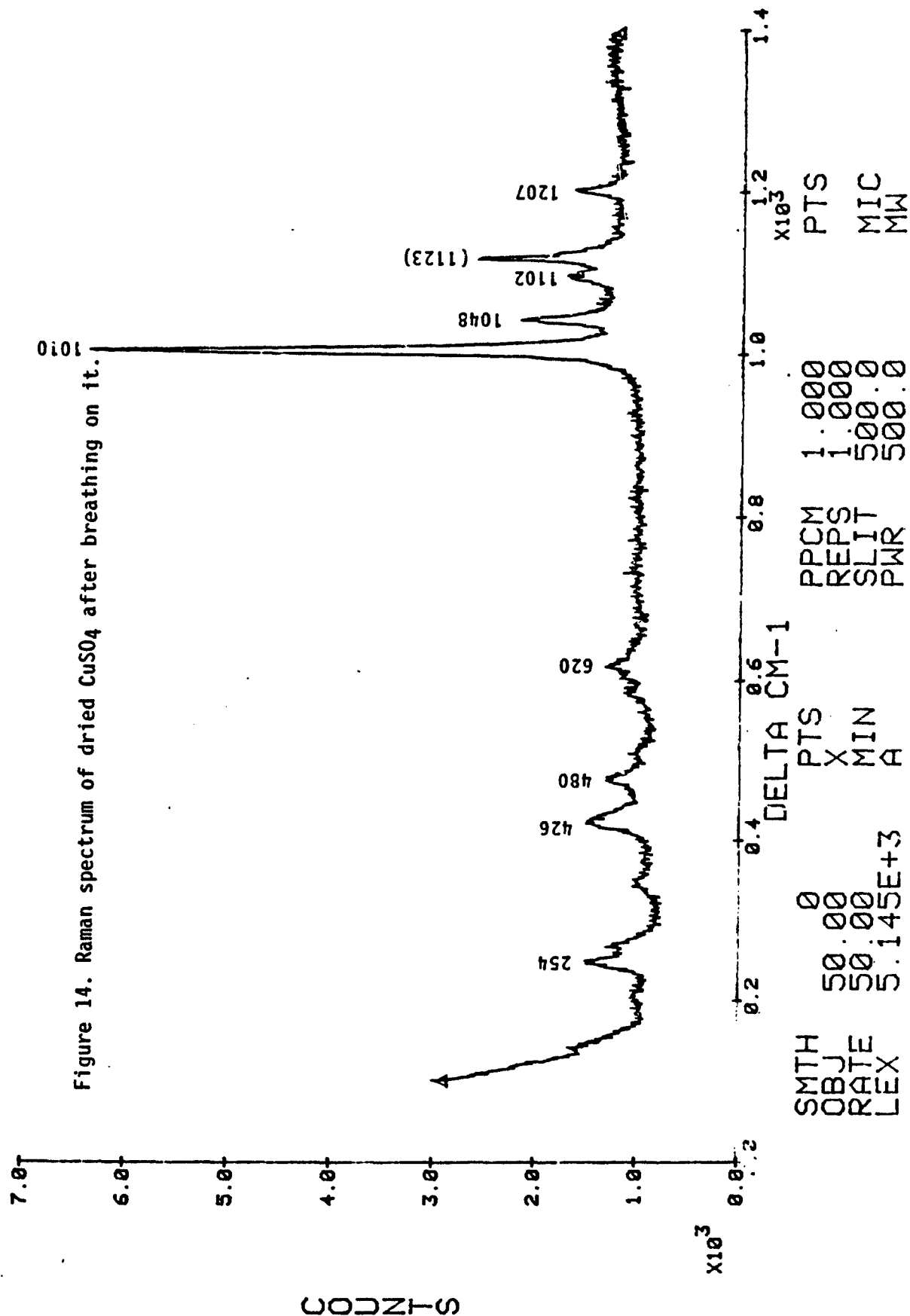
13:00:05



12/09/85

CUSO4 BREATHED

18:09:17



SECTION - #2

The Effect of Temperature and Alkali Metal Cation on the Cathodic Delamination of Polybutadiene from Steel

Principal Investigator: Henry Leidheiser, Jr.

Associate: John Catino (Graduate Student)

INTRODUCTION

An understanding of the principles underlying cathodic delamination has been an interest in this laboratory for several years [1-5]. Cathodic delamination occurs when a polymer-coated metal, usually having a defect in the coating, is polarized cathodically while immersed in an electrolyte. The coating loses adherence radially from the defect.

Cathodic delamination is important from a practical point of view because it occurs on ships and pipelines that are under cathodic protection, in the manufacture of circuit boards that are coated with a photoresist and in certain types of bimetallic couples in which the cathodic component is coated with an organic.

The primary factors controlling the rate of cathodic delamination are the nature of the substrate, the nature of the electrolyte, the applied potential and the characteristics of the coating. These factors control the delamination by affecting the cathodic reaction rate, the transport of species to or away from the reaction zone and the nature of the liquid at the periphery of the delaminated area.

The destructive species that bring about delamination are the hydroxyl ions that are formed by the cathodic reaction, $\text{H}_2\text{O} + 1/2\text{O}_2 + 2\text{e}^- = 2\text{OH}^-$. Thus the important reactants are water, oxygen, electrons and the cation counterion for the hydroxyl ions formed in the reaction. The critical questions relate to the route by which the reactants reach the metal surface and the rate determining step. Previous studies have shown that cations such as sodium and cesium have increased rates of migration through organic coatings when a cathodic potential is applied [6] and that the incubation or "delay time" before delamination occurs at a linear rate can be explained in terms of water migration into the coating [7]. These studies plus many more unpublished experiments have led us to the working hypothesis that the reactants, water, oxygen and cations, reach the delaminating front by migration through the coating. The present study has been carried out with the objective of obtaining additional information that might allow a better understanding of the means by which the reactants reach the metal surface. The method selected is based on the determination of activation energies for the delamination process with the expectation that the values obtained may aid in the analysis.

EXPERIMENTAL PROCEDURE

The substrate metal, 1010 steel, was wet abraded with 240 grit SiC metallographic paper, followed by rinsing and wiping in running distilled water, rinsing in methanol and wiping dry. The panels were sheared into 3" x 4" sections before coating. Immediately after shearing, the panels were coated with a polybutadiene known under the tradename RKY 662 Budium manufactured by Du Pont. This product undergoes an oxidative cure when heated at 190°-200° for 30 min. Since it was desired to use coatings about 25 μ m thick it was decided to cure the coating in two steps. A coating of approximately 13 μ m thick was applied to the panel by spin coating and the coating was given a superficial cure by heating at 185-190° for 10 min. After cooling, a second 13 μ m thick coating was applied, also by spin coating, and the two-coat system was heated for an additional 20 min at approximately 200°. The coating thickness was determined in all cases with a PPG Elconometer and was always 25 ± 2 μ m. This method of coating preparation avoided delamination at sites other than at the defect.

Coated panels were sheared into 1" x 2" samples and a 1 mm hole was drilled into one end for attaching a lead wire. The uncoated backside of the panel was protected by attaching a microscope slide with silicon caulking. The edges were protected by coating with a thick layer of an epoxy polyamide on all remaining steel. Panels were aged for a minimum of 10 days in a desiccator prior to testing.

Delamination experiments were conducted in 0.5M solutions of LiCl, NaCl, KCl, RbCl and CsCl. A few experiments were also carried out with 0.5M solutions of MgCl₂, CaCl₂, and ZnCl₂. All solutions were made from reagent grade chemicals and distilled water. Just prior to immersion in the electrolyte, a defect approximately 1 mm in diameter was punched into the coating and the coated panel was immersed in the electrolyte and polarized to a potential of -0.92 volt vs. SCE. The potential was maintained constant with the aid of the potentiostat described by Baboian et al. [8]. The delamination area was determined at the end of the experiment by touching adhesive tape to the surface and determining the area from which the coating had lost adherence. The boundary between the laminated and delaminated area was very sharp in all cases. Each experiment was thus a destructive test and provided only one point on a curve. A total of 213 experimental points, or an average of over 8 data points per curve, were utilized to calculate the delamination rates cited in the text.

EXPERIMENTAL RESULTS

The delaminated area increased linearly with time in all cases so the slope of the curve represents the delamination rate. The linear portion of the curve, however, did not pass through the origin. As indicated in an earlier publication [7], the intersection of the linear curve with the time axis is termed the "delay time," that is, the time required before the delaminated area becomes a linear function of time.

Data are summarized in Table I for 5 alkali metal chlorides at 5 different temperatures. Delamination tests were also run with the $MgCl_2$, $CaCl_2$ and $ZnCl_2$ solutions and no delamination was observed even at 53° for up to 96 hours.

The corrosion potentials of bare steel in the $LiCl$, $NaCl$ and KCl solutions were approximately the same in the three electrolytes at the same temperature as seen from the data summarized in Table II.

Table I

Delamination Rates and Delay Times as Determined by a Least Square Analysis of the Data. The Correlation Coefficient Is in Parenthesis

Electrolyte	Temp. ($^\circ C$)	Delamination Rate ($cm\ hr^{-1}$)	Delay Time (hr)
0.5M $LiCl$	8	.0003 (.94)	400
	23	.0021 (.79)	66
	35	.0024 (.87)	16
	53	.0066 (.96)	3
	73	.0284 (.92)	3
0.5M $NaCl$	8	.0006 (.93)	56
	23	.0026 (.83)	35
	35	.0073 (.93)	10
	53	.0439 (.96)	2
	73	.0546 (.95)	1
0.5M KCl	8	.0009 (.95)	38
	23	.0066 (.90)	30
	35	.0100 (.90)	5
	53	.0440 (.89)	0
	73	.0580 (.96)	0
0.5M $RbCl$	8	.0016 (.86)	70
	23	.0126 (.75)	30
	35	.0230 (.88)	13
	53	.0461 (.93)	1
	73	.0845 (.99)	2
0.5M $CsCl$	8	.0018 (.87)	40
	23	.0101 (.87)	25
	35	.0127 (.93)	9
	53	.0549 (.96)	2
	73	.0868 (.99)	2

Table II

Corrosion Potentials of Bare Steel in 0.5M Alkali Metal Halide Solutions at Different Temperatures

Electrolyte	Temperature (°C)	E_{corr} (volts vs. SCE)
0.5M LiCl	8	-.54
	23	-.57
	35	-.63
	53	-.66
	73	-.68
0.5M NaCl	8	-.57
	23	-.65
	35	-.63
	53	-.67
	73	-.70
0.5M KCl	8	-.56
	23	-.65
	35	-.61
	53	-.67
	73	-.70

DISCUSSION

The results reported herein confirm the previous observations [2] that the rate of cathodic delamination is strongly a function of the alkali metal cation present in the electrolyte. At 8° the rates decrease in the order, Cs, Rb, K, Na and Li. At higher temperatures the delamination rates in RbCl and CsCl solutions are approximately the same and the other cations exhibit the same ranking. In the case of the delay times, the shortest delay times were observed with KCl, with NaCl exhibiting longer delay times and LiCl exhibiting the longest delay times at all temperatures. The delay times observed with RbCl and CsCl were of the same order as those observed with KCl with the exception of the datum point at 8° which is anomalously high.

The negligible rates of delamination of the coating in solutions of $MgCl_2$, $CaCl_2$ and $ZnCl_2$ are probably a consequence of the fact that the hydroxides of these metals are unsufficiently soluble to form the necessary high pH to cause delamination. White corrosion product was indeed observed at the periphery of the defect after the polarization period in the case of these three salts.

Activation energies calculated from the delamination rates and from the delay times are summarized in Table III. The values for each alkali metal chloride as determined from the delamination rate and from the delay time were approximately the same with the exception of the anomalously high value for the activation energy calculated from the delay times in the case of KCl.

Table III
Calculated Activation Energies

Electrolyte	Activation Energies		
	From Delamination Rates (cals/mole)	From Delay Times (cals/mole)	Average (cals/mole)
0.5M LiCl	-12,100	-13,300	-12,700
0.5M NaCl	-13,500	-13,300	-13,400
0.5M KCl	-11,700	-16,400	-14,050
0.5M RbCl	-10,800	-10,500	-10,650
0.5M CsCl	-10,800	-9,300	-10,050

The only other published data on the activation energy for the cathodic delamination process is found in the work of Leidheiser and Wang [2] in which they calculated an activation energy of -9,500 cals/mole for a NaCl electrolyte and a polybutadiene coating on steel. This calculation was of limited accuracy, however, since the value was estimated on the basis of measurements made at three temperatures over a narrow range of 20°. Account must also be taken that the formulation of the coating may have been modified by the manufacturer in the time between these measurements.

It is unlikely that the activated process is the diffusion of water molecules through a bulk water phase in the polymer since the activation energy for diffusion of bulk water is 4.6 kcal/mole [9]. However, the activation energy for diffusion of water in confined internal volumes such as exist in zeolites can range from 8.7 to 11 kcal/mole. This capillary effect may exist in polymers as transport through the equivalent of narrow hollow cylinders as described by Crank and Park [10]. In fact, many polymers exhibit activation energies for water vapor diffusion in the range of 10-16 kcal/mole [11]. Activation energies for gas permeation through polymers are in the range of 6-12 kcal/mole over a temperature range of 21 to 62° [12]. It is unlikely that the measured activation energy represents oxygen diffusion since the activation energy for this process through polybutadiene is 6.8 kcal/mole in the temperature range of the present measurements [13].

Unfortunately, no information is available on the activation energies associated with the migration of anions and cations through organic coatings. Oyabu et al. [14] have determined the absorption of alkali metal chloride solutions into a polymer coating and found that the bulk migration properties were in the order $\text{LiCl} < \text{NaCl} < \text{KCl}$, an order similar to the order of delamination rates measured herein.

Parks and Leidheiser [6] have shown that the migration rates of cations such as Na^+ and Cs^+ are appreciably increased through a polybutadiene coating on steel when a cathodic potential is applied. The migration rate of water is also increased by the applied potential. It has also been shown [7] that both the delamination rates are appreciably increased and the delay times are appreciably decreased as the applied potential is increased. These facts, along with the delay times as determined herein, suggest that the critical factor is the diffusion of water into the coating and the subsequent or concurrent development of aqueous pathways for the migration of cations to the interface.

REFERENCES

- [1] H. Leidheiser, Jr., Croat. Chem. Acta 53, 197 (1980).
- [2] H. Leidheiser, Jr., and W. Wang, J. Coatings Technol. 53(672), 77 (1981).
- [3] H. Leidheiser, Jr., Ind. Eng. Chem. Prod. Res. Dev. 20, 547 (1981).
- [4] H. Leidheiser, Jr., W. Wang and L. Igetoft, Prog. Org. Coatings 11, 19 (1983).
- [5] J. M. Atkinson, R. D. Granata, H. Leidheiser, Jr., and D. G. McBride, IBM J. Res. Dev. 29(1), 27 (1985).
- [6] J. Parks and H. Leidheiser, Jr., Ind. Eng. Chem. Prod. Res. Dev., in press, March 1986 issue.
- [7] W. Wang and H. Leidheiser, Jr., Proc. INTERFINISH '84, 11th World Congr. Metal Finishing, Jerusalem, Israel, October 21-26, 1984, pp. 262-69.
- [8] R. Baboian, L. McBride, R. Langlais and G. Haynes, Mater. Perf. 18, 40 (1979).
- [9] J. H. Wang, C. V. Robinson and I. S. Edelman, J. Am. Chem. Soc. 75, 466 (1953).
- [10] J. Crank and G. S. Park, "Diffusion in Polymers," Academic Press: New York, 1968, p. 5.
- [11] R. Stannett, "Diffusion in Polymers," J. Crank and G. S. Park, Eds., Academic Press: New York, 1968, p. 41.
- [12] R. M. Barrer, Trans. Faraday Soc. 35, 628 (1939).
- [13] G. J. Van Amerongen, J. Polym. Sci. 5, 307 (1950).
- [14] Y. Oyabu, H. Kawai and S. Ikeda, J. Japanese Soc. Colour Mater. 37, 16 (1963).

SECTION - #3

Acid-Base Effects in Glass/Bead Phenoxo Model Coating Systems

Principal Investigator: John Manson, Prof. of Chemistry
Associate: Astrophel Tiburcio, Graduate Student

INTRODUCTION

In the two previous report periods [1,2], research has focused on the effect of pigment (filler)-binder interactions on various properties of the glass bead/phenoxo system, selected as a model for coatings [1,2]. Characterization of the filler surfaces by inverse gas chromatography (IGC) and qualitative analysis of the fracture surfaces of the composite by scanning electron microscopy (SEM) have shown that the filler-binder interactions were consistent with an interpretation based on Lewis acid-Lewis base (electron donor-acceptor) concepts. That is, combinations of electron-accepting fillers with electron-donating binders (or vice versa) are predicted to exhibit stronger adsorption and interfacial adhesion than combinations of donors with donors or acceptors with acceptors. Moreover, the degree of interfacial adhesion has been found to affect water vapor permeability and other properties of coatings used for corrosion resistance [1]; for example, strong adhesion reduced both the permeability to water and the retention of solvent. However, the dynamic mechanical response was affected primarily by the presence of residual solvent [2].

This report focuses on the viscoelastic behavior of glass bead-filled phenoxo as measured by dynamic mechanical response and the corrosion performance of the model coating as indicated by the cathodic delamination and accelerated salt solution experiments.

Thus a more detailed investigation of the viscoelastic behavior was undertaken. Compression-molded samples were prepared to ascertain separately the role of interfacial adhesion, filler content, and residual solvent. The effects of interfacial adhesion and pigment loading were analyzed using dry and water-saturated specimens. For comparison, dynamic mechanical response of solvent-cast films was also measured for both air-dried and oven-dried specimens.

Having established the base-line properties of the glass-bead-phenoxo system in the major areas of interest [1,2], i.e., characterization of the fillers, water vapor permeability and dynamic mechanical response, we thought it timely to investigate the corrosion performance of the model coating system. For these experiments, we selected cathodic delamination and accelerated corrosion tests in 3% NaCl solution.

Corrosion Tests

The method of cathodic delamination has been explained in detail in earlier reports by others [3,4]. Basically, the test measures the loss of adhesion of the coating from the metal substrate in the presence of an electrolyte under an applied potential. The results have shown significant differences between the delamination rates of air-dried and oven-dried specimens. Similarly, accelerated corrosion tests in salt solution provided interesting results concerning the corrosion performance of a coating material with and without filler and the effect of drying procedure on the inhibition of corrosion. In this case, conductance and potential measurements were made and micrographs taken to assess the property of the coating.

Dynamic Mechanical Behavior

The elastic and viscoelastic behavior is of interest because it reflects the state of the polymer as a result of the inclusion of a second phase. For composite systems, Equations 1 and 2 predict the upper and lower bounds of composite elastic modulus, E_c , for the simplest possible case [5].

$$\text{upper bound: } E_c = v_p E_p + v_f E_f \quad (\text{case of equal strains}) \quad (1)$$

$$\text{lower bound: } E_c = \frac{E_p E_f}{E_p v_f + E_f v_p} \quad (\text{case of equal stresses}) \quad (2)$$

where v represents the volume fraction, E the modulus, and the subscripts p and f the polymer matrix and particulate filler phases, respectively. Equations 1 and 2 typically correspond to glassy composites containing fibrous and particulate phases, respectively. More complicated equations may apply as well, e.g., Kerner's equation for particulate systems exhibiting good adhesion between the phases [5].

Changes in viscoelastic state are also manifested in the glass transition (T_g) of the material. For mixtures, Equation 3 can be used to estimate the change in T_g [6]:

$$\frac{1}{T_{g,c}} = \frac{w_1}{T_{g,1}} + \frac{w_2}{T_{g,2}} \quad (3)$$

where T_g is the glass transition, w is the weight fraction of each component, and the subscripts, c , 1 , 2 , represent the composite and components 1 and 2, respectively. Equation 3 (and variations thereof) also applies to plasticizers or diluents such as water or residual solvent [7-9].

EXPERIMENTAL

Materials

A high-molecular-weight linear phenoxy (Union Carbide) was the binder. This material is both a common coating material in its own right, and a linear analogue of an epoxy resin. For filler, glass beads of type 3000 (untreated) and 3000CP03 (treated with an aminosilane coupling agent) were supplied by Potters Industries; the mean particle size was 25 μm .

Sample Preparation

Free Films. The formulation consisted of 20-wt-% phenoxy resin in cellosolve acetate from which samples containing no filler and 0.4 volume fraction (v_f) glass beads (both untreated and treated with an aminosilane) were prepared. The films were cast on glass plates using a draw bar which delivers a wet film thickness of 4 mils. One set of samples was first allowed to "dry to touch" and then baked at 190°C for 20 min (oven-dried specimens) [10]. For the second group (air-dried specimens), drying was effected for 1 day at ambient temperature, followed by drying under vacuum for 24 h.

Compression-Molded Samples

Phenoxy pellets were subjected to vacuum drying at 100°C (above the T_g of the material) for 1 week to minimize the amount of residual monomer in the binder. (For comparison, one batch of neat resin was not dried before molding.) Appropriate amounts of phenoxy and glass beads (treated and untreated; volume fractions, 0.1 and 0.2) were mixed in a Banbury mixer at 120°C for 10 min to ensure uniform distribution of the filler in the composite material.

Neat resin (not dried previously) was molded at 150°C and 3.5 MPa pressure for 10 min; a two-step molding procedure was used for a second bath of neat resin (dried previously) and for the filled materials. The filled materials were compression-molded using a two-step process. In the initial step, samples were formed at 190°C under a pressure of 4.4 MPa for 10 min. Then, two samples from the first step were subjected to an initially low pressure at 190°C; the pressure was then gradually increased to the final pressure of 4.4 MPa, which was maintained for 30 min. The procedure yielded bubble-free specimens -2 mm thick.

Table I

Summary of Compression-Molded, Glass-Bead-Filled Phenoxy Specimens

v _f	Dry		Water Saturated ^c	
	unfilled	unfilled ^a	unfilled (1.23)	
0		unfilled ^{a,b}		
0.1	untreated	treated	untreated (1.43)	treated (1.38)
0.2	untreated	treated	untreated (1.56)	treated (1.44)

^aNeat resin (not dried previously) prepared using one-step molding procedure. All others were prepared using two steps.

^bVacuum-dried for 1 day before testing.

^cNumbers in parentheses represent wt % water in saturated binder.

Corrosion Test Specimens

The surfaces of commercially sandblasted steel panels (Q type) were polished with silicon carbide paper, 240 grit, while wetted with deionized water, and then rinsed with methanol. The panels were left to air-dry before the coating was applied (same formulation and procedures as for the free films). The panels were then cut to the required dimension for delamination and corrosion testing. Dried film thicknesses ranged from 1 to 2.5 mil (0.025 to 0.064 mm).

Test Procedures

Dynamic Mechanical Spectroscopy. Dynamic mechanical spectra (DMS) for the compression-molded samples were obtained at 110 Hz using an Auto-vibron Viscoelastometer Model DDV-IIIC. For thin films, DMS data were acquired using a manual Rheovibron Model DDV-II.

Cathodic Delamination. After a small defect was introduced in the coating material (by a sharp-pointed counter punch), the specimen was immersed in a 3% NaCl solution and cathodically protected by an applied potential of -0.800 V relative to a standard calomel electrode. At specified times, the specimen was disconnected, allowed to dry, and the area of delamination estimated using commercial Scotch tape to separate the delaminated portion from the metal substrate. For more specific details, see References [11] and [12].

Accelerated Corrosion Test. Specimens were cut into circular disks and assembled in a small polyethylene bottle in such a way that the coated side could be continually exposed to 3% NaCl solution. Conductance and potential data were acquired at specific time intervals while the corrosion of the coating was observed visually and photographed.

RESULTS AND DISCUSSION

Viscoelastic Behavior

The complexities of a composite system are manifested in the dynamic mechanical response. Several factors contribute to overall behavior: the type and amount of filler, the polymer, the degree of interfacial adhesion between filler and binder; and residual solvent [2,5]. Thus the glass-phenoxy system, the intrinsic behavior of the composite may be expected to be modified by the latter and, hence, by the nature of the drying process (air vs. open drying).

As expected [5], the addition of filler particles increases the storage modulus (E') in the glassy state (Figure 1 and Table II). Except for the untreated glass ($v_f = 0.1$), the increase appears to be slightly higher than that predicted by the lower bound limit of Equation 2, but slightly lower than predicted by Kerner's equation.

Table III shows that the addition of glass beads raised the T_g by up to 3 or 5 degrees ($v_f = 0.1$ and 0.2 , respectively); an increase in the T_g of this magnitude of change is comparable with those found for glass-bead-filled epoxy and phenoxy resins [13-15]. However, for both treated and untreated beads, the increase was essentially independent of filler content. Interestingly, at each volume fraction of filler in the dry sample, the untreated glass (which adheres poorly to the resin) appeared to raise the T_g slightly more than the treated glass—a behavior reported by Lewis and Nielsen [12] for glass beads in an epoxy.

Analysis of the mechanical spectra (Figure 1) indicates three regions of damping behavior ($\tan \delta$), below the β -peak region ($< -60^\circ\text{C}$), the β -peak region ($-60^\circ\text{C} < T < 15^\circ\text{C}$), and above 15°C . The β -transition for the phenoxy system corresponds to the motion of the free hydroxyl group on the polymer chain. Above and below the β -transition, the filler tends to decrease damping of the polymer resin (with one exception); the magnitude of change is more noticeable above the β -transition than below. Such a decrease is expected since the filler does not contribute to the damping. In the β -transition region, the beads increase damping with respect to the unfilled resin, a behavior consistent with studies by Hirai and Kline [16] and Jenness [17]. While the order of increase does not follow a particular pattern [$\tan \delta$ for $0.1 v_f$ (treated) $>$ $\tan \delta$ for $0.2 v_f$ (treated) $>$ $\tan \delta$ for $0.2 v_f$ (untreated) $>$ $0.1 v_f$ (untreated)], it appears that the treated systems exhibit higher damping than the resin or the resin-containing untreated glass.

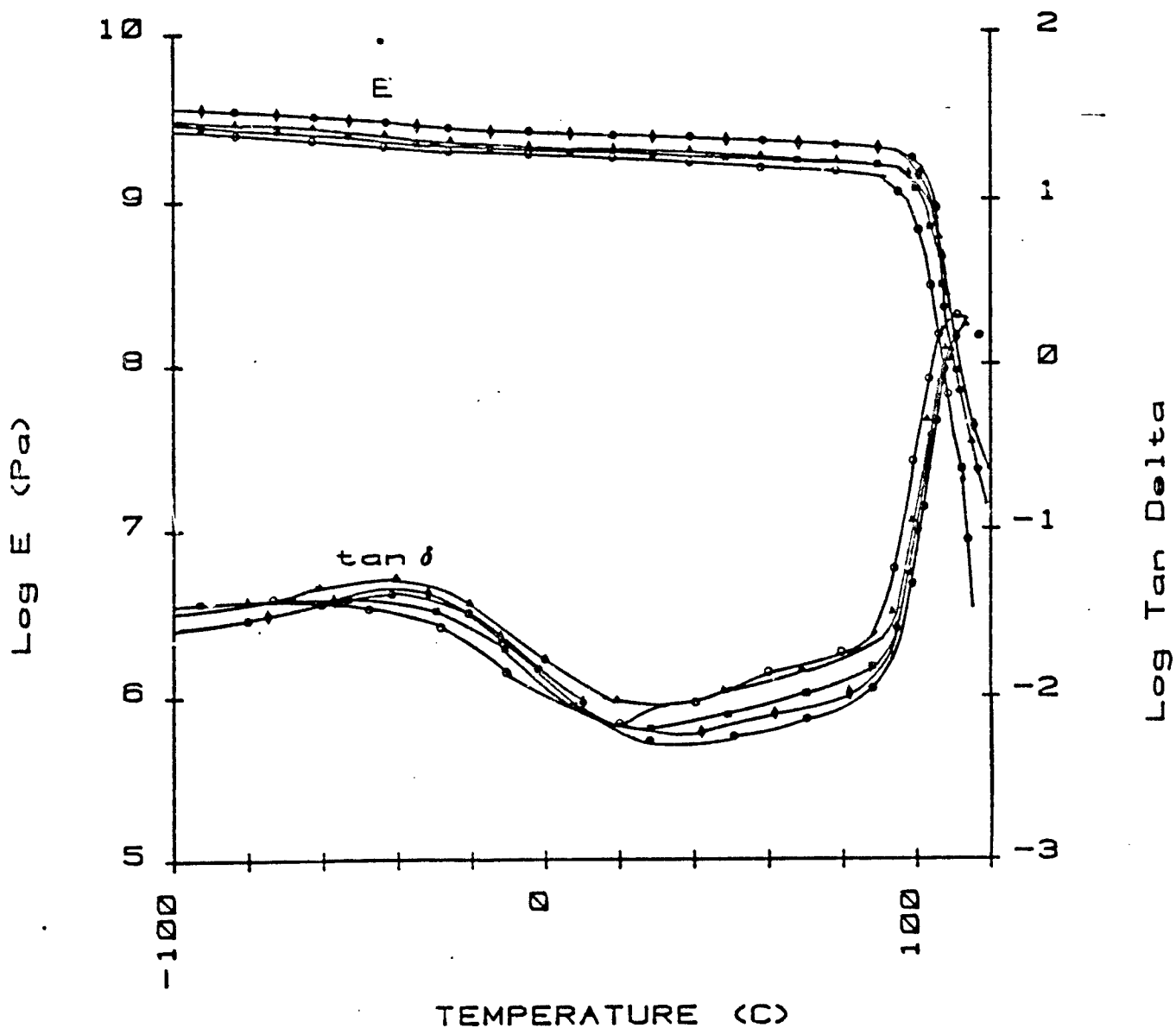


Figure 1. E' and $\tan \delta$ for dry glass-bead-filled phenoxy resin: O, dry unfilled resin; \square, \triangle , $v_f = 0.1$ for untreated and treated beads, respectively; \bullet, \blacklozenge , $v_f = 0.2$ for untreated and treated beads, respectively.

Table II

Storage Moduli^a at -100°; for Glass-Bead/Phenoxy Materials
(Dry and Water-Saturated) as a Function
of Volume Fraction Filler (v_f)

v_f	State	E'^b (predicted)	Untreated	Treated
0	dry	--	2.58	2.58
0.1	dry	2.86 (3.21)	2.80	3.01
0.2	dry	3.20 (3.92)	3.51	3.64
0	sat.	--	2.48	2.48
0.1	sat.	--	2.53	2.79
0.1	sat.	--	2.92	3.16

^aYoung's modulus; E' is the storage component of the complex modulus E^* .

^bValues in parentheses predicted by Kerner's equation, assuming a Poisson's ratio of 0.37; others predicted by Equation 2.

Table III

Glass Transition Temperatures^a for Compression-Molded Glass
Bead/Phenoxy Systems (Dry and Water Saturated) as a
Function of Volume Fraction of Filler (v_f)

v_f	Specimen Type	T_g (dry), °C	T_g (saturated), °C
0	Unfilled	102	87
	Unfilled ^{b,c,d}	95	--
	Unfilled ^{b,c}	89	--
0.1	Filled	106 (105) ^e	91 (93) ^e
0.2	Filled	107 (105) ^e	91 (91) ^e

^a T_g is defined as T at maximum E'' (not shown in the figures).

^bNot dried before molding.

^cOne-step molding.

^dOne-day vacuum oven drying before testing.

^eNumbers in parentheses correspond to specimen containing treated rather than untreated glass.

Comparison of the different filler types at the same filler concentration reveals that the treated glass has higher damping throughout most of the temperature range, the difference being more pronounced for $v_f = 0.1$. This enhancement in damping by silane treatment can be attributed to the interfacial acid-base interactions [1,2,5]. Thus, frictional motion of the interface contributes more energy dissipation when acid-base interactions are present (due to the displacement of partial charges of opposite kind) than when they are absent.

The effects of specimen preparation must also be considered. Figure 2 illustrates the spectra of the four unfilled phenoxy specimens while Tables II and III contain E' and T_g data. At low temperatures ($T < T_g$), the storage modulus (E') increases in the following order: dry unfilled > unfilled reference (1-day vacuum-drying prior to testing) > saturated unfilled > unfilled reference. Above the β -transition, the value of E' parallels the degree of dryness of the sample (dry unfilled > reference unfilled with 1 day vacuum drying > reference unfilled > saturated unfilled). Since drying removes absorbed species (residual water or monomer) in the polymer matrix which may plasticize the resin, the presence of the plasticizer lowers E' above the β -peak. At least with this system, an antiplasticization effect below T_g due to water does not materialize, though water has such an effect in some polymers [2]. In any case, the

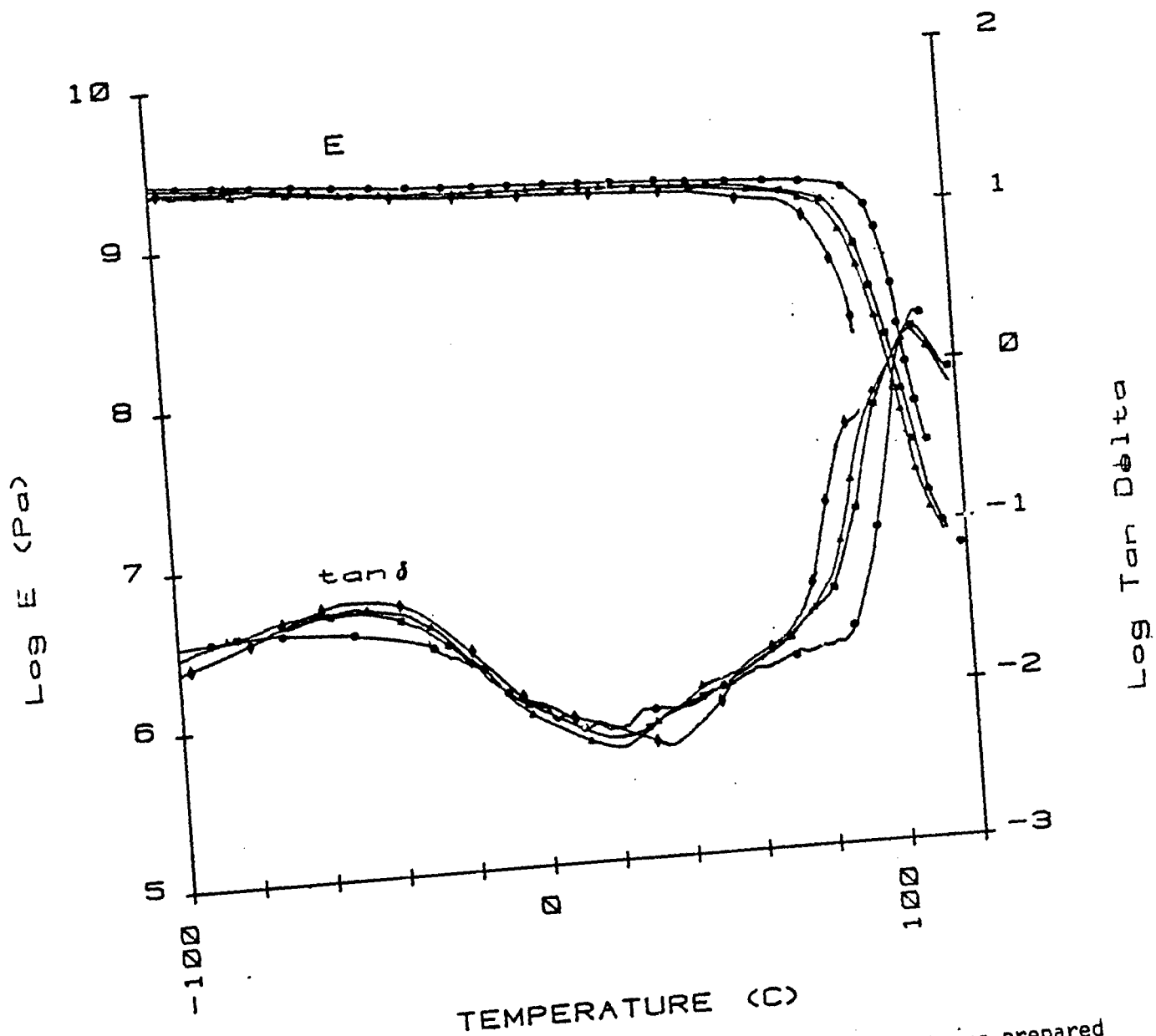


Figure 2. Dynamic mechanical response of unfilled phenoxy specimens prepared in different ways (see Table I): ●, dry unfilled; ▲, neat resin (not dried before molding); ■, neat resin (not dried before molding but vacuum dried before testing); ◆, unfilled saturated with water.

water tends to lower T_g . Also, water increases damping in the β -transition region and at temperatures above 50°C but decreases damping below the β -transition region, a behavior consistent with an earlier study [2]. At temperatures above -10°C but below 50°C , the scatter of the data makes analysis difficult.

Figures 3 and 4 present the mechanical spectra of the two sets of compression-molded samples for each filler type—dry and saturated with water.

From Table I, the untreated glass absorbs more water than the treated glass. This effect may well be due to the hydrogen bonding of water at the acid/base interface. Such water may, however, be sufficiently bonded that permeability is not increased (earlier results [2,18]) showed that surface treatment of the glass reduced the permeability to water). In this section, the effects of water on the DMS of composite materials are discussed.

As expected, the presence of water plasticized the saturated specimens relative to the dry samples (Table III), lowering the T_g by 12 to 16°C . However, filler type or concentration does not appear to significantly affect the T_g . In the glassy state region, the differences in E' primarily reflect the differences in volume fraction filler rather than the amount of retained water (Table II). In this respect, these results are consistent with Figures 1 and 2 where the increase in filler content raises the modulus for the dry filled specimens and antiplasticization effects are absent for the unfilled samples, respectively.

In general, water appears to have a more pronounced effect on the damping behavior of the untreated filler than the treated glass. Contrary to the results of the dry specimens where damping decreases as the volume fraction of filler increases, the presence of water raises $\tan \delta$ as the filler content is increased. This is true for both treated and untreated glass. Thus above the β -transition, damping increases in the following order: $0.2 v_f$ (saturated) $> 0.1 v_f$ (saturated) $> 0.1 v_f$ (dry) $> 0.2 v_f$ (dry). These results suggest that above the β -transition the effect of water on damping overrides the effect of filler. Correspondingly, the greater differences in the $\tan \delta$ values between the two samples of the saturated untreated glass (Figure 3), in comparison to the two samples of saturated treated glass (Figure 4), reflect the more dominant role of water on damping. In this case, the difference in the magnitude of the water content of the two saturated untreated glass samples (0.12%) is much higher than the differences between the two saturated treated glass (0.06%).

It appears that the saturated unfilled phenoxy control has lower damping than the saturated filled samples between the β and glass transitions. However, on a comparative basis (Table I), the saturated unfilled specimen contains less water in the binder than the saturated filled samples. Thus, the behavior is self-consistent.

In addition, the presence of absorbed water produces a new peak just before $\tan \delta$ reaches maximum. Manson and Chiu [19] observed a similar behavior for glass-bead-filled epoxies and attributed the extraneous peak to absorbed water.

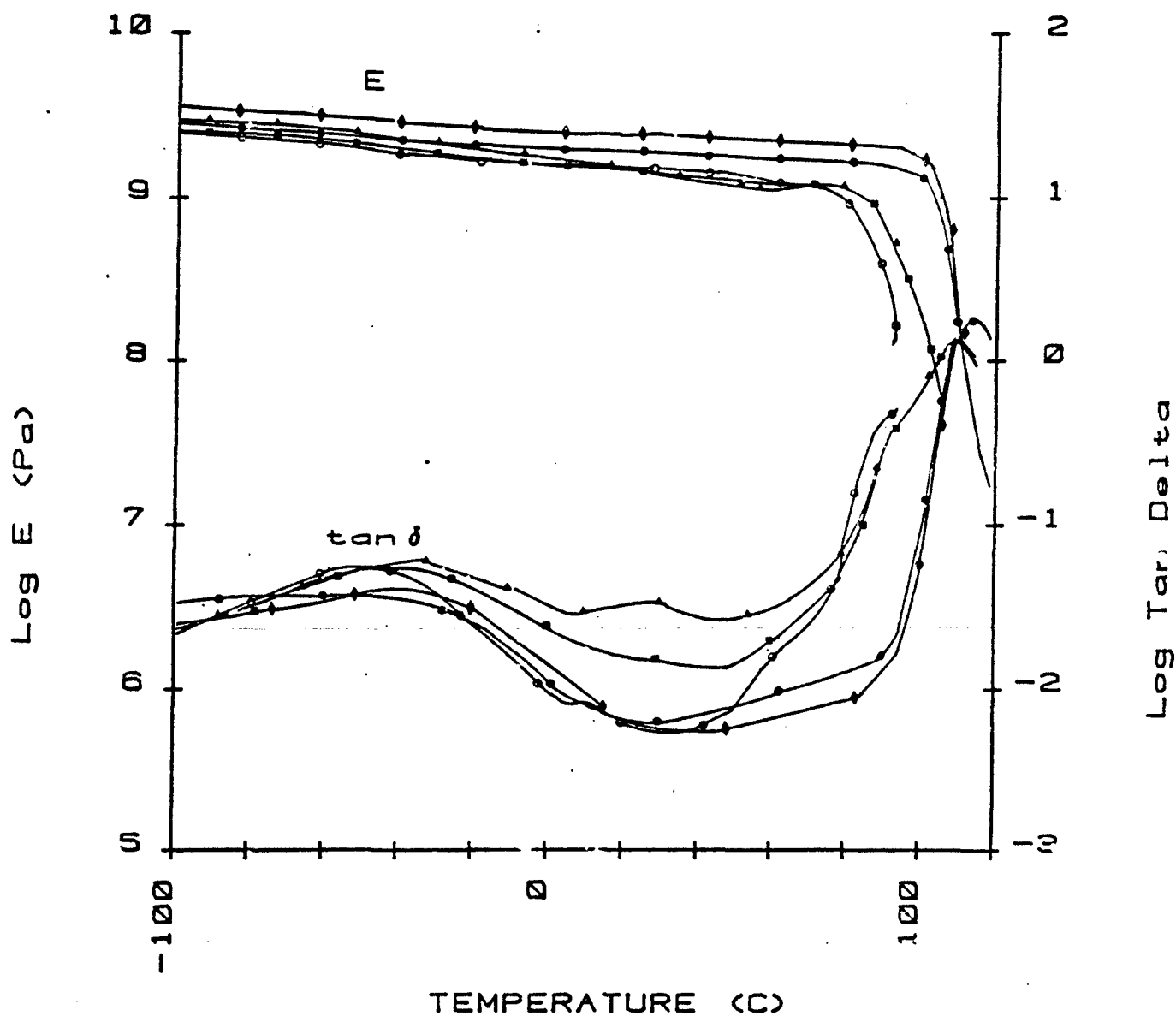


Figure 3. Dynamic mechanical response of dry and water saturated glass-bead-filled phenoxy with the untreated glass as filler: water saturated unfilled control; ●, ■, $v_f = 0.1$ for dry and water saturated specimens, respectively; ♦, ▲, $v_f = 0.2$ for dry and water saturated specimens.

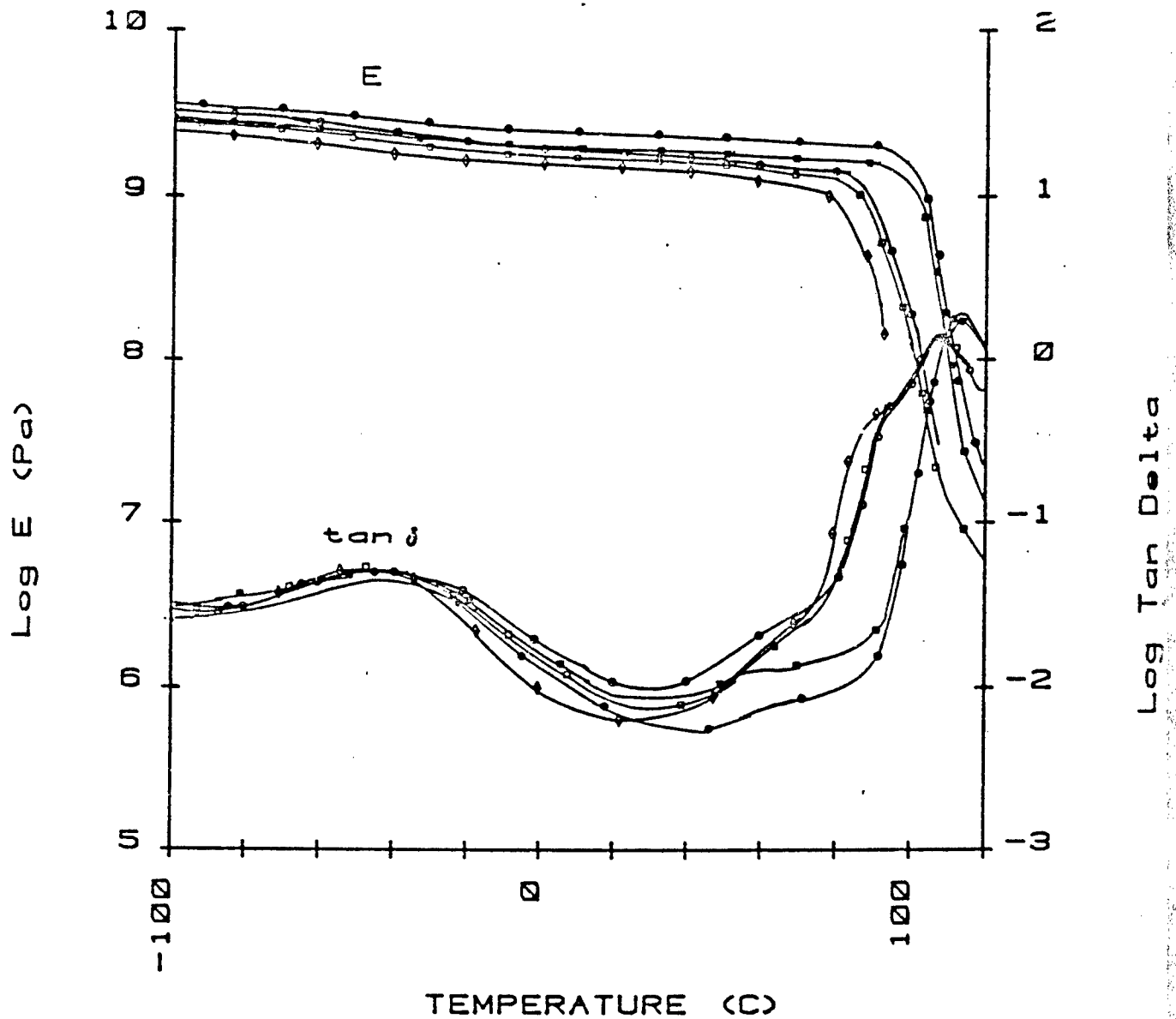


Figure 4. Dynamic mechanical response of dry and water saturated glass-bead-filled phenoxy with the treated glass as filler: ◇, water saturated unfilled control; ■, ●, $v_f = 0.1$ for dry and water saturated specimens, respectively; □, ○, $v_f = 0.2$ for dry and water saturated specimens.

It is now of interest to examine the viscoelastic behavior of solvent-cast films in comparison with molded specimens. Figures 5 and 6 illustrate E' and $\tan \delta$ for the thin-film specimens (0.5-2.5 mil thick). In some cases, particularly the oven-dried specimens, the brittleness of the sample made it difficult to acquire a complete spectrum into the rubbery region, failure usually occurring at the T_g region. However, the measurements are sufficient to illustrate trends.

Figure 5 exhibits the classical effect of solvent as a plasticizer. In this case, strong Lewis acid-Lewis base interactions enable the acidic phenoxy binder to retain the basic cellosolve acetate solvent, confirming earlier studies on this system [2]. As noted earlier, below T_g , E' was increased in the presence of residual solvent in the air-dried phenoxy, and T_g was decreased. The decrease in T_g parallels the increase in the amount of retained solvent in the film^g (molded < oven-dried < cast). Table IV summarizes the T_g values and the solvent content in the binder estimated from the T_g lowering using Equation 3. As expected, the presence of solvent produces higher damping: air-dried > oven-dried > compression-molded.

Table IV
Effect of Residual Solvent on T_g of Unfilled Phenoxy Films

Specimen Type	T_g^a , °C	Wt % Solvent ^d	
Unfilled (air-dried)	60	5.9 ^b	7.6 ^c
Unfilled (oven-dried)	73	2.8 ^b	5.5 ^c
Unfilled (comp. molded)	88	—	—
Unfilled (comp. molded, dry)	102	—	—

^a T_g is defined as T at E'' maximum.

^b T_g (solvent) = 143 K

^b T_g phenoxy = 88°C (compression-molded, neat resin)

^c T_g phenoxy = 102°C (dry unfilled, Table II)

^dCalculated using Equation 3.

The inclusion of a filler particle, particularly those with different surface treatments, adds complexity to the spectra. In an earlier report [2], the untreated glass system was said to possess a greater propensity for retaining solvent than the treated glass, a characteristic attributable to the higher entropy of the matrix phase compared to the matrix with treated glass. Similarly, more rigorous drying reduces the amount of retained solvent in the binder, a behavior which has been shown in an earlier report [20]. In this regard, the trends in Figure 6 seem to reflect primarily the extent of dryness of the sample rather than the

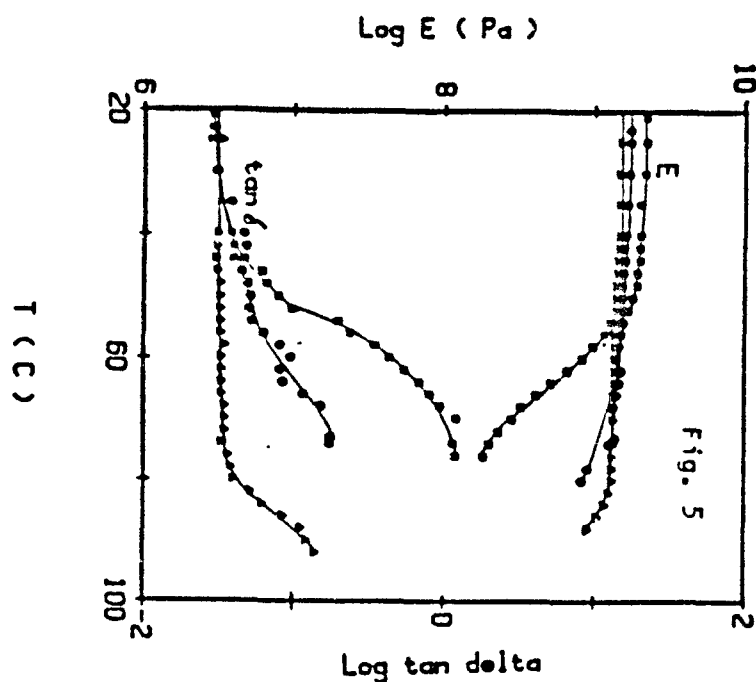


Figure 5. Dynamic mechanical response of unfilled phenoxy films: ▲, compression-molded; ■, solvent-cast and air-dried; ●, solvent-cast and oven-dried.

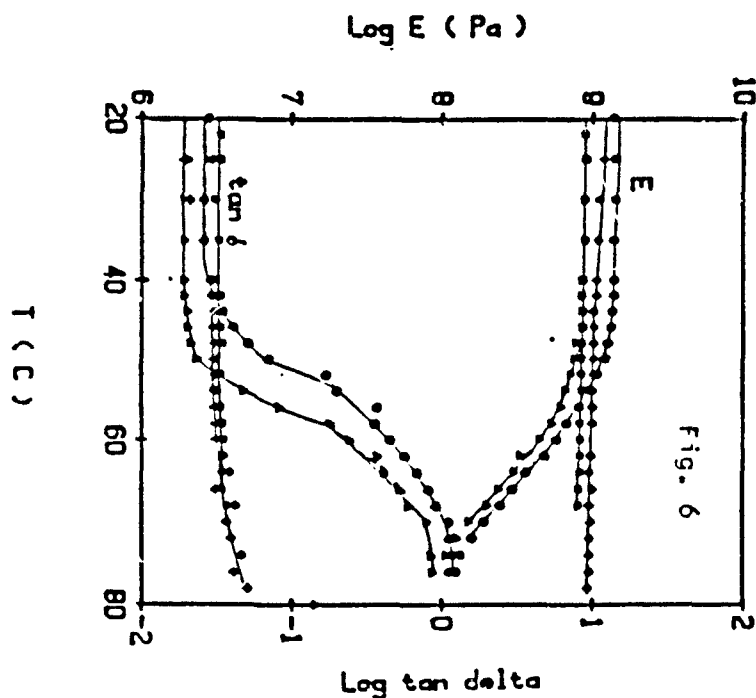


Figure 6. Dynamic mechanical response of solvent-cast-glass-filled phenoxy films ($v_f = 0.4$) with different drying conditions: ▲, ●, for air-dried untreated and treated glass, respectively; ■, ◆, for oven-dried and treated glass, respectively.

effect of filler on solvent retention. In the glass transition region, the oven-dried specimens exhibit higher E' than the air-dried, though for the same drying procedure the treated glass increases E' . In terms of damping behavior (solvent increases damping), the air-dried specimens (which may be expected to retain more solvent) show higher damping than the oven-dried samples near the glass transition region.

Cathodic Delamination

Cathodic delamination measurements reflect the ability of the coating material to inhibit the transport of permeants at the coating/metal substrate interface. The passage of oxygen and water molecules is of particular interest because the mechanism of cathodic delamination is generally believed to be an electrochemical process with the oxygen and water species as major reactants [3,4]. These results attempt to relate the cathodic delamination measurements with the water vapor permeability behavior of the glass-bead-filled phenoxy system [2] and to use these findings to help interpret the accelerated corrosion results below.

The results from the two sets of experiments (air drying vs. oven drying) show that oven drying significantly reduces the delamination rate of the unfilled coating. For the unfilled specimen -1 mil thick, analysis of the data (the slope of delamination area vs. time) yields a delamination rate of $0.010 \text{ cm}^2/\text{hr}$ for the oven-dried samples but a rate of $0.87 \text{ cm}^2/\text{hr}$ for the air-dried. Extrapolation of the delamination curve to zero delamination area produces a delay time, the time required to establish a steady-state condition. The delay times for the oven-dried and air-dried samples are 20.8 hours and 1.1 minutes, respectively. In comparison, an alkyd coating of comparable thickness exhibits a delamination rate of $0.17 \text{ cm}^2/\text{hr}$ and a delay time of less than 1 hour (in 0.5 N NaCl using a steel substrate under an applied potential of -0.8 volt (vs. a standard calomel electrode) [4]. Thicker alkyd and epoxy-polyamide coatings (3.6 and 2.5 mils, respectively) yield delamination rates of 0.015 and $0.030 \text{ cm}^2/\text{hr}$, respectively [12]. (Note, however, that the test conditions are different for those used in this study.) Hence, phenoxy resin is very resistant to cathodic delamination, at least when baked.

For the glass-bead-filled coatings containing 0.4 volume fraction filler, rapid delamination rates and wet adhesion problems make measurement difficult. In the case of oven-dried samples, the entire portion of the coating immersed in the electrolyte delaminates from the metal substrate in less than 6 hours. Judging from the results of the unfilled specimens, the loss of adhesion for the filled air-dried samples will occur at an even faster rate.

Comparison of the film thickness and the filler size may explain the rapid delamination behavior of the filled phenoxy specimens. Dry film thickness for the oven-dried films is approximately 2 mils ($\sim 50 \mu\text{m}$) while the average glass bead diameter is $25 \mu\text{m}$. Thus, the path length for diffusion nearly equals the size of the filler particles. Since water vapor permeability studies show the filled coatings to be more porous than the unfilled material [2], particularly at higher filler loadings, permeation through the filled coating in the electrolyte solution may also be

expected to be significantly higher than for the unfilled. In effect, the interfacial region around the filler particles act as microscopic defects in the coating. The use of thicker films could provide sufficient barrier properties so that it will be possible to observe differences due to filler-matrix adhesion.

Accelerated Corrosion

A common method to assess the corrosion performance of a coated metal is to expose it to a corrosive agent and then appraise the results. The corrosive agent accelerates the corrosion process, reducing the duration of the experiment to a more reasonable time period. As a continuation of the study on corrosion behavior, conductance and potential measurements were made of various phenoxy coatings on sandblasted Q-panels in 3% NaCl solution.

In general, the unfilled coating achieves the best corrosion performance for both systems studied: oven-dried at 190°C and air-dried. Figure 7 illustrates the conductivity behavior of the air-dried specimens. The conductance reflects the properties of a coating as a barrier to permeants while the potential (not shown) reveals conditions at the coating/metal substrate interface. Thus, the better coating exhibits lower conductivity and higher potentials (in the positive direction).

Judging from Figure 7 and potential measurements, for the air-dried specimens, the unfilled coating should provide the best corrosion protection for the metal. The conductance measurements show a dramatic difference between the unfilled and the 0.4 volume fraction glass-bead-filled samples, while for the filled samples the treated glass has lower conductivity than the untreated glass. The corresponding potential measurements yield no significant differences among the various samples, though the unfilled tends to have higher potential.

The appearance of micrographs of the actual specimens after exposure to the salt solution for a specified period of time is consistent with the electrical measurements. The typical brown rust associated with aerated corrosion was observed for the filled systems after 10 days. In contrast, the unfilled coating shows little or no evidence of corrosion. Qualitatively, rusting appears shortly after a conductivity of 800 μ Siemens. For the unfilled coatings, the treated filler provides better corrosion protection than the untreated, at least during the early part of the experiment. Visual observation and the conductance measurements correlate well with one another, suggesting a role of filler-matrix adhesion in corrosion behavior. In this regard, the corrosion behavior of the air-dried specimens parallels the water vapor permeability of the glass-bead-filled films [2]: the order from most permeable (worst corrosion protection) to least permeable (best corrosion protection) being untreated > treated > unfilled.

Close examination of photomicrographs reveals the presence of "dark spots" on the metal substrate underneath the coating. We believe that these defects arise because the sandblasting process introduces microscopic pits on the metal surface [21]. After coating, the more elevated areas have less coating material above them, making them susceptible to

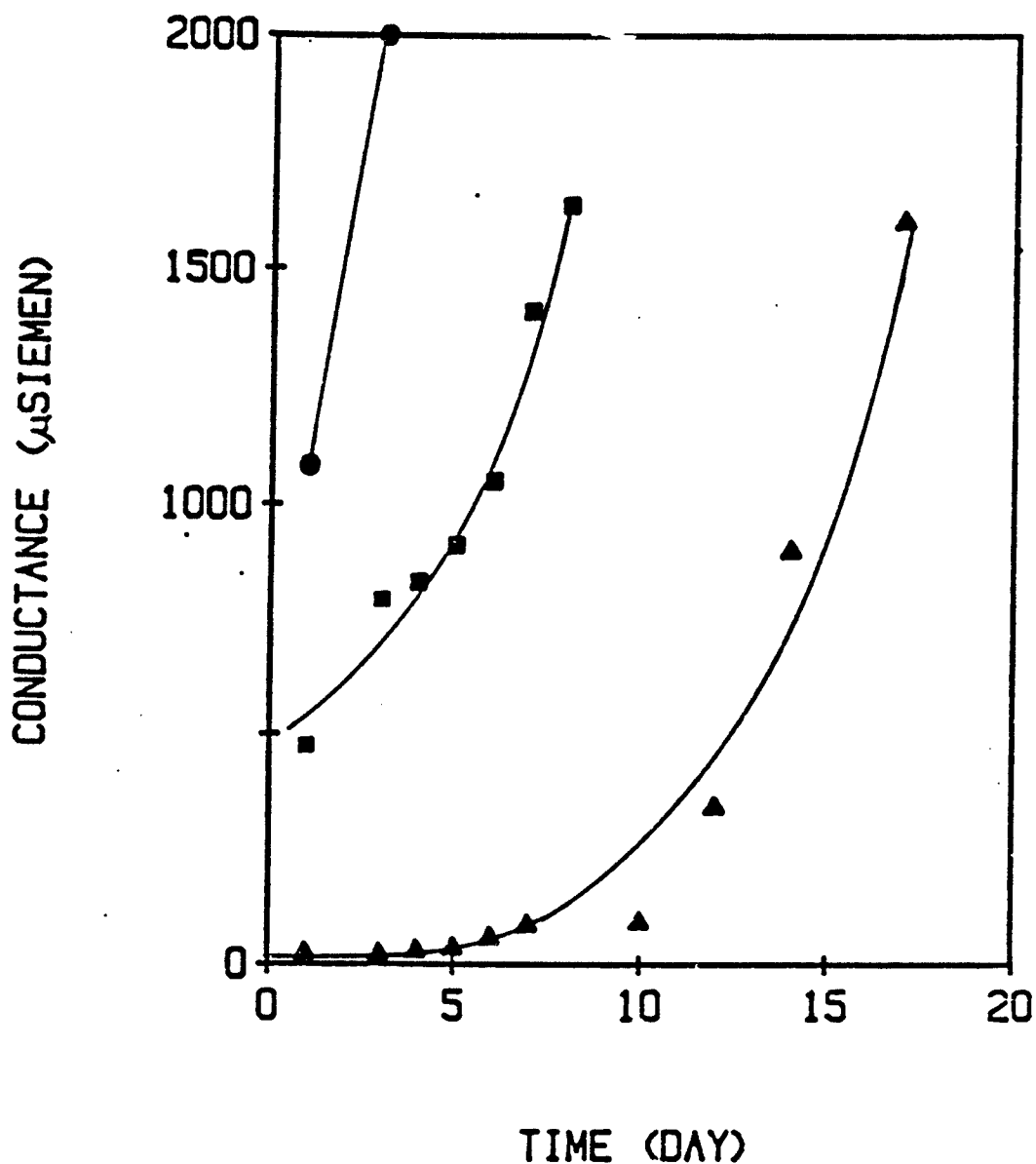


Figure 7. Conductivity behavior of phenoxy coatings as a function of time (The phenoxy coatings were applied onto sandblasted Q-panels and exposed to 3% NaCl solution.): ▲ corresponds to the unfilled coating while ● and ■ refer to glass-filled coatings containing untreated and treated glass at $v_f = 0.4$, respectively.

corrosion. In this respect, the "dark spots" may serve as precursors to corrosion.

Similarly, for the oven-dried specimens, the electrical measurements predict the oven-dried unfilled material to perform the best in the following group of coating materials: oven-dried unfilled, 0.4 volume fraction glass-bead-filler of both types, and air-dried unfilled. The electrical behavior from the lowest conductance and more positive potential (best corrosion protection) to the highest conductivity and more negative potentials (worst corrosion protection) follows the order: oven-dried unfilled > oven-dried filled > air-dried unfilled. In contrast to the air-dried-filled coatings, the conductance and potentials of the untreated and treated glass sufficiently overlap so that no distinct differences between the two glass types are apparent.

Micrographs of the various coatings support the trends in the electrical measurements. After 7 days, the oven-dried unfilled coating exhibits minimal corrosion while the air-dried filled coatings show significant amounts of rusting. For the oven-dried system, the two types of glass appear to offer relatively the same degree of corrosion protection, in comparison to the oven-dried unfilled. As expected, the air-dried unfilled coating behaves much more poorly than the oven-dried unfilled, as evidenced by the presence of numerous "dark spots" and some rust areas. Actually, after only 3 days, the air-dried unfilled performed more poorly than the glass-bead-filled coatings. Thus, the order of corrosion performance parallels the electrical measurements, particularly during the early parts of the experiment.

For the unfilled coatings, the difference in corrosion performance relates to the stronger adhesion of the oven-dried coating onto the metal substrate. The delamination studies above clearly support this finding. Correspondingly, the poor performance of the oven-dried glass-bead-filled coatings, in comparison to the oven-dried unfilled, may also reflect the delamination behavior of these materials and the water vapor permeability behavior of an earlier report [2]. In this case, the presence of the fillers increases the porosity in the polymer binder, making the composite more porous for permeants and more susceptible to corrosion.

CONCLUSIONS

Dynamic Mechanical Spectroscopy Studies

1. For dry specimens

- Inclusion of filler raises the modulus and increases T_g relative to that of the unfilled resin.
- The glass filler reduces damping with higher filler loadings below and above the β -transition while the converse is true at the β -transition region.
- Good filler-matrix adhesion increases damping.

2. Unfilled dry specimens

- Sample preparation changes the dynamic mechanical response.
- A plasticizer (water or residual monomer) increases damping above the β -transition and lowers the T_g of the resin.

3. Water-saturated filled samples

- Water plasticizes the saturated filled specimens relative to that of the dry filled specimens.
- The effect in E' in the glassy state is primarily due to the volume fraction filler rather than absorbed water.
- In terms of damping behavior above the β -transition, the effect of water predominates over the effect of filler. The untreated glass is affected more significantly than the treated glass.

4. Unfilled-solvent-cast films

- Exhibits the classical plasticization anti-plasticization effect. The retained solvent (a plasticizer) lowers T_g , raises E' in the glassy state region, and increases damping.

5. Filled-solvent-cast films

- The extent of dryness significantly affects the modulus and damping behavior in the glass transition region.

Corrosion Studies

1. Cathodic delamination

- "Baking" significantly increases the adhesion of the phenoxy coating onto the metal substrate, the rate of delamination being better than other commercially available polymer binders.

2. Accelerated corrosion test

- The results are consistent with the cathodic delamination studies and earlier investigations on the permeability behavior of glass-bead-filled films.
- Generally, the unfilled resin offers better corrosion protection than the filled phenoxy while "baking" dramatically improves the corrosion performance of the unfilled specimens relative to that of an unbaked, unfilled resin.

ACKNOWLEDGEMENTS

We wish to thank Mr. John Catino and Dr. Malcolm White for their assistance on the delamination and accelerated corrosion experiments, respectively. Also, we are grateful to Dr. Henry Leidheiser for his suggestions on the interpretation of the results for the accelerated corrosion studies.

REFERENCES

1. Annual Report, this project, 1984.
2. Annual Report, this project, 1983.
3. Annual Report, this project, 1983, Program #4.
4. Annual Report, this project, 1981, Program #1.
5. John A. Manson and Leslie H. Sperling, "Polymer Blends and Composites," Plenum Press: New York, 1976, Chapter 12.
6. Ibid., Chapter 2.
7. O. Olabisi, L. M. Robeson, and M. T. Shaw, "Polymer-Polymer Miscibility," Academic Press: New York, 1979.
8. P. R. Couchman, *Macromolecules* 11, 1156 (1978).
9. F. N. Kelly and F. Bueche, *J. Polym. Sci.* 50, 549 (1961).
10. Private communications with Mr. George Salensky, Union Carbide Corp., Boundbrook, NJ.
11. John Catino, Master's Thesis, Dept. of Metallurgy and Materials Science, Lehigh University, Bethlehem, PA, 1985.
12. Wendy Wang, Ph.D. Dissertation, Dept. of Chem. Eng., Lehigh University, Bethlehem, PA, 1983.
13. T. B. Lewis and L. E. Nielsen, *J. Appl. Polym. Sci.* 14, 95 (1970).
14. J. A. Manson and E. H. Chiu, *J. Polym. Sci. Symp.* 41, 95 (1973).
15. D. H. Droste and A. T. DiBenedetto, *J. Appl. Polym. Sci.* 13, 2419 (1969).
16. T. Hirai and D. E. Kline, *J. Compos. Mat.* 7, 160 (1973).
17. R. E. Jenness, Ph.D. Thesis, The Pennsylvania State University, December 1972.
18. Annual Report, this project, 1982.
19. J. A. Manson and E. H. Chiu, *Polymer Preprints* 14, 469 (1973).
20. Annual Report, this project, 1981.
21. Private communication with Dr. H. Leidheiser, Jr., Lehigh University, Bethlehem, PA.

SECTION - #4

Surface Acidity of Ferric Oxides Studied by Flow Microcalorimetry

Principal Investigator: Frederick M. Fowkes, Prof. of Chemistry
Associate: Sara T. Joslin (Ph.D. awarded)

ABSTRACT

The molar heats of adsorption of nitrogen and oxygen bases from neutral hydrocarbons onto the surface sites of α -ferric oxides have been determined by using a UV concentration detector in series with a flow microcalorimeter. Since the strongest sites are neutralized first, the distribution of molar heats of adsorption is determined from their time dependence. Molar heats of adsorption for nitrogen and oxygen bases depended very strongly on the amount of adsorbed moisture, so the development of methods for controlling moisture levels in the liquids and on the solids of these studies became an important issue. The acidic surface FeOH sites were found to be hard acids with a range of acid strengths. The stronger acid sites had a concentration of about $1 \mu\text{mol}/\text{m}^2$, and their Drago E and C constants were found (by the heats of adsorption of pyridine, triethylamine, and ethyl acetate) to be $C_A = 0.8 \pm 0.2$ and $E_A = 4.5 \pm 1.1 \text{ (kcal/mol)}^{1/2}$. The adsorption of poly(vinylpyridine) was found to occur rapidly as a 0.1% solution in benzene flowed through the bed. The polymer occupied 68% of the acidic surface sites of the ferric oxide as determined by subsequent adsorption of pyridine, and 52% of the pyridine groups of the adsorbed polymer molecules were bound to the surface.

INTRODUCTION

Intermolecular interactions such as adsorption have been described as polar and nonpolar, following the principle that polar groups bond to polar surfaces and that nonpolar groups develop "hydrophobic bonds" to nonpolar surfaces; thus we have the old rule that "like bonds to like." Current studies of polar interactions, however, have found that all polar interactions are actually Lewis acid-base interactions, that all substances except saturated hydrocarbons are Lewis acids or bases, and that the rule of polar bonding should actually be "acids bond to bases" (Fowkes et al., 1984; Fowkes, 1984).

Quantitative calorimetric and spectrometric studies of the interactions of simple organic liquids by Drago and co-workers (1971, 1977) showed that the heats of mixing of organic liquids (ΔH_M) are entirely predictable as Lewis acid-base interactions between electron donors (such as nitrogen, oxygen, sulfur, or π -electron bases) and electron acceptors (such as the "active" hydrogens of alcohols, phenols,

carboxyls, or partially halogenated hydrocarbons; or the non-Brønsted acids such as iodine and the chlorides or alkyls of boron, aluminum, antimony, etc.). A quantitative correlation of heats of mixing

$$-\Delta H_M = C_A C_B + E_A E_B \quad (1)$$

was shown to predict heats of mixing generally to within 0.1-0.2 kcal/mol, except for situations where steric factors prevent optimum donor-acceptor bond angles and bond distances.

The adsorption and adhesion of polymers to inorganic substrates has also been shown to be entirely governed by acid-base interactions between acidic or basic sites of the polymer and of the inorganic substrate. Basic polymers include polystyrene, polyester, polyamides, polyethers, polyamines, and polycarbonates, while acidic polymers include halogenated polyolefins, polymers of vinyl halides, and polymers with "active" hydrogens such as polyvinylbutyral. The E and C constants for polymers such as poly(methyl methacrylate) (PMMA) are easily measured by infrared spectral shifts (Fowkes et al., 1984), and the E and C constants for inorganic substrates such as silica and titania have been measured with high surface area powders by calorimetry or by infrared spectral shifts (Fowkes et al., 1985). We can therefore predict with precision the heats of adsorption of polymers per adsorption site on silica and titania, but we must have further information on the number of sites adsorbed to determine the heats of polymer adsorption per mole of polymer.

The heats of polymer adsorption per site are important parameters for understanding the conformation of adsorbed polymers. The heats of acid-base interactions of polymers with inorganic substrates are often large multiples of kT per site; for PMMA on silica or titania the heats of adsorption per site are about $-7 kT$. As Silberberg (1984) has just made clear, such heats of adsorption cause a large fraction of the adsorbed polymer chains to be in the adsorbed "trains" and a smaller fraction to be in "loops" and "tails". Such conformations are believed to lead to strong adhesive bonding.

This paper is concerned with the principles governing the adhesion of polymers to the surface of steel, where acid-base interactions determine the energy of adsorption. Iron oxides can bond to acids or to bases, but this study is limited to the interactions of basic polymer groups with the acidic FeOH sites. The acid strength of these sites has been determined by measuring the heats of adsorption of test bases (pyridine, triethylamine, ethyl acetate), and Drago E and C constants were determined for these sites. Most of the studies have been done with a commercial α -iron oxide, but some were also done with a γ -iron oxide. Much of the effort in these studies concerned controlling the water content of the oxides, the solvents, and the test bases. Water is both an acid and a base; it adsorbs as a base onto the acidic FeOH sites and can very appreciably reduce the acidity. Our concern was not to make the oxides as dry as possible and thereby maximize their acidity but to work with controlled water activities in the dryer part of the range normally encountered in polymer coating technology.

The technique used in these studies was a novel combination of flow microcalorimetry with a flow concentration detector suggested to us by

George Salensky of Union Carbide. As a solution of the test base is pumped through the iron oxide powder bed, the heat of adsorption is measured by thermistors, and when the solution is pumped on through the flow UV detector, the depletion of base due to adsorption is measured; the combination of these two measurements allows determination of the heat of adsorption of the test base in kcal/mol. Furthermore, because dilute solutions of base are pumped through the bed and the rates of adsorption are fast, the stronger acidic sites are neutralized first and the weaker last, so that the time distribution of heats of adsorption is a good site distribution of heats of adsorption. An unexpected bonus of this approach was that after adsorbing polymers onto the oxide we could measure the surface concentration of bare sites directly (with a solution of test base in the same solvent) and thus determine what fraction of the basic sites of the polymers was bound to the acidic sites of the ferric oxide.

EXPERIMENTAL

Oxides and Reagents. Most of the experiments were done with a single sample of an α -ferric oxide reported to be free of any flocculants or surface modifiers (R-1299, lot E9036, from Charles Pfizer, Inc., Easton, PA) having $9.9 \text{ m}^2/\text{g}$ of surface area by BET analysis of argon adsorption data (courtesy of Vital and Micale) and a sulfur concentration of about 0.5% in the surface region as determined by ESCA (courtesy of Prof. David W. Dwight of VPI).

The principal solvent for these studies was HPLC grade cyclohexane from Fisher Scientific, but some additional work was done with decalin (mixed decahydronaphthalenes) from Aldrich Chemical, 99% mole purity n-hexane from Fisher Scientific and Reagent grade benzene from J. T. Baker. These were distilled before use to minimize thiophene. Solvents were dried with 8-12 mesh Davison 3-Å molecular sieves (activated for at least 1 h under vacuum at 250°C), stored under Drierite-dried nitrogen, and dispensed through a sealed buret into HPLC delivery syringes or into adsorption study vials with syringe needles through septa shields for the vials, so as to eliminate any contact of the dried solvent or solutions with air. All glassware was oven dried for at least 16 h at 50°C immediately prior to use, and the water content of the solvents was monitored with an Aquatest IV automatic Karl Fischer titrimeter (Photovolt Corp., NY). Solvents were stored over freshly activated molecular sieves, but not for longer than 2 weeks, for in that time enough water entered from the glass to raise the dissolved water content despite the presence of the molecular sieves. Solutions were made fresh daily.

The organic bases used for titration of surface acidity included pyridine (99+% mole purity, Aldrich Chemical), triethylamine (99 mol % from Aldrich Chemical), ethyl acetate (Certified ACS grade from Fisher Scientific), and poly(2-vinylpyridine) with M_w 92000 and M_n 89000 (Scientific Polymer Products, Ontario, NY).

Flow Calorimeter. The flow calorimeter (Microscal Ltd., London, U.K.) has a central stainless steel block with a long 6-mm-diameter

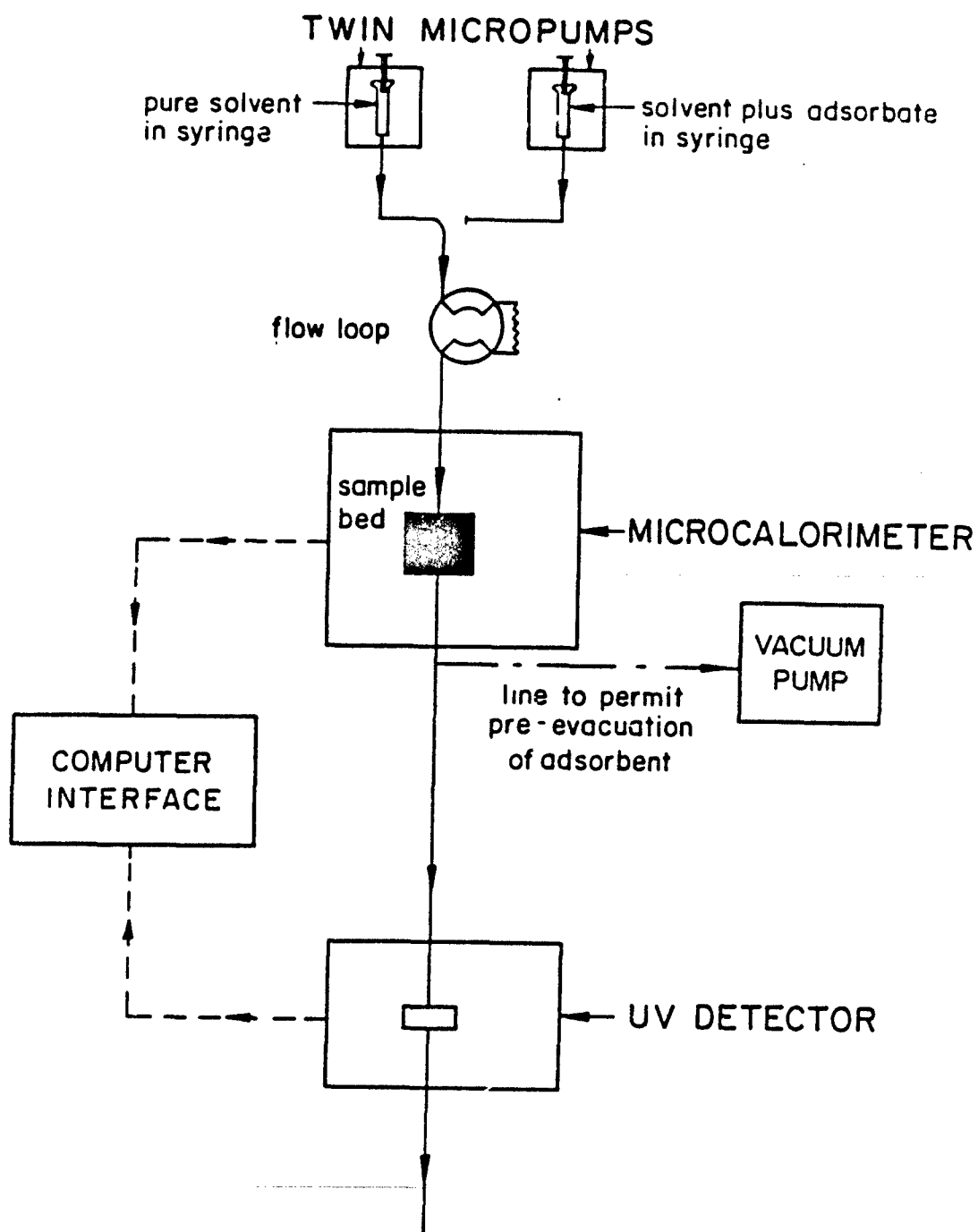
cylindrical cavity in which a 6-mm-deep adsorption bed is enclosed between inlet and outlet tubes. The two thermistors that project into the bed and the two thermistors in the block are in a Wheatstone bridge circuit that is very sensitive to the bed temperature. The efficiency of the calorimeter depends on the degree of filling of the bed; maximum efficiency was found with 150 mg of iron oxide, thus leaving about 120 μ L of pore space in the bed. The unit is operated just like an HPLC unit (see Figure 1) with syringe pumps for pumping solvent or solution (usually at 100 μ L/min) and two Valco HPLC valves (with loops) for switching from solvent to solution and back again. The liquid that flowed through the bed was conveyed directly into a Perkin-Elmer LC-75 UV flow detector by HPLC Teflon tubing so that the UV absorbance (and concentration) of solutes could be determined, thereby allowing quantitative measurement of solute adsorption.

The calorimeter was equipped for evacuation of the bed with a vacuum pump and liquid nitrogen trap attached through the bed outlet. We attached a Hastings gauge just upstream of the inlet on a "T" into the Teflon tubing connecting the Valco valves to the bed, and the pressures measured there during bed evacuation were a bit higher but considered indicative of those attained in the bed. During pump-down of a freshly loaded bed of 150 mg of α -ferric oxide the decrease in pressure at the Hastings gauge is monitored. However, during pump-down we also observe a marked endotherm sensed by the thermistors, resulting from evaporative cooling of the bed as traces of adsorbed water evaporate (Figure 2). Reproducibly low moisture levels in the bed can be obtained by pump-down through the evaporative cooling process, and even lower moisture levels can be obtained by pump-down to low Hastings gauge readings.

Calibration of the heat-sensing system is done with a calibration coil of fine wire placed in the adsorption bed and attached to an outlet tube (supplied by the manufacturer). The calibration is done by passing known amounts of electrical energy through the coil in the packed bed while the solvent is being pumped through the bed at the desired rate.

Typical adsorption exotherms and UV absorption plots are shown in Figures 3 and 4; these and all others in this paper were determined at 40°C. The UV absorption plot compares the absorption of pyridine solution passing through the bed of ferric oxide with the absorption of the same solution passed through an empty bed. The amount of pyridine adsorbed (in moles) is proportional to the area between the two curves in that time period.

Because of the need to relate the time dependence of the exotherms and endotherms observed by the heat sensors to the time dependence observed by the concentration sensor, a laboratory microcomputer became an essential part of the unit. We chose an MTU-130 from Microtechnology Unlimited (Raleigh, NC), and Douglas Eadline of this laboratory wrote the data recording and display software in CODOS, the machine language of this computer. The data were recorded at two points per second for adsorption exotherms or desorption endotherms of 400-1000-s duration and also for the UV calibration and absorption measurements; the data were displayed on the screen as stripchart data by software entitled STRIPCHART. After the experiments were completed, the data were analyzed with a light-pen operated program (DATAPENCIL-2, written in BASIC); this included base-line selection, integration, and "time slicing" of both the thermal and UV data



FLOW DIAGRAM

Figure 1. Block diagram for the microcalorimetric experimental arrangement.

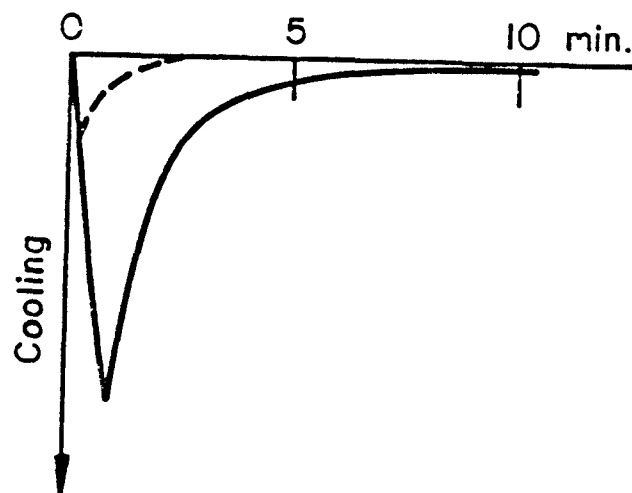


Figure 2. Evaporative cooling in the micro-calorimeter bed during vacuum pump-down, used as a measure of the removal of adsorbed water. Dashed line is for an empty bed and solid line is for a bed of 150 mg of α -ferric oxide.

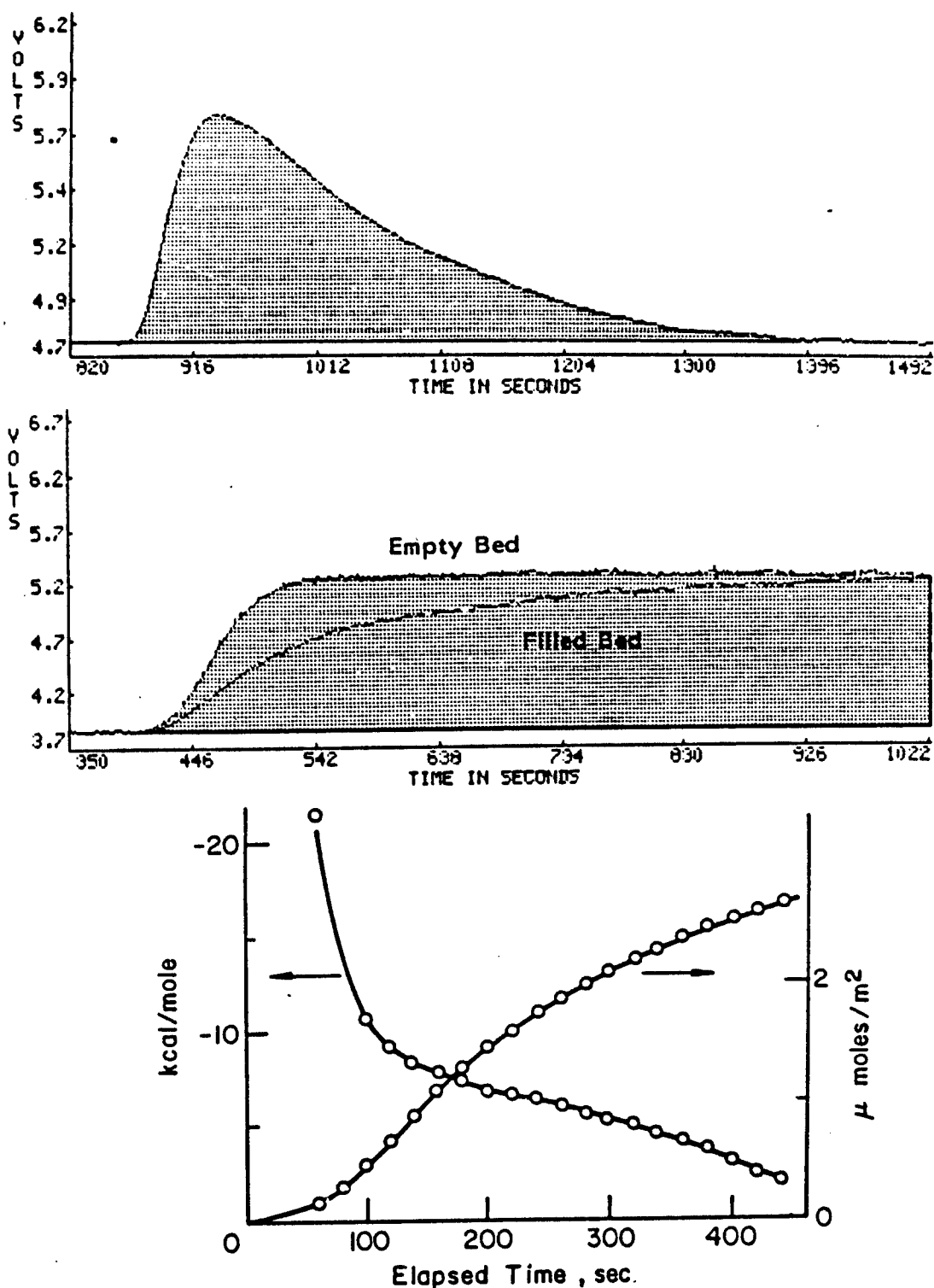


Figure 3. Typical flow calorimetric adsorption exotherm (top) and UV absorption plot (center) for a 25 mM solution of pyridine in cyclohexane flowing through a bed of 150 mg of α -ferric oxide. Bottom, differential heats of adsorption and rates of adsorption calculated from the above data.

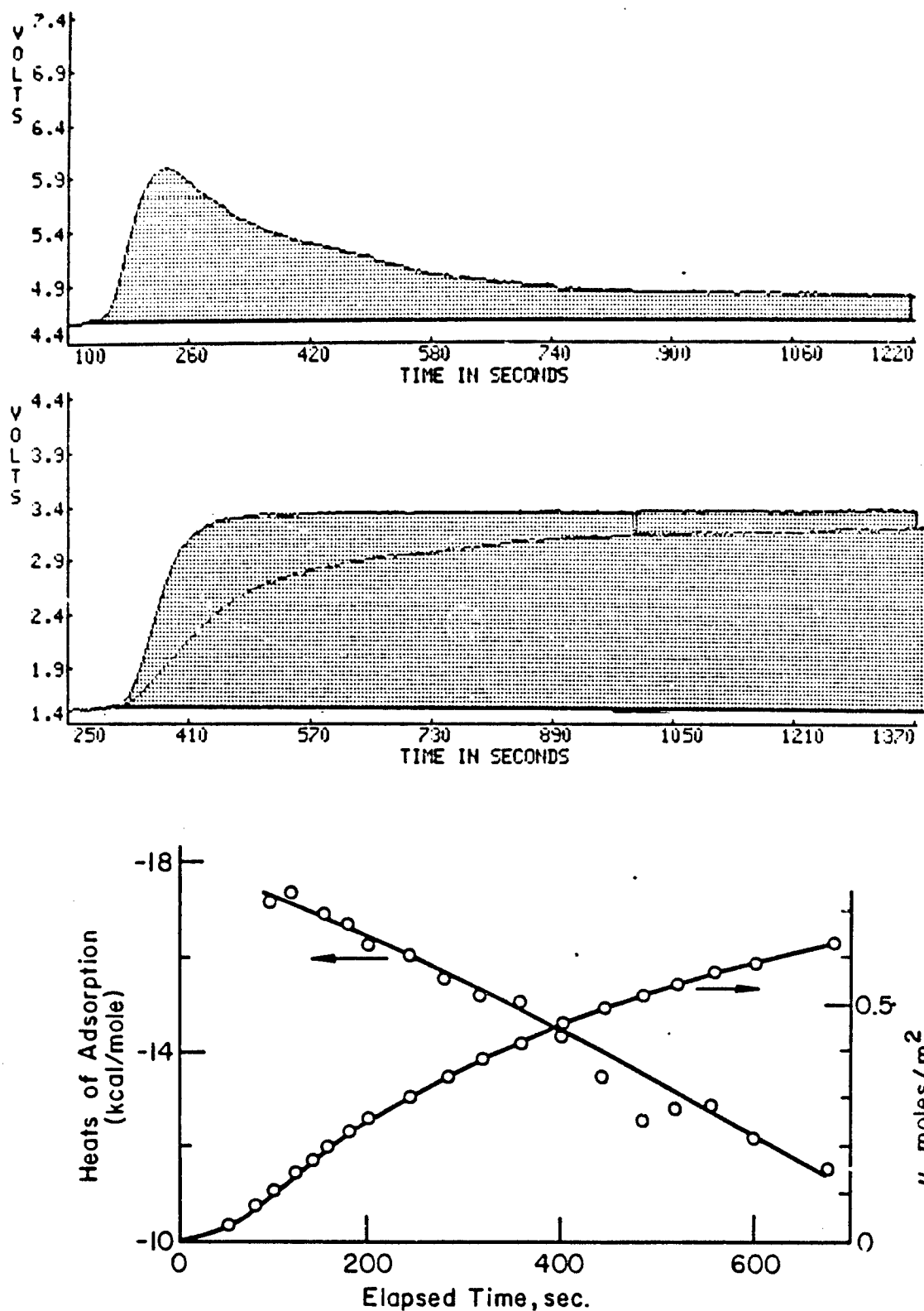


Figure 4. Flow calorimetric adsorption exotherm (top) and the UV absorbivity of a 3.2 mM pyridine solution flowing from the adsorption bed (middle). Bottom, differential heats of adsorption and rates of adsorption calculated from above data.

so that the time dependence of molar heats of adsorption could be determined.

Absorption Isotherms. The equilibrium adsorption of pyridine onto α -ferric oxide was studied in several hydrocarbon solvents and at several temperatures by using tightly sealed vials containing 10 mL of solution and 0.8 to 3.0 g of powder that were shaken in a water bath for 3 days to reach equilibrium. Supernatant solutions were diluted into a range where Beer's law held for the UV absorption at 252 nm as measured on a Hitachi UV spectrophotometer.

EXPERIMENTAL RESULTS AND DISCUSSION

Importance of Moisture Control in Adsorption on Ferric Oxides. Exploration of the importance of moisture content and development of procedures to control moisture content of the flow system, oxide, and solutions was done largely with pyridine and with 1-butanol solutions in cyclohexane. Butanol, like water, is both a base and an acid, and it can adsorb on the acidic or basic sites of ferric oxide. Pyridine is much more basic, has little self-association, and adsorbs strongly onto acidic sites. The Drago E and C constants for the acidity of water (Drago, Vogel, and Needham, 1971) show that its heat of mixing with pyridine is -5.0 kcal/mol. Thus, if all of the ferric oxide surface were water covered, the observed heat of adsorption of pyridine should be close to the above value.

We chose the following procedure to ensure reproducibly dry liquids and powder beds. It was found unnecessary to first dry the powder in a vacuum oven, for too much moisture was picked up during transfer through the air into the bed. The as-received powder was dry-loaded into the bed and evacuated at 40°C with a vacuum pump and liquid nitrogen trap for 5-10 min (when the Hastings gauge reached about 5 torr), and then the solvent, dried to the required degree of water saturation (usually 10% or less), was pumped through the bed for 2 h at a flow rate of 6 mL/h. This procedure ensured that the oxide bed and the solvent had a controlled degree of water saturation.

Heats of Adsorption of Pyridine on Ferric Oxide. Figure 3 shows a typical adsorption exotherm and ultraviolet absorption plot for a 25 mM solution of pyridine in cyclohexane containing 20 ppm of dissolved water as it flows through the 150-mg bed of ferric oxide in the flow microcalorimeter. At these higher pyridine concentrations the adsorption is complete in about 8 min, as evidenced by the return of the exotherm nearly to the base line and the close approach of the pyridine concentration to the empty bed value. The bottom plot of Figure 3 shows the rate of adsorption and the incremental values of the heat of adsorption as a function of elapsed time, determined by time-slicing the integrated areas of the upper plots. About 8 bed volumes of solution flow through the bed during the exotherm, and after the first bed volume most of the pyridine flowing through is unadsorbed; therefore, it is proposed

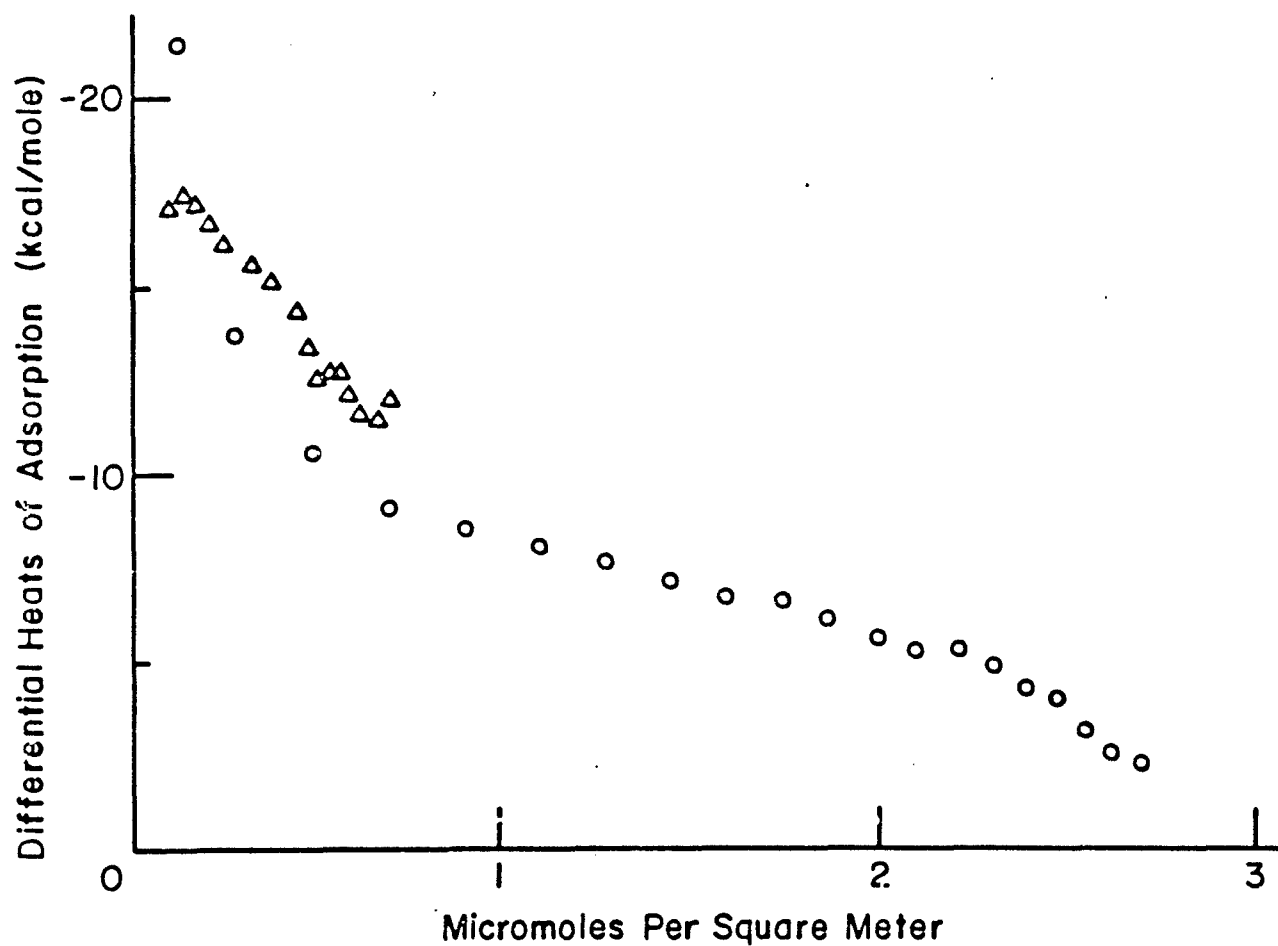


Figure 5. Comparison of differential heats of adsorption of pyridine adsorbing from a 3.2-mM solution in cyclohexane with 8 ppm water (Δ) and from a 25-mM solution with 18-20 ppm of water (O).

that the distribution of heats of adsorption vs. time is a good representation of the distribution of equilibrium heats of adsorption.

An adsorption exotherm and UV absorption plot for a more dilute pyridine solution, 3.2 mM in cyclohexane with 8 ppm of dissolved water, are shown in Figure 4. Even though this run extended twice as long as the run of Figure 3, only about $0.7 \mu\text{mol}/\text{m}^2$ was adsorbed as compared to 2.8 in Figure 3. This comparison illustrates the marked concentration dependence of the rates of adsorption. It should also be noticed that the exotherm of Figure 4 did not return as close to the base line as did the one in Figure 3, nor did the concentration of pyridine flowing from the bed return as close to the empty bed value as did the concentration in Figure 3. At first glance it appears that the exotherm has established a higher base line, but the heats of adsorption calculated with a flat base line are seen to decrease in the same manner as those of Figure 3.

In Figure 5 the heats of adsorption as a function of coverage are shown for the two runs of Figures 3 and 4. The 3.2 mM solution averages about -14 kcal/mol over the range $0-0.7 \mu\text{mol}/\text{m}^2$ whereas the 25 mM solution averages about -12 kcal/mol over the same range; this is attributed to their water contents (8 ppm vs. 20 ppm, respectively). The average heat of adsorption of pyridine from the 25 mM solution over the whole range ($0-2.8 \mu\text{mol}/\text{m}^2$) is found to be -7.5 kcal/mol .

Similar runs have been made with a wide range of pyridine concentrations, shown in Table I. The water content of these solutions was 10-20 ppm. The decline of heats of adsorption with coverage results simply from the larger number of sites sensed by the higher pyridine concentrations, as illustrated in Figure 5 and discussed in the preceding paragraph.

Adsorption of pyridine onto the same oxide and from the same solvent was determined at two temperatures (see the Langmuir plots of Figure 6), and by using the temperature coefficient of the equilibrium constant K determined from those isotherms, we can determine the heat of adsorption with the van't Hoff equation, as was done previously (Fowkes et al., 1981). In these studies the pyridine concentration varied from 2 to 30 mM, and the amount of oxide equilibrated with each solution was chosen so that 30% to 70% of the pyridine was adsorbed. Consequently, the vials contained such a high ratio of oxide surface to water content of the solvent (19-35 ppm) that even if all the water adsorbed onto the oxide it could provide less than 10% of a monolayer and could not affect the results significantly. The results obtained at 28 and 48°C (shown in Figure 5) predict a heat of adsorption of -7.2 kcal/mol . This heat should be compared to the integral heat at the same coverage, which would be about the midpoint of the concentration range in Table I, or -7.0 kcal/mol . This perfect agreement between calorimetric heats of adsorption by flow microcalorimetry and the heats of adsorption determined from the temperature coefficient of adsorption isotherms is helpful in demonstrating the significance of these flow microcalorimetric results.

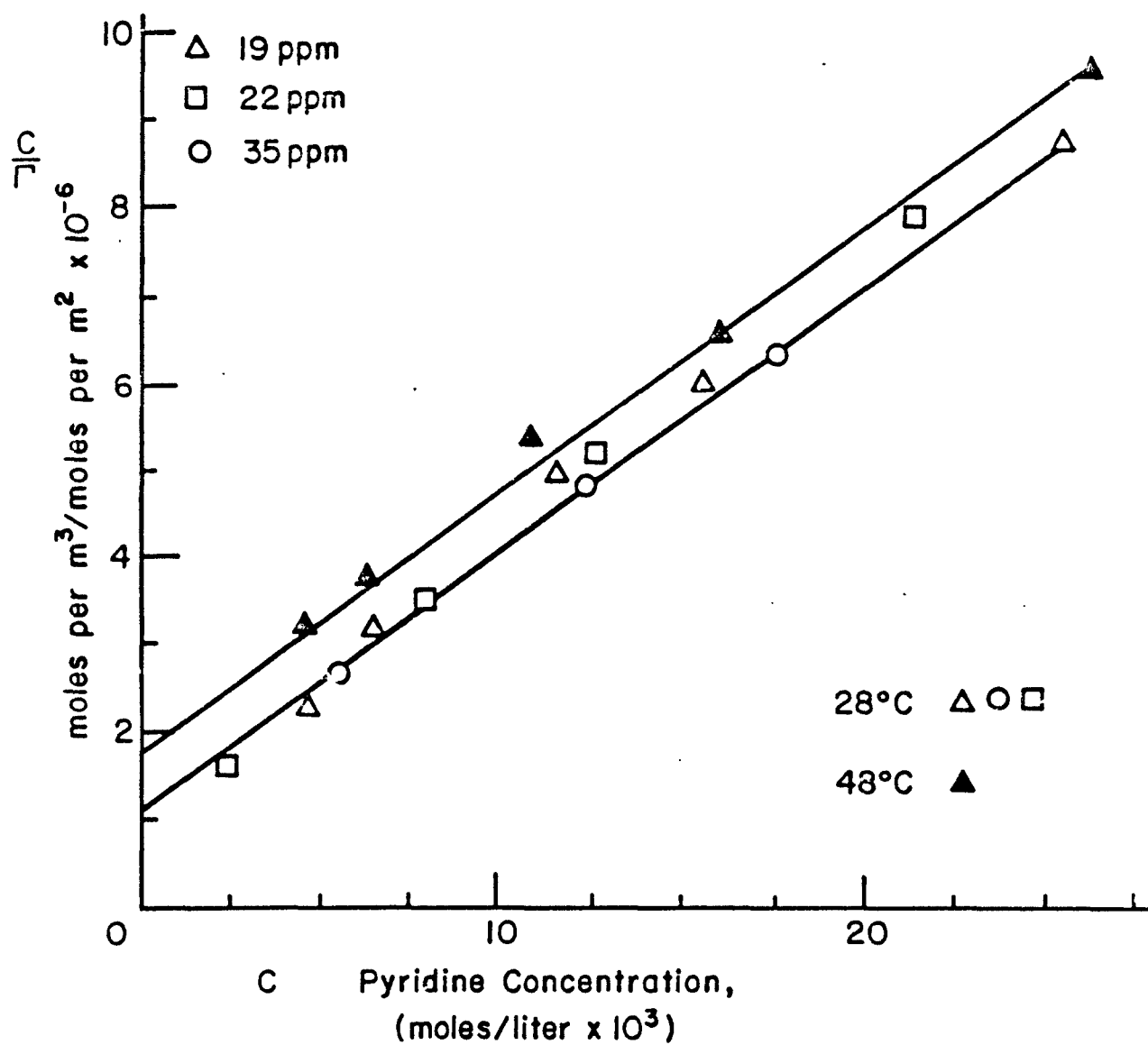


Figure 6. Langmuir adsorption isotherm plots for pyridine adsorption from cyclohexene onto α -ferric oxide. The temperature dependence of the vertical displacement of these lines is used to calculate heats of adsorption.

Table I

Total Amounts Adsorbed and Total Integral Heats of Adsorption
of Pyridine onto R-1299 α -Ferric Oxide vs. Concentration
of Pyridine in Cyclohexane
(20-30 min, 40°C, 10-20 ppm Water)

Pyridine Concn., mM	Amount Adsorbed mol/m ²	Area/ Molecule nm ²	Heats of Adsorption kcal/mol
3.6	1.42	1.17	-12.1
10.4	1.61	1.03	-12.0
10.4	1.73	0.96	-11.9
16.9	3.19	0.52	-7.0
23.5	3.02	0.55	-6.5
23.5	3.19	0.52	-6.8
29.5	3.69	0.45	-6.45
30.3	3.77	0.44	-5.95
35.0	4.15	0.40	-5.75

Determination of the Drago E and C Constants of Ferric Oxide. In previous studies with silica and rutile (Fowkes et al., 1985; Fowkes, 1984) it was shown that basic adsorbates interact with the acidic surface sites much as they do with the acid sites of small molecules and that heats of adsorption of bases onto acidic surfaces obey the Drago correlation of Equation 1. When the heats of adsorption of these solids with bases of different C/E ratios were measured, the E and C parameters of the acidic surface sites were determined: for silica, $C_A = 1.16 \pm 0.02$ and $E_A = 43 \pm 0.1$; for rutile, $C_A = 1.02 \pm 0.03$ and $E_A = 5.7 \pm 0.2$ (kcal/mol)¹. These earlier heats of adsorption were determined by two different techniques, calorimetric and spectrometric. A Tronac calorimeter was used with a stirred suspension of powder that was titrated with solutions of bases in neutral hydrocarbons to provide very accurate heat measurements; after the heat of adsorption was generated, the concentration of residual base was determined by UV absorption. Heats of adsorption were also determined by the shift of carbonyl infrared absorption peaks upon adsorption of esters and ketones. Both methods gave identical E and C constants for silica.

In these flow microcalorimetric studies we used three bases of appreciably different C/E ratios so that C and E constants could be accurately determined. Pyridine, triethylamine, and ethyl acetate were chosen as the test bases for microcalorimetric heats of adsorption studies on the R-1299 ferric oxide equilibrated with cyclohexane having 10-20 ppm of water. All three bases absorb in the UV region well enough to be monitored with the UV detector in the same manner as pyridine. Figure 7 compares the integral heats of adsorption of the three bases as a function of the surface concentration of sites neutralized. The integral heats were used because of their greater accuracy and because integral heats

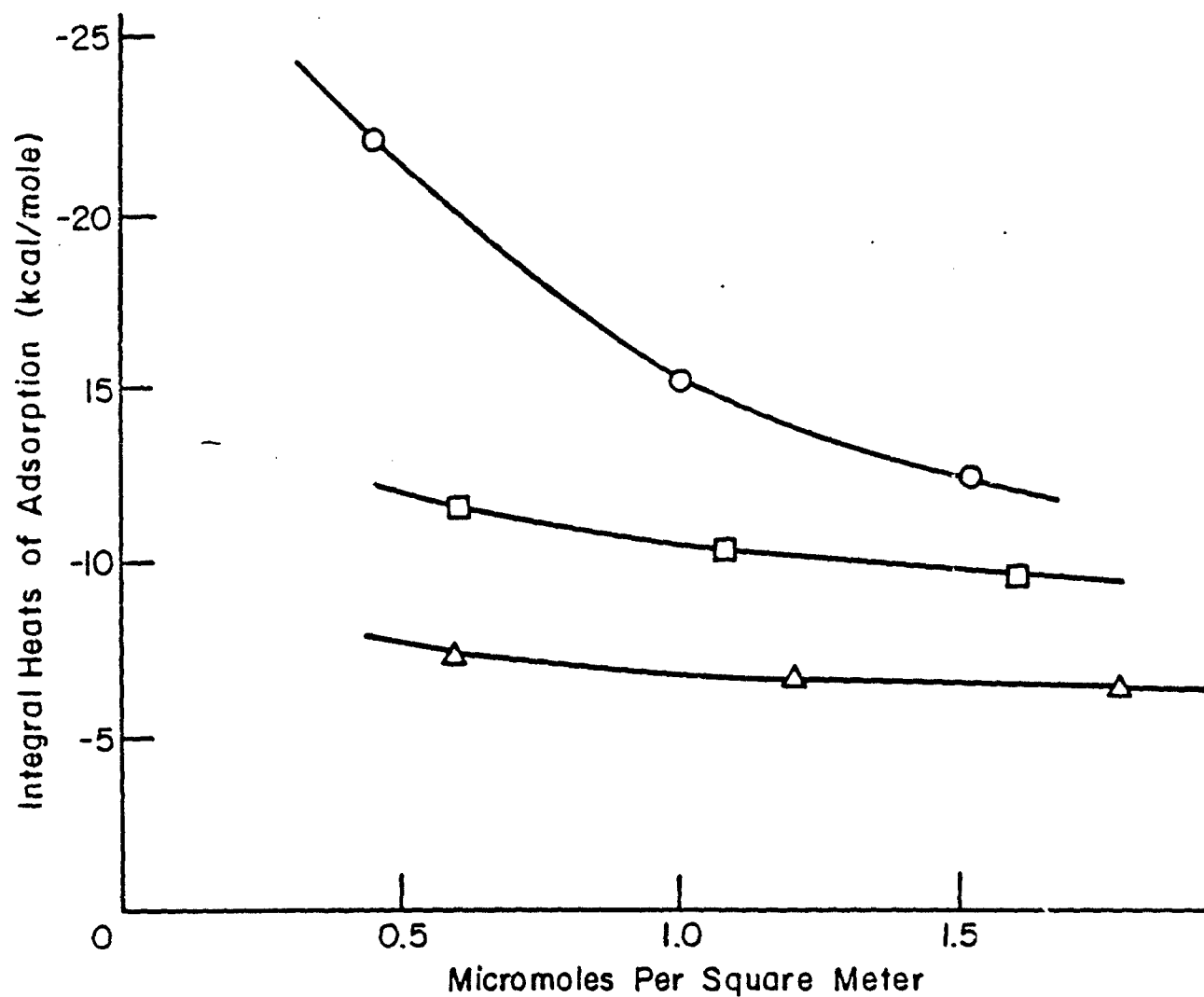


Figure 7. Distribution of the integral heats of adsorption of three bases on α -ferric oxide determined by "time slicing" adsorption exotherms and the corresponding UV adsorption traces: triethylamine (O), pyridine (□), and ethyl acetate (Δ). All concentrations 25 mM and water contents 13-20 ppm.

were used in the earlier studies with silica and titania.

The E and C constants for the acidic surface sites of the R-1299 α -ferric oxide can be determined from the heats of adsorption of the three bases. We have chosen to use the integral heats of adsorption of 1.1 $\mu\text{mol}/\text{m}^2$ (-14.2, -10.0, and -6.5 kcal/mol for triethylamine, pyridine, and ethyl acetate, respectively) and to determine the E and C parameters for these stronger acidic sites of ferric oxide by a graphical technique (Figure 8). The "E and C plot" is based on a rearrangement of Equation 1:

$$E_A = -\Delta H_{\text{ads}}/E_B - C_A(C_B/E_B) \quad (2)$$

As can be seen in Figure 3, the heat of adsorption of each base gives a straight line of slope C_B/E_B , and the intersection of the lines gives the E and C constants for the acidic surface sites. The line for triethylamine is the steepest ($C/E = 11.1$), the line for ethyl acetate is the flattest ($C/E = 1.78$), and the pyridine line falls in between ($C/E = 5.47$). The average intersection of these three lines gives the Drago E and C parameters for the stronger FeOH sites of α -ferric oxide: $C_A = 0.8 \pm 0.2$ and $E_A = 4.5 \pm 1.1$.

As can be seen in Figure 7, these oxides have a wide distribution of heats of adsorption, so either lower or higher E and C constants could be obtained, depending at what surface coverage we choose to compare. Clearly the FeOH sites are somewhat less acidic than either the SiOH or TiOH sites, but their C/E ratio of 0.18, which is a measure of "hard" or "soft" acid character, is rather more like the TiOH sites (0.18) than the SiOH sites (0.27).

Table III compares the heats of adsorption predicted from E and C constants for the adsorption of various bases (from Drago's tables) onto the SiOH sites of silica, the TiOH sites of rutile, and the FeOH sites of ferric oxide. These three kinds of surface sites are seen to be rather similar, and we also see a similarity of magnitudes of heats of adsorption of the various nitrogen bases, or of the oxygen bases, or of the π -electron bases. These predictions apply to the stronger acid sites of ferric oxide, where we see about -11 kcal/mol for the heats of adsorption of nitrogen bases, about -7 kcal/mol for oxygen bases, and about -4 kcal/mol for π -electron bases.

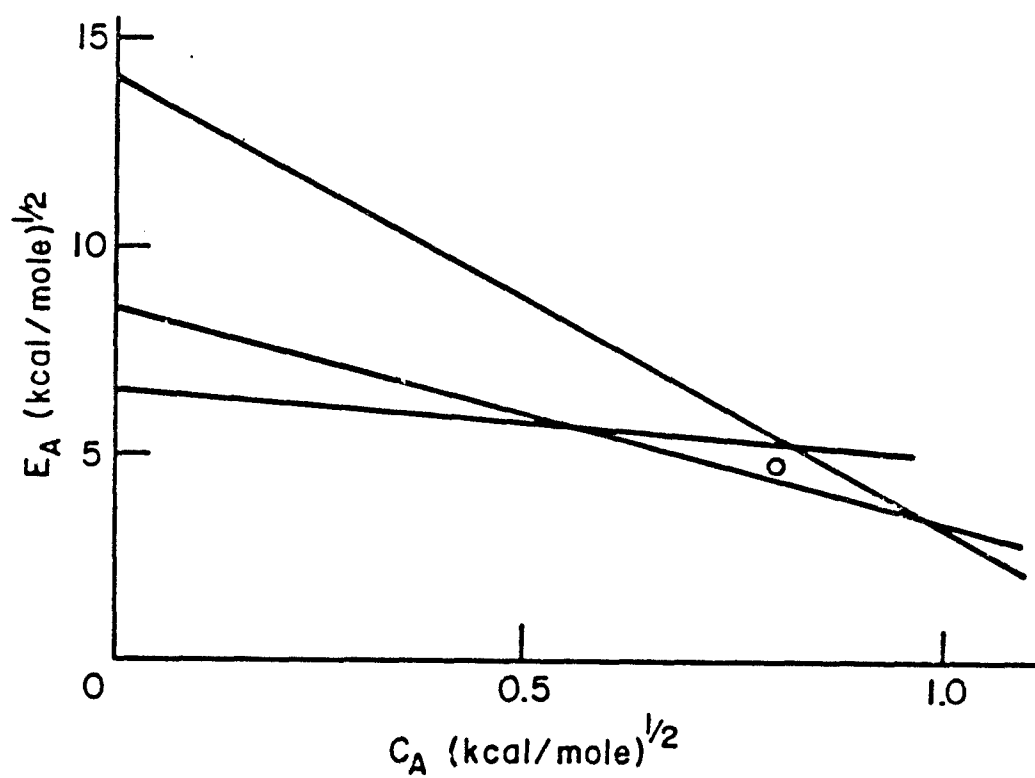


Figure 8. Graphical determination of the E and C parameters for the acidic FeOH sites of α -ferric oxide using the heats of adsorption of the plateaus of Figure 6 and the principle of Eqn. (2). The average intersection (O) predicts $C = 0.73$ and $E = 4.6$ for these FeOH sites.

Effect of Solvent on Heats of Adsorption. The adsorption of pyridine onto the R-2299 α -ferric oxide was measured in four solvents: n-hexane, cyclohexane, decalin, and benzene. The Langmuir-type adsorption isotherms obtained with saturated solvents, shown in Figure 9, all have the same slope. That means the site area for adsorbed pyridine is not affected by the differences in solubility parameter or the differences in work of adhesion of these saturated solvents. The heats of adsorption of pyridine from these three solvents were found to be nearly identical by flow microcalorimetry (Table II).

The case of benzene is quite different, however, for its π -electrons provide sufficient basicity for it to compete against pyridine for the FeOH sites, and this results in weaker pyridine adsorption and lower surface concentrations of adsorbed pyridine. The site area per pyridine molecule was 0.97 nm^2 in benzene as compared to 0.40 nm^2 in saturated hydrocarbons and the integral heat of adsorption by flow microcalorimetry at this coverage was -6.4 kcal/mol in benzene vs. -9.5 kcal/mol in cyclohexane. If we use the E and C constants for benzene (Drago et al., 1971) together with those determined for ferric oxide in this work, the heat of benzene adsorption is predicted to be -2.6 kcal/mol , in good agreement with the observed difference of -3.1 kcal/mol for the adsorption of pyridine from saturated hydrocarbon solvents vs. the adsorption from benzene.

The reduction of the heat of adsorption of pyridine onto ferric oxide from benzene as compared to adsorption from saturated solvents (3 kcal/mol) is thus found to equal the heat of adsorption of benzene from saturated solvents. Extension of this principle would allow us to predict that the heat of adsorption of pyridine onto ferric oxide from an oxygen base such as ethyl acetate would be about $6-8 \text{ kcal/mol}$ less than the heat of adsorption from cyclohexane and, as we can see from Table III, this order of magnitude would apply to most oxygen bases. This principle may be a guide to understanding the effect of the water content of solvents or powders on the heats of adsorption of nitrogen bases on ferric oxide. Water may be acting just as any other oxygen base, and depending on its degree of saturation, would simply compete like any oxygen-base solvent and tend to decrease the heats of adsorption of nitrogen bases by up to $6-8 \text{ kcal/mol}$. The observed effects of water on the heats of adsorption of pyridine onto ferric oxide are in agreement with this principle.

Adsorption of Poly(vinylpyridine) from Benzene onto Ferric Oxide. Flow microcalorimetry studies were made of the adsorption of a 90000 mol wt poly(vinylpyridine) from benzene onto the R-1299 α -ferric oxide. All of the previously described precautions for drying the solvent, the adsorbate, and the adsorbent were rigorously followed. The bed contained the usual 150 mg of oxide, and the concentration of polymer in the incoming stream of the flow calorimeter was 0.1% . The concentration of polymer in the outflowing stream was determined by UV absorption at 285 nm , where Beer's law was found to hold.

The UV sensor indicated that the adsorption was rapid and that saturation of the bed ($9.36 \text{ } \mu\text{mol}$ of repeat units on 1.5 m^2 of oxide surface) was reached in 6 min . However, the heat sensor showed evolution of heat for 25 min , for a total of 28 mcal . Evidently the polymer molecules take some time to reach the configurations that maximize interaction

Table II

Effect of Carrier Solvent on Heat of Adsorption of Pyridine
onto R-1299 α -Ferric Oxide

Solvent	Water, ppm	Pyridine mM	Area/ Molecule nm ²	Heat of Adsorption	
				mcals/m ²	kcal/mol
hexane	8	29.2	0.48	23.5	-6.8
	3	28.8	0.40	20.5	-5.5
cyclohexane	6	29.5	0.45	23.8	-6.45
	3	30.3	0.44	22.5	-5.95
decalin	1	30.5	0.45	24.7	-6.7
	4	29.8	0.42	20.7	-5.3

Table III

Heats of Adsorption of Bases on Oxides Predicted from
Their E and C Values, kcal/mol

Base	SiO ₂	TiO ₂	α -Fe ₂ O ₃
pyridine	-12.4	-13.1	-10.3
ethylamine	-12.8	-13.9	-10.9
diethylamine	-13.9	-13.9	-10.9
triethylamine	-17.1	-16.9	-13.3
ethyl acetate	-6.2	-7.3	-5.7
acetone	-6.9	-8.0	-6.3
ethyl ether	-7.9	-8.8	-6.9
THF	-9.1	-9.9	-7.8
DMF	-8.1	-9.5	-7.5
Me ₂ SO	-9.0	-10.5	-8.2
diethyl sulfide	-10.0	-9.5	-7.4
benzene	-3.7	-3.9	-2.7
mesitylene	-5.3	-5.5	-4.3
PMMA	-4.0	-4.8	-3.8
poly(vinylpyridine)	-12.0	-12.7	-10.0

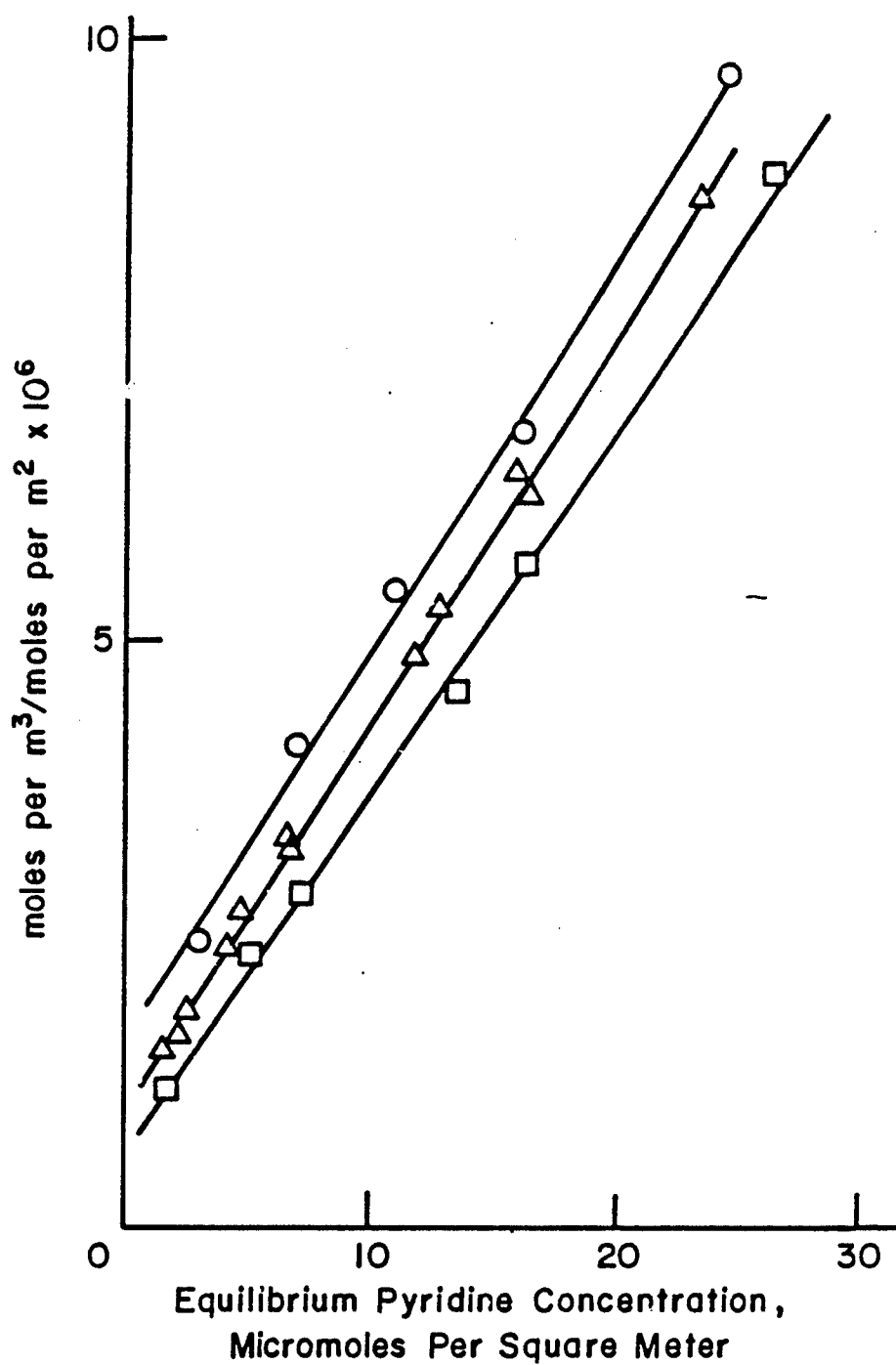


Figure 9. Langmuir plots for the adsorption of pyridine at 28°C onto α -ferric oxide from hexane (O), cyclohexane (Δ), and decahydronaphthalene (\square).

with the surface.

After the polymer was completely equilibrated on the oxide surface, we probed the amount of bare surface by pumping through the bed a 30 mM solution of pyridine in benzene; 8.05 mcal was evolved as 1.32 μmol of pyridine was adsorbed. This amounted to a heat of adsorption of -6.1 kcal/mol, a little less than the -6.5 kcal/mol found with no adsorbed polymer. By using the previously determined surface concentration of pyridine adsorbed from benzene, we could determine the number of 0.40-nm² pyridine sites blocked by the polymer, and from this information we find that an average of 52% of the polymer repeat units were bonded to the surface, with a heat of adsorption per mole of repeat units of -5.7 kcal/mol. This slightly lower heat of adsorption for pyridine groups in the polymer as compared to ordinary pyridine (-6.4 kcal/mol) could result from steric limitations. The high percentage of repeat units bound to the surface is not too surprising when the energy of bonding per repeat unit is this strong (-9 kT).

CONCLUSIONS

The FeOH surface sites of ferric oxides are acidic and adsorb nitrogen and oxygen bases with appreciable heats of adsorption, which can be quantitatively correlated and predicted with the Drago E and C equation.

The measured heats of adsorption of test bases of different C/E ratios predict that the stronger acidic surface sites have the following Drago constants: $C_A = 0.8 \pm 0.2$ and $E_A = 4.5 \pm 1.1$ (kcal/mol)^{1/2}. These constants are similar to those already measured for the SiOH sites of silica and the TiOH sites of titania, all of which are hard acid sites similar to, but about twice as strongly acidic as, alcohol groups.

Poly(vinylpyridine) adsorbed rapidly onto ferric oxide from a dilute solution in benzene, with 52% of the repeat units bonded to acid sites and with a heat of adsorption of -9 kT per site.

Flow calorimetry with a UV solute concentration detector downstream of the calorimeter bed can give accurate distributions of heats of adsorption.

Moisture levels of solvents, solutes and adsorbents strongly influence heats of adsorption. In the flow microcalorimeter, control of the moisture levels was attained by pumping down with a vacuum pump with liquid nitrogen trap while monitoring evaporative cooling and pressure of the bed. Karl Fischer analyses of water contents of solvents and solutions were necessary to achieve proper dryness.

A laboratory microcomputer to collect and correlate data from the heat and concentration sensors was an important part of this project.

REFERENCES

- Drago, R. S.; Vogel, G. C.; Needham, T. D. J. Am. Chem Soc. 1971, 93, 6014.
- Drago, R. S.; Parr, L. R.; Chamberlain, C. S. J. Am. Chem. Soc. 1977, 99, 3203.
- Fowkes, F. M. Rubber Chem. Technol. 1984, 57, 328-43.
- Fowkes, F. M.; Sun, C.-Y.; Joslin, S. J. In "Corrosion Control by Organic Coatings," Leidheiser, H., Jr., Ed. NACE: Houston, TX, 1981; p.1.
- Fowkes, F. M.; Tischler, D. O.; Wolfe, J. A.; Lannigan, L. A.; Ademu-John, C. M.; Halliwell, M. J. J. Polym. Sci. Polym. Chem. Ed. 1984, 22, 547-66.
- Fowkes, F. M.; McCarthy, D. C.; Tischler, D. O. J. Polym. Sci. Polym. Chem. Ed., in press.
- Silberberg, A., Plenary Address, 53th Colloid and Surface Science Symposium, Pittsburgh, PA, June 1984.

SECTION - #5

Inhibition of Iron Corrosion by Carboxylates in the Presence of Oxidants

Principal Investigator: Richard D. Granata, Research Scientist
Associates: Henry Leidheiser, Jr., Prof. of Chemistry
Patricia C. Santiesteban, Graduate Student

ABSTRACT

Inhibition properties of carboxylate-oxidant additives were studied. The investigation has focused on inhibition and inhibitive film formation by combinations of organic compounds with oxidizing agents in a system consisting of steel in a moderately corrosive, chloride-containing environment. More than 25 organic compounds were tested in combination with 7 oxidants. Immersion tests were performed for both preliminary screening at room temperature and 60°C and for long-term testing. Electrochemical testing included polarization resistance, polarization curves and AC impedance measurements. Crevice corrosion resistance was studied with specimens sealed with O-rings. Nearly 100% inhibition was obtained with several carboxylates in moderately alkaline media and at high concentrations using oxygen or nitrite oxidants. The investigation focused on acetate, m-nitrocinnamate, cinnamylideneacetate and cinnamate in solutions containing dissolved oxygen. Cinnamylideneacetate provided the best inhibition at low concentrations.

INTRODUCTION

The basis for this research is the process described by Leidheiser and Konno [1] in which an electrochemical oxidation process caused incorporation of an organic compound into the surface layers of steel, thereby improving corrosion resistance. Adaptation of the process to certain practical applications requires elimination of the electrochemical step. Observations made in our laboratory suggested that inhibition by acetate in chloride-containing solution may have the same origin. Therefore, a chemical step was sought to provide incorporation of organic inhibitor compounds into the surface layers of steel. Selection of compounds was oriented towards materials having low toxicity.

Acetate and many carboxylates, designated Type I-adsorption inhibitors, are dependent upon the presence of oxygen for their effectiveness. Thomas [2] has suggested that the Type I inhibitors catalyze the oxidation of ferrous ion. Mayne and Page [3] have used autoradiography to show that inhibition is associated with repair of defects and oxide or insoluble material formation. Mansfeld et al. [4] distinguished between an interface, 2-dimensional adsorbed-inhibitor layer and an interphase, 3-dimensional oxide-inhibitor layer system. Inhibition by carboxylates in the presence of dissolved oxygen is probably an interphase inhibitor system.

Aal and Wahdan [5] have reported increased passivation of steel with acetate and nitrite in deaerated solutions. Mercer [6], reporting tests in tap water containing chloride and sulfate, noted a sudden loss of inhibition at long immersion times and recommended long-term evaluations.

EXPERIMENTAL

Experimental methods used to evaluate corrosion inhibition properties of the test media with or without additives were immersion tests and electrochemical measurements. The immersion tests were evaluated in terms of the degree of appearance of corrosion products or corrosive attack of the substrate. The electrochemical measurements determined the corrosion potential of the substrate as a function of time, the effect of carboxylate on the polarization behavior, and the effect of carboxylate on the AC impedance behavior at selected DC potentials.

Immersion Methods

Evaluation of inhibition effects was made with steel specimens immersed in test media during a period of 7 days unless stated otherwise. The specimens were SAE 1010 steel obtained in the form of Q-Panels (Q-Panel Co., Cleveland, Ohio), cut to 2 cm x 4 cm pieces using a shearing cutter, then degreased with methyl alcohol before exposure to the test medium. Duplicate experiments were run to test reproducibility of the data. Additional experiments were run in cases of poor agreement of the duplicates or in cases where results were considered critical. The specimens were placed and inclined at a 45-60° angle in 50 ml beakers. The test medium was added to the beaker to completely cover the specimen (40 ml). The beaker was covered by a glass plate or watch glass to decrease evaporation and dust accumulation. Appearance evaluations and ratings were made on the following bases:

<u>Rating</u>	<u>Evaluation/Criteria</u>
1	Excellent: No change in solution appearance, no change in sample appearance.
2	Good: Some edge corrosion (spots) or solution discoloration.
3	Fair: Some spots on flat surface areas or some surface darkening. Noticeable edge corrosion.
4	Poor: Precipitation present; some change in color of solution. Darkening or spotting of surfaces.
5	Very Poor: Blackening or severely changed surface appearance. Large change in solution appearance with heavy precipitation.

In cases where the evaluation was judged to be intermediate, a half unit was assigned. For example, a rating of 1.5 indicates an evaluation intermediate between excellent and good.

Long-term immersion tests were made with some of the better performing inhibitors and under selected conditions.

An additional type of immersion experiment was performed with organic compounds to test the persistence of inhibition due to oxide-incorporated organic compounds after removal of the specimen from contact with dissolved inhibitor. After 7 or 16 days' immersion in test medium containing the organic compound, the sample was removed, rinsed with fresh test medium, and immersed in fresh test medium not containing the organic compound. Immersion ratings were made for these samples after 4 days.

Solutions and Test Media

All solutions were prepared from distilled water and reagent grade materials, except for some organic materials which were not readily available in purified form. A Corrosion Medium (CM) was selected to provide a minimum concentration of ions and aggressive species for each test medium. All test media were prepared using CM as the diluent/solvent. The CM composition was:

Fluoride (F)	10 ppm
Potassium (K)	10 ppm
Calcium (Ca)	50 ppm
Sulfate (SO_4)	100 ppm
Chloride (Cl)	300 ppm
Sodium (Na)	188 ppm

The CM was prepared from 100X stock solutions of the individual components. The stock solutions were prepared with distilled water as given below:

Sodium fluoride (NaF)	- 2.2 g/l
Potassium chloride (KCl)	- 1.9 g/l
Calcium chloride (CaCl_2)	- 13.9 g/l
Sodium sulfate (Na_2SO_4)	- 14.8 g/l
Sodium chloride (NaCl)	- 33.1 g/l

For preparation of 1000 ml of CM, 10 ml of each stock solution were added to a 1 liter volumetric flask which was half filled with distilled water. The calcium chloride stock solution was added first to avoid precipitation problems. After addition of each of the stock solutions, the volumetric flask was filled to the mark with distilled water. The pH of the CM was 5.5-6.0 as prepared with the available distilled water and reagents.

Inhibited test media were prepared with a variety of organic materials, with or without oxidizing agents. Organic materials with limited solubility were first dissolved in a small amount of methanol or ethanol, then diluted with CM such that the final concentration of alcohol was only a few percent. Several oxidizing agent/inhibitor combinations in CM were evaluated. Inhibited solutions were approximately pH 9, unless stated

otherwise. The organic compounds, the oxidizing agents and the test data are listed in the Results section.

Measurements at 60°C

Immersion and corrosion potential measurements were made at 60°C in a convection air oven. Immersion specimens were placed in small, screw-top polyethylene bottles containing the test electrolyte and incubated in the oven at 60°C. Corrosion potential measurements were made at room temperature after exposure at 60°C in the test solution. The O-ring sealed, glass joint method was used for corrosion potential measurements for specimens exposed at 60°C. The method is described in the following section.

Electrochemical Potential Measurements

Corrosion potential measurements were made on test specimens in various test media using a saturated calomel electrode (SCE) and an electrometer. The specimens were prepared for measurement by insulating the edges and making an electrical contact or by use of an O-ring seal. In the former preparation, samples were cut 2.5 cm square, a small hole drilled in a corner, a wire was inserted into the hole and twisted to make an electrical contact and the connection was coated with a conductive nickel-filled paint which was allowed to dry overnight. The edges and wire connection were given three coats of a fast-drying lacquer designed for electroplating mask uses (Microshield®) to insulate and seal them from the electrolyte. In another set of experiments, a 25 mm O-ring sealed, glass joint was clamped onto the specimen test area (8.8 cm²). The glass joint was filled with the test solution (approximately 25 ml), a reference electrode immersed in the electrolyte, and electrometer measurements made between the reference electrode and the specimen. Specimens coated with Microshield® were immersed in a beaker with a reference electrode to make the corrosion potential measurements.

Polarization Curve Determination

Polarization resistance and polarization curve determinations were performed on an EG&G Princeton Applied Research Model 350 Corrosion Measurement Console with specimens having 8.8 cm² area exposed to the test electrolyte. Most experiments were performed using the O-ring sealed, glass joint arrangement described above. Polarization curves were determined at a scan rate of 1 or 0.3 mv/s and were begun at the corrosion potential. Polarization resistance measurements were determined at a scan rate of 0.1 mv/s from -0.015 to +0.005 v vs the corrosion potential of the specimen. All potentials are reported versus the saturated calomel electrode (SCE).

AC Impedance Measurements

AC impedance measurements were made to help determine the nature of the corrosion inhibition observed for selected samples. An EG&G Princeton Applied Research Corporation Model 368 AC Impedance System was used for

taking the measurements. Specimens were tested using the O-ring sealed, glass joint arrangement described above, or, in the case of acetate measurements, a 1 cm² area was masked with molten (160°C) thermoplastic cement (Buehler Ltd., #40-8100) and tested, while hanging vertically, in 80 ml of test solution. Measurements were in the range of 0.02 Hz to 20 kHz. A three electrode measurement system was used. The DC bias potential was set to the corrosion potential. Measurements were at room temperature.

RESULTS

Substituted Acetate and Propionate Compounds

Table I shows the results of the immersion tests done with substituted acetate and propionate carboxylate compounds. While several of these compounds have excellent inhibition properties at a 0.1M concentration, few are effective at the lower 0.01M concentration. Hydroxyacetate, in some cases, exhibited a unique behavior versus the other compounds: After 4-8 days' immersion, a bronze-like iridescent film developed on the surface. The film was adherent to the specimen surface. Comparison of the dissociation constant values (pK_a) with inhibition behavior revealed no specific value for greatly enhanced inhibition. Generally, a range of 3.8-5.0 for pK_a values yielded similar results in these tests.

The best performance at low concentration was obtained with cinnamylideneacetate. Cinnamylideneacetate yielded excellent results at a concentration of 0.01M without an added oxidant such as nitrite. The results of long-term tests with this material are given in a later part of this section.

Substituted Aryl Acids

Substituted aryl carboxylates were evaluated by immersion testing and the results are given in Table II. Many of these aromatic carboxylates performed well at 0.1M concentration and fair results were obtained in certain cases at 0.01M concentration. The first aryl compound identified as giving good performance at low concentration in CM was cinnamate. Derivatives of cinnamate and benzoate showed better inhibition at the lower concentrations than did the derivatives of the acetate and propionate.

Effect of Oxidizing Agents

Table III shows the immersion test ratings obtained in the presence of oxidizing agents. A concentration of 0.001M was selected to be approximately equal to that of dissolved oxygen at room temperature. The best ratings with oxidants under these conditions were obtained for nitrite, followed by dichromate, and followed by molybdate. Note that the results obtained with dissolved oxygen as the oxidizing agent were nearly as good at pH 8 as for the nitrite or dichromate. Results for tests conducted under additional conditions of temperature and oxidant concentration are

Table I

Immersion Test Ratings of Substituted Acetate and Propionate

Compound (Sodium salt)	Concentra- tion (M)	Rating	pK _a	pH Change Initial-Final
Acetate	0.1	1	4.8	7.8-7.5
"	0.01	4	"	7.0-7.0
" (magnesium salt)	0.05	1.5	-	7.6-7.2
" "	0.005	4.5	-	7.3-6.6
Chloroacetate	0.1	4.5	2.9	9.1-7.8
Ethoxyacetate	0.1	4.5	3.7	9.7-7.6
Hydroxyacetate ^a	0.1	1.5	3.8	9.1-6.4
" ^b	0.1	1	"	8.8-7.8
" ^c	0.1	1	"	9.3-9.2
" ^b	0.01	4.5	"	9.0-6.9
Aminoacetate	0.1	3.5	2.3	9.0-8.8
2-Naphthylacetate	0.1	1	4.3	8.9-7.8
"	0.01	4.5	"	9.3-7.2
Phenylacetate	0.1	1	4.3	9.0-(7)
Cinnamylideneacetate	0.1 ^{ss}	1	-	- - -
"	0.01	1	-	- - -
Propionate	0.1	1	4.8	8.6-7.5
"	0.01	4.5	"	- - -
2-Chloropropionate	0.1	4.5	2.8	9.4-6.7
3-Chloropropionate	0.1	4	4.0	9.0-6.0
"	0.01	4.5	"	9.7-6.3
Formate	0.1	5	3.8	7.1-7.3

Notes: Ratings are for 7-day immersion period.

ss - Denotes saturated solution.

a - Initial test, film formed in 4-8 days.

b - Repeat test, film formed in 8 days.

c - Repeat test, with fresh material, no apparent film in 16 days.

Table II

Immersion Test Ratings of Aryl Carboxylates

Compound (Sodium salt)	Concentra- tion (M)	Rating	pK _a	pH Change Initial-Final
Benzoate	0.1	1	4.2	9.0-7.8
"	0.01	4.5	"	9.5-7.1
o-Aminobenzoate	0.1	4.5	5.0	9.0-8.7
m-Aminobenzoate	0.1	1.5	4.7	7.9-7.4
"	0.01	3	"	7.8-7.2
p-Aminobenzoate	0.1	1	4.9	8.1-7.3
"	0.01	2.5	"	7.5-6.9
m-Bromobenzoate	0.1	1	3.8	9.0-8.0
"	0.01	2.5	"	9.6-7.3
p-Chlorobenzoate	0.1	1	4.0	9.0-7.6
"	0.01	4.5	"	9.6-6.0
Cinnamate (trans)	0.1	1.5	4.4	7.6
"	0.01	3.5	"	7.5
"	0.001	5	"	7.3
m-Nitrocinnamate	0.1	1	4.1	9.9-7.6
"	0.01	2.5	"	9.7-8.0
p-Nitrocinnamate	0.1	1	4.0	9.3-9.0
"	0.01	3	"	9.5-8.4
Cinnamide	0.1	4.5	-	9.2

Note: Ratings are for 7-day immersion period.

Table III
Immersion Test Ratings with Oxidizing Agents

Oxidizing Agent (0.001M)	Solution					
	CM, 0.1M Acetate			CM, 0.01M Acetate		
	pH 6	pH 8	pH 10	pH 6	pH 8	pH 10
H ₂ O ₂	4	2.5	2	—	—	—
K ₂ Cr ₂ O ₇	3.5	1.5	1.5	1.5	1.5	1.5
K ₂ S ₂ O ₈	4	3	3.5	3.5	3.5	3.5
KMnO ₄	4	3.5	3.5	3.5	3.5	3.5
NaNO ₂	3.5	1	2	1	1	1
Na ₂ MoO ₄	5 ^a	2 ^a	3 ^a	3.5 ^a	2.5 ^a	3.5 ^a
Dissolved O ₂	5	2 ^b	2.5	—	—	—

Notes: Ratings are for 7-day period.
a - Ratings are for 10-day period.
b - Rating for pH 7 was 1.

shown in Table IV. Due to toxic effects and water management problems associated with chromate, nitrite and dissolved oxygen were selected for additional testing in combination with selected organic compounds.

Table IV

Immersion Test Ratings of Steel at Room Temperature and 60°C

Carboxylates in CM, Sodium Salts	Concen- tration Molar	Temperature/Oxidant Concentration		
		RT —	60°C —	60°C 0.01M nitrite
4-Hydroxybutyrate	0.01	4.5	—	1.5
"	0.1	1.5	5	2.5
Chloroacetate	0.1	4	—	5
"	1	1.5	4	4.5
γ-Phenylbutyrate	0.01	2.5	—	4
"	0.1	1	2	1.5
m-Aminobenzoate	0.01	4.5	—	2
"	0.1	1.5	2	2
Acetate	0.001	4	—	2
"	0.01	3	—	1
"	0.1	1	4.5	1
Propionate	0.001	—	—	3
"	0.01	4.5	—	1.5
"	0.1	1	5	1

Note: Ratings are for 7-day immersion period.

Long-Term Immersion Tests

Long-term immersion test results are given in Table V. The test specimens have been immersed for periods of up to 14 months. Some of the test specimens showed little, if any, signs of corrosion. Note that the rating system (1 to 5) was initially designed to evaluate signs of corrosion appearing within 7 days. The same criteria were used to evaluate these long-term specimens and may be considered a very harsh rating system for the long-term tests. Ratings of 2 or 3 should be considered very good performance in these long-term tests. Almost all of the solutions tested in this experimental set yielded good results. Particularly significant is the generally good results for the cinnamate derivatives. The best performance may be that for cinnamylideneacetate, especially at the lower concentration of 0.01M. Additional tests are planned for cinnamylideneacetate. Poor ratings were observed for the uninhibited CM and for the CM with an old lot of hydroxyacetate. The poor rating for the hydroxyacetate may have been due to impurities (amber-colored) in the material. The fresh

lot of hydroxyacetic acid was water-white in appearance and did not form an iridescent film as was observed with test solutions of the older material.

Table V
Long-Term Immersion Test Ratings

Test Conditions	Immersion Time (days)	Ratings*
CM (corrosion medium) only.	427	5
0.1M acetate, pH=7.8, CM	456	2.5
0.05M magnesium acetate, CM.	260	2.5
0.1M propionate, CM.	407	2.5
0.1M hydroxyacetate, CM.	260	5
0.005M propionate, 0.1M acetate, CM.	407	1.5
0.005M propionate, 0.01M acetate, CM.	404	2
0.004M phenylthiourea, 0.1M acetate, 0.001M nitrite, pH=8, CM.	421	4
0.1M cinnamylideneacetate, CM.	295	1.5
0.01M cinnamylideneacetate, CM.	245	2
0.005M cinnamylideneacetate, 0.005M hydroxyacetate, CM.	232	3
0.1M hydroxyacetate ^a , CM.	233	1
0.1M cinnamate, CM.	310	1
0.1M m-nitrocinnamate, CM.	259	1.5
0.1M p-nitrocinnamate, CM.	240	1
0.1M m-bromobenzoate, CM.	261	2
0.1M p-aminobenzoate, CM.	239	2.5
0.01M γ -phenylbutyrate, 0.01M nitrite, CM.	349	1.5
0.1M chloroacetate, 0.01M nitrite, CM.	349	1.5
0.1M 2-naphthylacetate, CM.	261	2.5
0.1M 4-hydroxybutyrate, CM.	376	2.5
0.01M 4-hydroxybutyrate, 0.01M nitrite, CM.	349	2.5

Notes: * Rating system is the same as that used in 7-day tests.
^a New lot of compound, colorless.

Additional Immersion Tests

A set of experiments was initiated to test the effect of pre-oxidation of the steel surface prior to exposure to the inhibitor. Pre-oxidation with 0.001M persulfate, molybdate, chromate, nitrite, nitrate or hydrogen peroxide followed by immersion in 0.01M hydroxyacetate in CM or cinnamate in CM showed no significant improvement in inhibition.

A set of experiments was performed to help evaluate the corrosion protection properties of films on specimens immersed for up to 16 days in 0.1M inhibitor in CM. Inhibitors included in this experimental set were

acetate, propionate, hydroxyacetate, m-aminobenzoate, p-aminobenzoate, γ -phenylbutyrate, and cinnamylideneacetate. After removal of the specimen from the inhibited CM solution, the specimen was rinsed and immersed in CM. After 4 days' immersion, the ratings of the specimens were 4-4.5 in all cases, or slightly better than untreated steel. However, in the first few hours of immersion, very little corrosion was observed, especially in the case of the specimen pretreated in hydroxyacetate for 16 days. These results suggest that a corrosion resistant film was formed which provided some protection in the absence of the dissolved inhibitor.

Some experiments were begun to determine the effect of preconditioning test specimens at high concentrations of inhibitor for short periods before immersion at lower concentrations for longer periods. Table I shows that for 0.01M acetate after 7 days, a rating of 4 was obtained. However, a specimen immersed in 0.1M acetate for 2 days before immersion in 0.01M acetate yielded a rating of 2 after 25 days. Preconditioning at higher concentrations of inhibitor enhances the inhibition observed in these tests.

Polarization Resistance Measurements

Corrosion potential and polarization resistance measurement data are presented for cinnamate, m-nitrocinnamate and cinnamylideneacetate in Figures 1 and 2, respectively. Experiments were made at three concentrations, 0.03M, 0.01M, and 0.003M. Generally, all three compounds provided excellent inhibition. Potentials below approximately -0.5 v vs SCE correspond to freely corroding specimen behavior. In Figures 1 and 2, the corrosion potential and R_p values for steel in 0.01M cinnamate are shown to drop to values representative of freely corroding steel. In the 0.003M inhibitor measurements, steel in cinnamylideneacetate maintained the highest values of corrosion potential and R_p while showing some corrosion product formation at the O-ring seal with the remaining area corrosion-free. Steel in 0.003M cinnamate or m-nitrocinnamate was severely corroded. Visible corrosion usually began adjacent to the O-ring in the crevice region and correlated with potentials below -0.5 v.

Polarization Curves

Figures 3-5 show the polarization curves for steel in the presence of 0.1M acetate, 0.03M cinnamate, 0.03M m-nitrocinnamate, and 0.01M cinnamylideneacetate. These concentrations were selected on the basis of having the minimum effective inhibitor concentration or approximating the maximum solubility of the inhibitor in CM. The electrolyte was CM. Figure 3 shows anodic polarization curves begun at the corrosion potential at a scan rate of 1 mv/s. The lowest currents were observed for cinnamate and the highest for acetate from the corrosion potential to 0.4 v. These observations showed that cinnamate formed a more resistive film than the other compounds. Figure 4 shows the cathodic polarization curves for steel begun at the corrosion potential at a scan rate of 0.3 mv/s. The lowest currents were observed for cinnamate and the highest for acetate from the corrosion potential to -0.7 v. The curve for m-nitrocinnamate shows no diffusion currents expected for oxygen reduction in the potential range of -0.6 to -1.0 v, presumably due to reduction of the $-\text{NO}_2$ group.

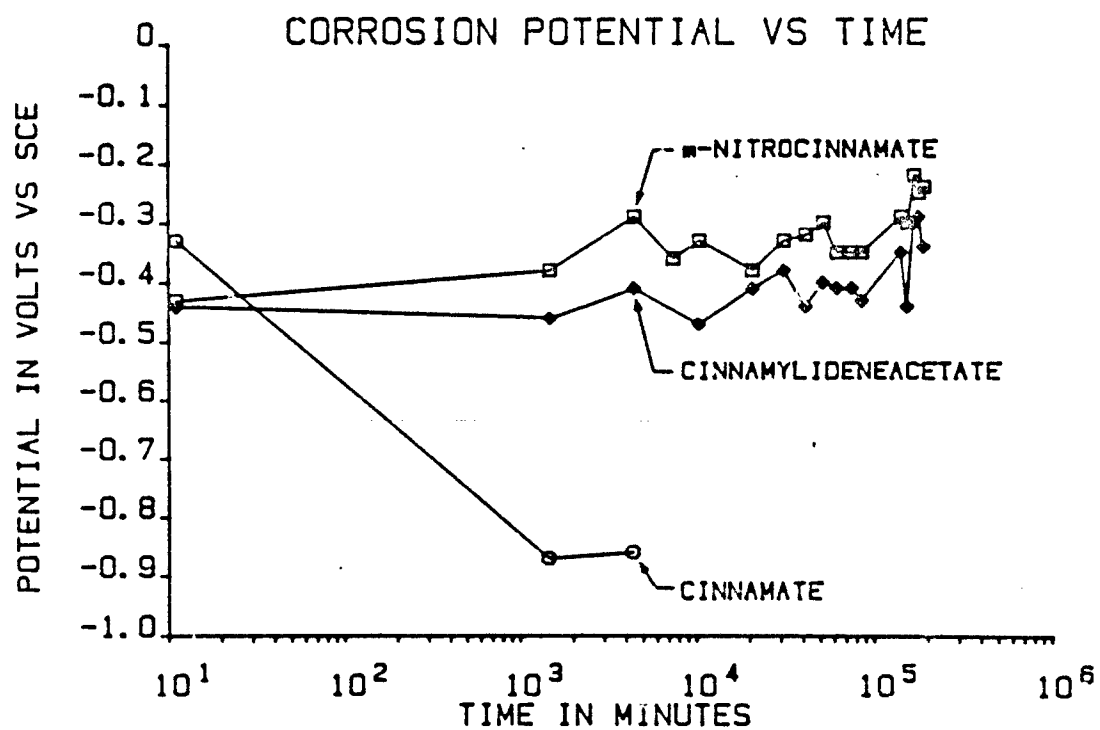


Figure 1. Corrosion potential versus time for steel specimens exposed to 0.01M inhibitor in corrosion medium. Specimens were assembled with an O-ring seal.

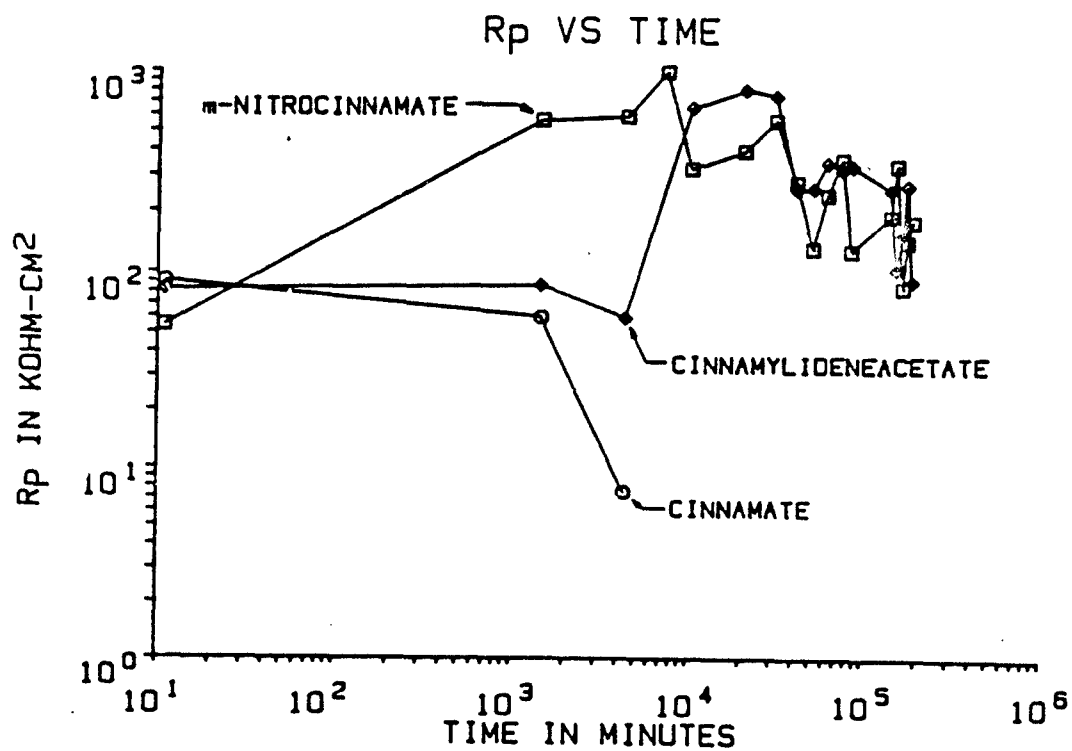


Figure 2. Polarization resistance versus time for steel specimens exposed to 0.01M inhibitor in corrosion medium. Specimens were assembled with an O-ring seal.

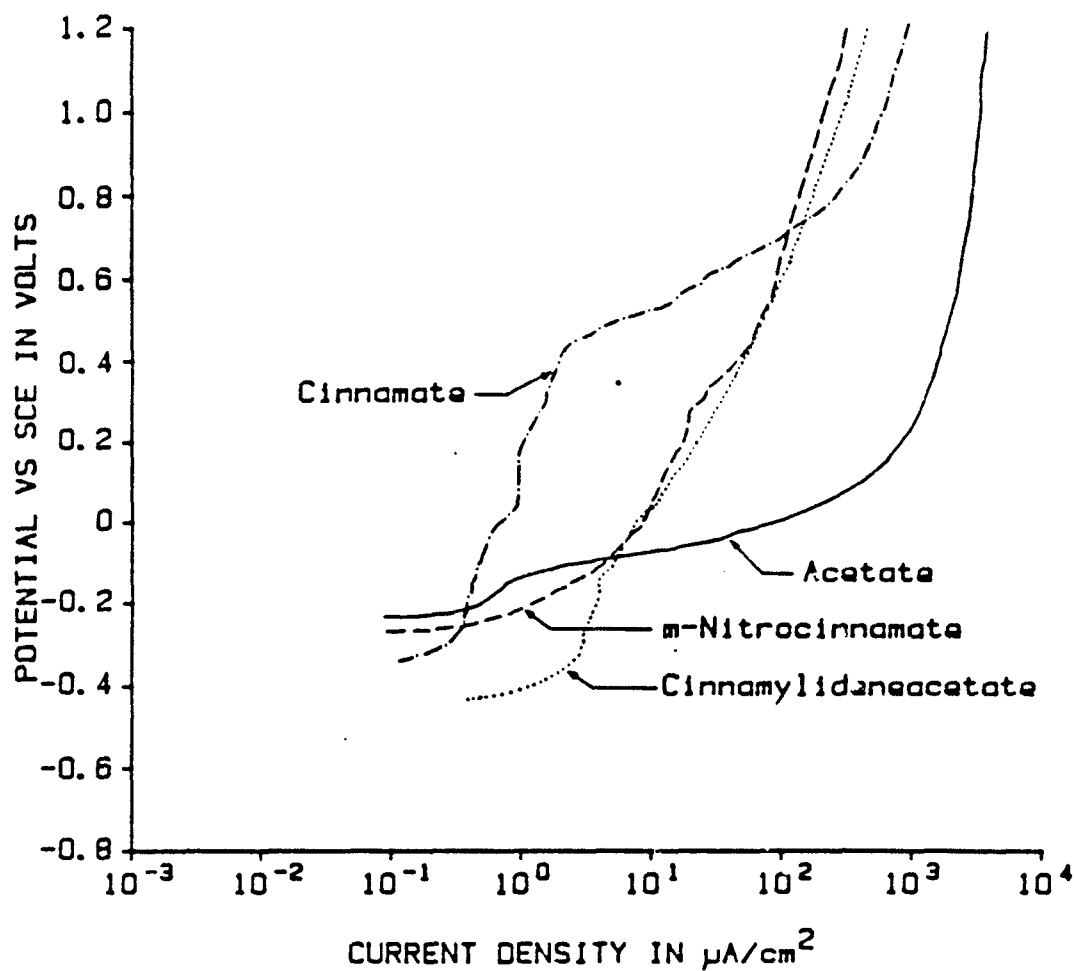


Figure 3. Anodic polarization curves of steel in corrosion medium for 0.1M acetate, 0.03M m-nitrocinnamate, 0.03M cinnamate, and 0.01M cinnamylideneacetate. Scan rate was 1 mv/s.

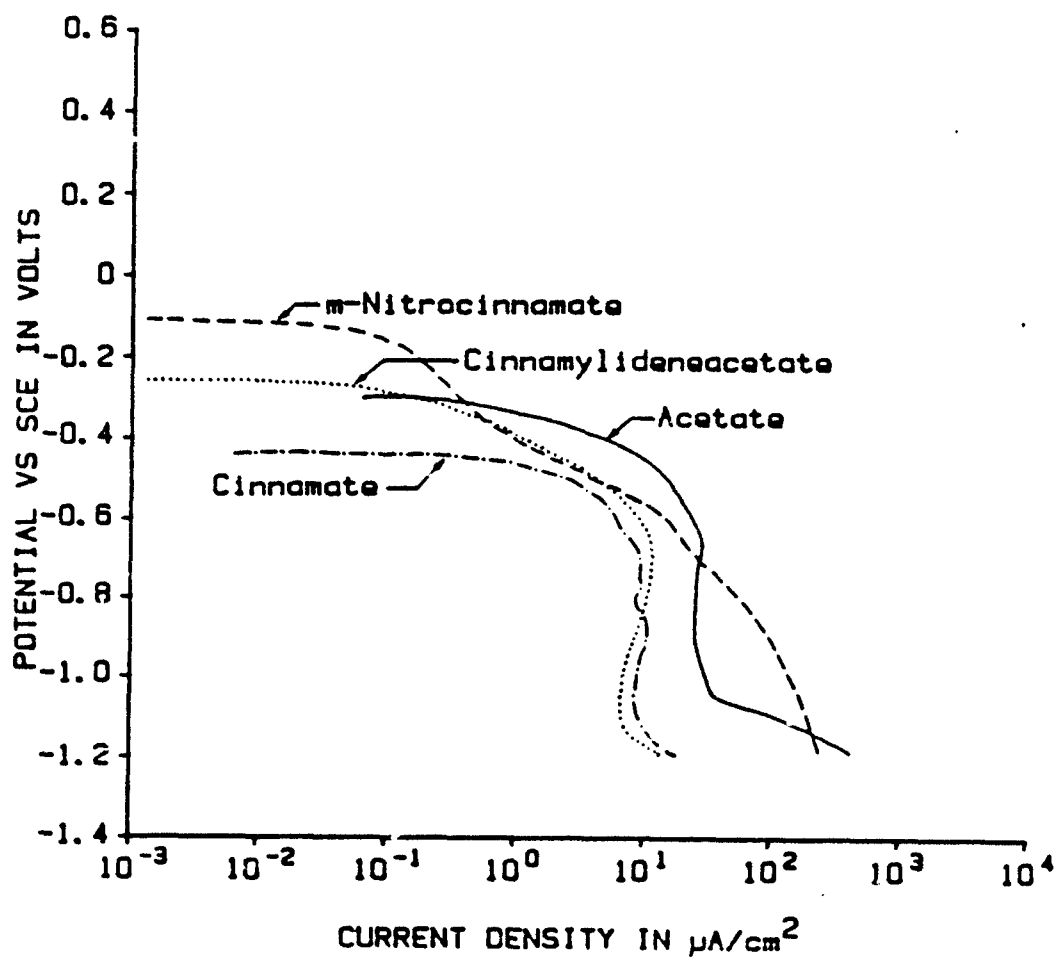


Figure 4. Cathodic polarization curves of steel in corrosion medium for 0.1M acetate, 0.03M m-nitrocinnamate, 0.03M cinnamate, and 0.01M cinnamylideneacetate. Scan rate was 0.3 mV/s.

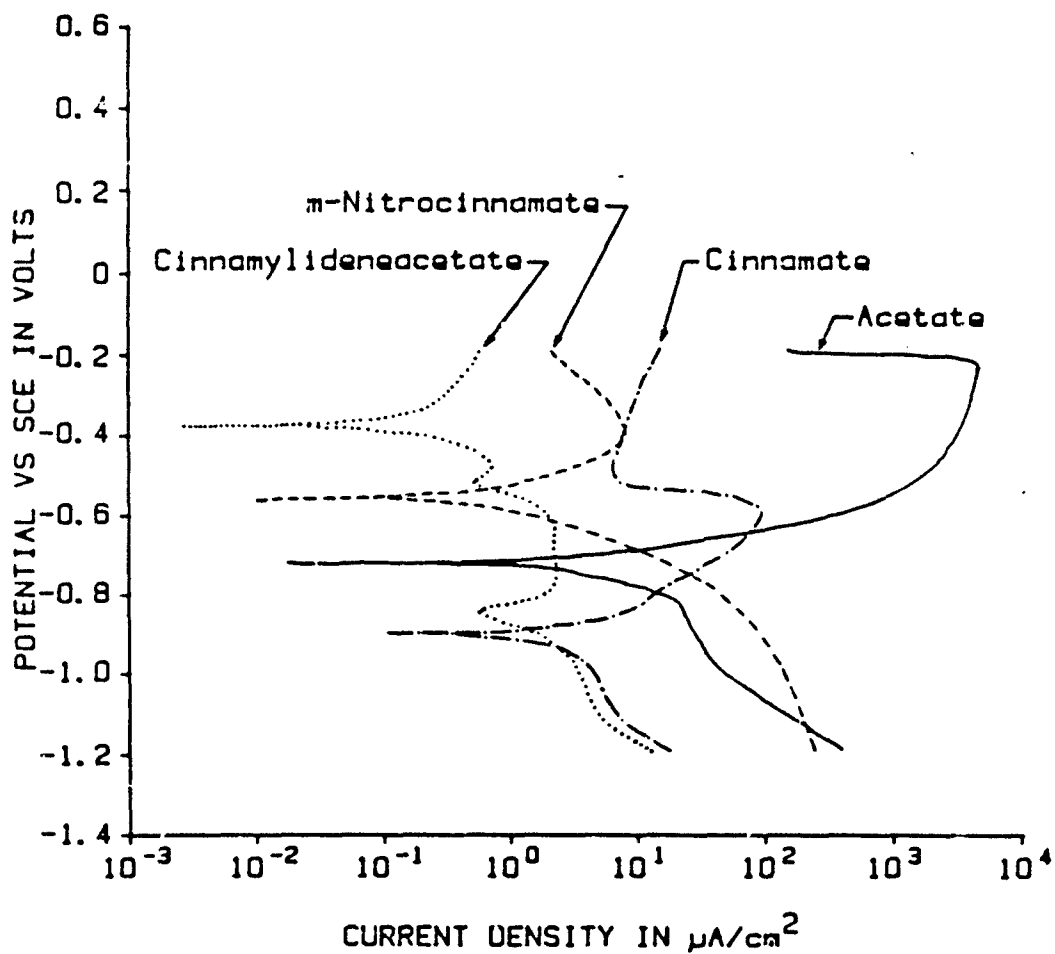


Figure 5. Polarization curves of steel in corrosion medium for 0.1M acetate, 0.03M m-nitrocinnamate, 0.03M cinnamate, and 0.01M cinnamylideneacetate obtained upon reversal of the scan direction after completion of the cathodic polarization curve (Figure 4). Scan was from -1.2 v to -0.2 v at a scan rate of 0.3 mv/s.

These observations along with those from the anodic polarization curves suggest that the film formed in cinnamate is more resistive than the other three compounds. Figure 5 shows the polarization curves obtained upon reversal of the scan direction at -1.2 v. These curves show the behavior of the steel substrates polarized from the hydrogen evolution potential region to -0.2 v. The curves show the largest anodic currents for acetate, much smaller currents for cinnamate, and very small currents for m-nitrocinnamate and cinnamylideneacetate. These results suggest that cinnamylideneacetate and m-nitrocinnamate form protective films most readily, cinnamate less readily, and acetate with difficulty.

Impedance Measurements

A series of impedance measurements was made at different DC bias potentials. Figure 6 shows the results obtained with 0.01M cinnamylideneacetate in CM. The impedance diagrams are given as Bode plots. The test cell was an O-ring sealed glass joint. The plots show that at low frequencies the resistance was higher, while the phase angle was lower for the curves obtained at the initial corrosion potential and again at 0 v versus the other four curves. Similar but smaller differences were obtained with 0.03M m-nitrocinnamate and 0.03M cinnamate. These results suggest that the inhibition is dependent upon the presence of either an air-formed or electrochemically formed oxide layer.

XPS Surface Analysis

Steel specimens were subjected to X-ray photoelectron spectroscopic (XPS) analysis after immersion in 1.0M acetate for 1 day or 0.03M cinnamate for 2 days. The specimen was not rinsed after removal of the specimen from the solution, but was immediately and rapidly blown dry in a stream of dichlorodifluoromethane (Freon). The spectra are shown in Figure 7. The major elemental peaks observed were for Fe, O, C, and Na. An analysis was made of the carbon and sodium relative intensities based upon peak height and sensitivity factors for the two elements. The analytical ratios of C/Na were calculated to be 25 for cinnamate and 6 for acetate. The stoichiometric ratios of C/Na for these sodium carboxylate salts were 9 (cinnamate) and 2 (acetate). Comparing the calculated analytical ratios to the stoichiometric ratios yielded a ratio of approximately 3 molecules of carboxylate per sodium ion; hence, a larger ratio of carboxylate was associated with protons or iron ions than sodium ions. This analysis suggests that the carboxylates were partially adsorbed in the acid form, or iron carboxylate compounds were formed and incorporated in the surface layer.

CONCLUSIONS

This work supports the initial hypothesis that chemical treatments may be used to incorporate organic inhibitors in the surface layers of steel. The chemical treatment method was designed to be an alternative to the electrochemical treatment developed by Leidheiser and Konno [1].

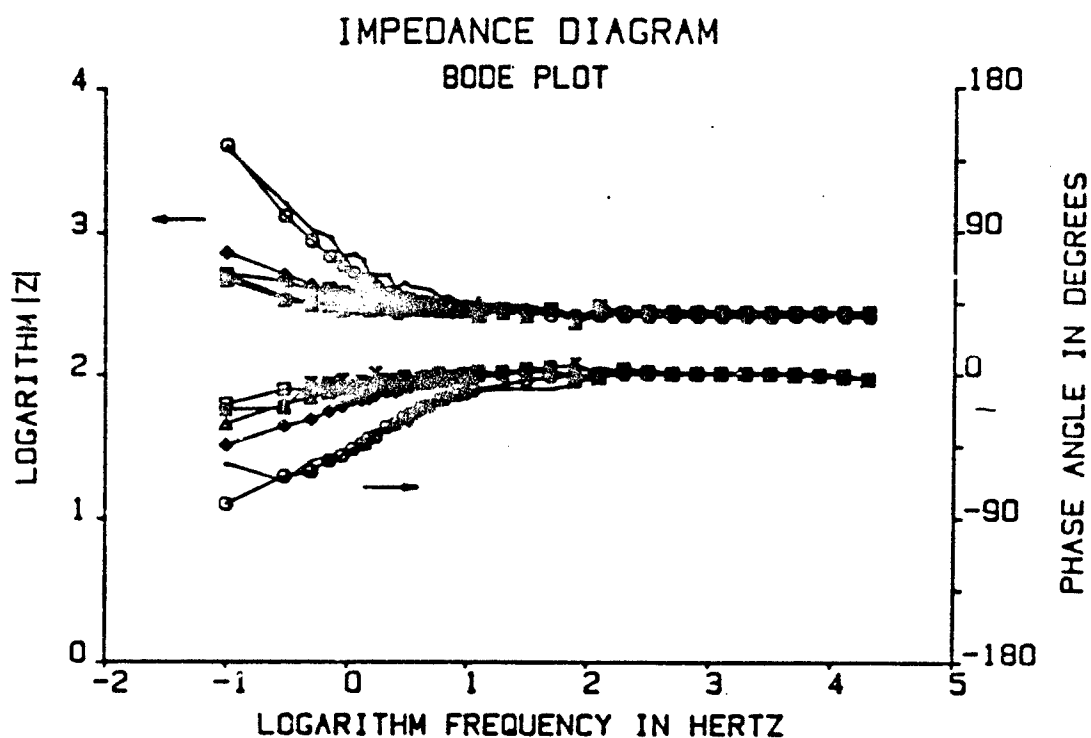


Figure 6. AC impedance data presented as Bode plots for steel in 0.01M cinnamylideneacetate in corrosion medium. Specimen area was 8.8 cm^2 . Consecutive experiments on same sample. Legend: (—) 1st data set obtained after 1h equilibrium; (\circ) 2nd data set obtained at -0.8 v ; (\square) 3rd data set obtained at -1.2 v ; (\triangle) 4th data set obtained at -0.8 v ; (\times) 5th data set obtained after 10 min equilibrium; (\ominus) 6th data set obtained at 0 v .

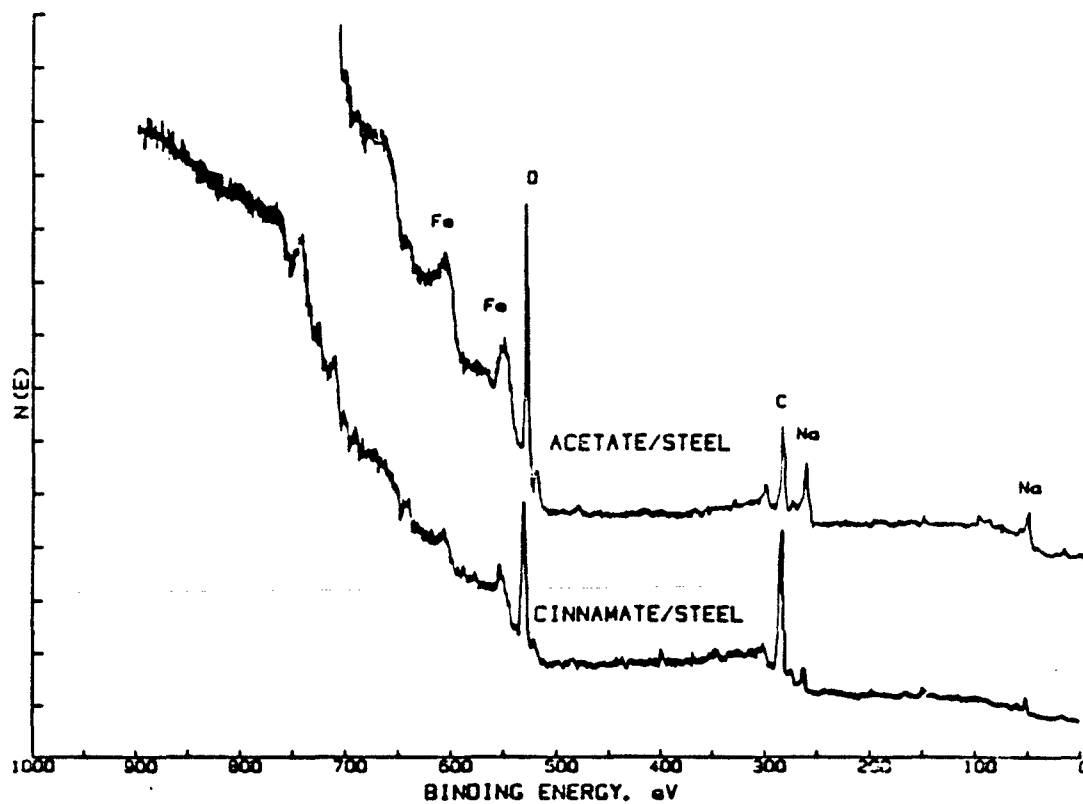


Figure 7. X-ray photoelectron spectra of steel immersed in corrosion medium containing 1M acetate or 0.03M cinnamate.

Conditions have been identified in which carboxylates, oxidants and controlled pH yielded corrosion-free environments for steel in chloride-containing aqueous solutions.

Based upon the results given in Tables I and II, several carboxylates were shown to be effective in the chloride-containing medium. There was a significant difference in the minimum effective concentration for inhibition among the different inhibitors. For example, the minimum concentration for acetate is approximately 0.1M, whereas for cinnamylideneacetate, it is less than 0.003M.

Tests with oxidizing agents showed that nitrite was more effective than dissolved oxygen and approximately as effective as chromate.

Electrochemical measurements with O-ring sealed specimens showed that some carboxylates were more effective in the inhibition of crevice corrosion. Acetate at concentrations 10 times greater than that required for general corrosion inhibition were ineffective at inhibiting crevice corrosion. Cinnamate, substituted benzoates and cinnamyl derivatives were effective in inhibiting crevice corrosion at concentrations similar to that for general corrosion inhibition. Crevice corrosion occurred within minutes in 1M acetate. No evidence of crevice corrosion was observed in 0.01M cinnamylideneacetate or m-nitrocinnamate after more than 100 days.

Long-term immersion tests have shown that 0.01M cinnamylideneacetate provided excellent protection for steel for at least 245 days. O-ring sealed specimens with 0.01M inhibitors also have received excellent ratings after more than 100 days.

Immersion tests at 60°C yielded good results with γ -phenylbutyrate and m-aminobenzoate at 0.1M concentration. With the addition of 0.01M nitrite, 4-hydroxybutyrate, acetate and propionate also yielded good results.

Pre-treatment of steel specimens in 0.001M solutions of oxidizing agents did not improve inhibition in 0.01M hydroxyacetate. Air oxidation appears to be sufficient to provide any required oxide surface for inhibitor interaction.

Films appeared to be formed on steel in the presence of inhibitors as evidenced by the iridescent films obtained in impure (discolored) hydroxyacetate and the persistence of the inhibition observed when specimens were removed from solution and immersed in the corrosion medium without inhibitor.

Pre-conditioning the specimens in high concentrations of inhibitor solutions for short periods was found to enhance the inhibition observed when the specimens were transferred to solutions containing lower inhibitor concentrations.

Corrosion potential and polarization resistance measurements were consistent with most of the visual rating observations. The exceptions were related to the crevice corrosion observed at the O-ring seal for some specimens, especially acetate at low concentrations.

Polarization curves showed that the protective film formed in the presence of cinnamate is more resistive than m-nitrocinnamate, cinnamylideneacetate or acetate. However, on specimens polarized to cathodic potentials, protective films reformed more readily with m-nitrocinnamate and cinnamylideneacetate than with cinnamate. This behavior suggests that their greater crevice corrosion resistance versus cinnamate is related to their ability to form protective layers on a surface with little or no oxide.

AC impedance results with cinnamylideneacetate, m-nitrocinnamate, cinnamate and acetate suggested that the inhibition is dependent upon the presence of oxide or oxide-forming conditions.

Comparison of XPS results for steel treated with acetate or cinnamate revealed that the ratio of carboxylate to sodium on the surface was 3 and indicated adsorption of carboxylates, at least partially, in the acid form, or indicated formation on the surface of iron carboxylates.

REFERENCES

1. H. Leidheiser, Jr. and H. Konno, J. Electrochem. Soc. 130, 747 (1983).
2. J.G.N. Thomas in "Proceedings of the 5th European Symposium on Corrosion Inhibition", Vol. 2, Ferrara, Italy (1980), pp.453-70.
3. J.E.O. Mayne and C.L. Page, Br. Corr. J. 9, No. 4, 223 (1974).
4. F. Mansfeld, M.W. Kendig and W.J. Lorenz, J. Electrochem. Soc. 132, 290 (1985).
5. M.S.A. Aal and M.H. Wahdan, Br. Corr. J. 16, No. 4, 205 (1981).
6. A.D. Mercer in "Proceedings of the 5th European Symposium on Corrosion Inhibition", Vol. 2, Ferrara, Italy (1980) pp.563-81.

Corrosion Behavior of Steel Pre-Treated with Silanes

Principal Investigator: Henry Leidheiser, Jr., Prof. of Chemistry
Associates: Richard D. Granata, Research Scientist
Michelle DeCrosta, Graduate Student

ABSTRACT

Steel panels were coated with 10 different silanes by brushing the silane or a diluted silane on the surface, and the coated panels were evaluated for corrosion protection by R_p measurements, anodic and cathodic polarization curves, and by accelerated rusting. Cathodic delamination tests were also performed on panels treated with 3 different silanes. The best overall corrosion protection was afforded by a coating formed from methyl triacetoxysilane. XPS, AES and FTIR studies suggest that the active silanes provide a continuous coating that is not removed from the surface upon exposure to aqueous solution. The more protective silanes show Si-O-Si bonds indicative of polymerization.

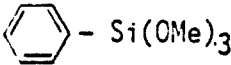
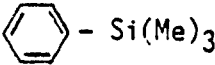
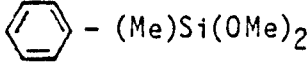
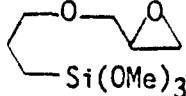
EXPERIMENTAL

The silanes used in this study and their acronyms are given in Table I. They were all obtained from the Dow Corning Co.

All experiments were performed on cold-rolled steel Q panels that were degreased in trichloroethane, rinsed in methanol, polished with 600 grit SiC suspended in deionized water, rinsed in methanol and stored in a desiccator until time for coating. The coating was applied either by brushing the pure silane or a 5-10% solution in 90% deionized water/10% absolute methanol onto the surface in a thin film and allowing to dry in a desiccator for 3-5 days. In a few cases the coated metal was heated in air at 60°C for 20-25 min.

The organic coating applied over the silanized surface was polybutadiene as used in previous studies [1]. The coatings were applied using a spin-coating technique and were cured at 200° in air for 20 min. Cathodic delamination studies were carried out in 0.5M NaCl using an applied potential of -0.80 v vs. SCE. The defect was made by scribing a 1 mm² hole in the coating. The radial growth of the delaminated region, which manifested itself as a lighter-colored area adjacent to the defect, was periodically measured. The final delaminated area was confirmed by a tape-pull test.

Table I
Organosilane Selection

Silane	Abbreviation	Structure
Phenyl trimethoxy silane	PTS	 $\text{C}_6\text{H}_5\text{-Si(OMe)}_3$
Phenyl trimethyl silane	PTMS	 $\text{C}_6\text{H}_5\text{-Si(Me)}_3$
Methylphenyl dimethoxy silane	MPDS	 $\text{C}_6\text{H}_5\text{-(Me)Si(OMe)}_2$
Dimethyl diethoxy silane	DDS	$(\text{Me})_2\text{Si(OEt)}_2$
Ethyl triethoxy silane	ETS	$(\text{Et})\text{Si(OEt)}_3$
Dichloro dimethyl silane	DCS	$\text{Cl}_2\text{Si(Me)}_2$
Trichloro methyl silane	TCS	$\text{Cl}_3\text{Si(Me)}$
Glycidoxy propyl trimethoxy silane	GPTS	 $\text{CH}_2\text{CH}_2\text{CH}_2\text{O-CH}_2\text{CH}_2\text{CH}_2\text{Si(OMe)}_2$
Methyl triacetoxysilane	MTS	$(\text{Me})\text{Si(OOCCH}_3)_3$
Hexamethyl disiloxane	HMDS	$(\text{Me})_3\text{Si-O-Si(Me)}_3$

All potentiodynamic experiments were carried out using a Princeton Applied Research Model 350 Corrosion Measurement Console with a K47 electrochemical cell. AC impedance measurements were made using a Princeton Applied Research Model 368 AC Impedance Measurement System.

Surface analysis studies were performed on a Physical Electronics ESCA/AUGER/SAM 549 spectrometer with argon sputtering capabilities, a GCA Corp. Ion Microprobe Analytical Mass Spectrometer, and a Mattson Sirius 100 FTIR Spectrometer.

Accelerated rusting experiments were conducted on 1 cm diameter disks punched from the silanized steel sheet. The edges, the underside and the perimeter of the test side were coated with Microshield® lacquer. The uncoated surface was treated with a solution composed of 3 μ g NaCl plus 10 μ g kaolin per ml MeOH while the sample was placed in a closed chamber containing a saturated solution of NaBr to maintain a relative humidity of 58%. The samples were visually inspected every 24 hours and photographs were taken.

RESULTS

Polarization Resistance

Tables II - V summarize the polarization resistance and corrosion potentials in 0.15M sodium borate-0.05M NaCl for two series of experiments for steel treated with the silanes. The data in Tables II and III are for silanized steel panels that were cured for 3-5 days in a desiccator. The data in Tables III and IV are for silanized steel that was heated for 20-25 min in air at 60°.

It will be noted in Table II that six of the silanes (PTS, MTS, GPTS, MPDS, DDS and HMDS) yielded R_p values that were significantly higher than that of the blank and remained high for at least 2 h after exposure to the borate-chloride solution. The only silane that provided high R_p values after the heat treatment was MTS, as shown by the data in Table IV. Four silanes (PTS, MTS, GPTS and TCS) yielded noble potentials initially and after 2 h exposure for the panels cured at room temperature but none of the silanes yielded noble potentials after 2 h in the case of the panels heated at 60°. It is thus concluded that moderate heat treatment degrades the corrosion resistance in borate-chloride medium.

Table II

Initial and Two-Hour Polarization Resistance Values
for Silanized Cold-Rolled Steel Specimens*

Silane	Log $R_{p,i}$	Log $R_{p,2h}$
PTS	4.76	4.33
MTS	4.36	4.17
GPTS	4.13	4.16
MPDS	3.84	3.75
DDS	3.54	3.81
HMDS	3.62	3.65
ETS	3.56	3.24
TCS	3.19	3.53
PTMS	3.09	3.18
BLANK	3.09	3.17
DCS	3.03	3.22

*Polarization Resistance in $V/A/cm^2$.

Table III

Initial and Two-Hour Corrosion Potential Values
for Silanized Cold-Rolled Steel Specimens*

Silane	$E_{corr,i}$	$E_{corr,2h}$
PTS	-.202	-.302
MTS	-.326	-.348
GPTS	-.294	-.313
MPDS	-.637	-.675
DDS	-.299	-.439
HMDS	-.260	-.675
ETS	-.322	-.733
TCS	-.270	-.333
PTMS	-.720	-.705
BLANK	-.697	-.690
DCS	-.695	-.715

*Corrosion Potential in Volts vs. SCE.

Table IV

Initial and Two-Hour Polarization Resistance Values for Silanized and Heat Treated Cold-Rolled Steel Specimens*

Silane	Log $R_{p,i}$	Log $R_{p,2h}$
MTS	4.11	4.16
MPDS	3.04	3.30
GPTS	3.51	3.23
DDS	2.89	3.25
PTS	3.03	3.21
ETS	3.55	3.17
PTMS	2.89	3.18
HMDS	3.21	3.15
BLANK	3.13	3.11

*Polarization Resistance in $V/A/cm^2$.

Table V

Initial and Two-Hour Corrosion Potential Values for Silanized and Heat Treated Cold-Rolled Steel Specimens*

Silane	$E_{corr,i}$	$E_{corr,2h}$
MTS	-.516	-.575
MPDS	-.707	-.707
GPTS	-.273	-.678
DDS	-.660	-.673
PTS	-.681	-.697
ETS	-.324	-.685
PTMS	-.864	-.695
HMDS	-.348	-.699
BLANK	-.624	-.699

*Corrosion Potential in Volts vs. SCE.

Additional R_p experiments were conducted on panels that were immersed in 5% organosilane solutions in 95% deionized water/5% absolute MeOH. Table VI shows the results obtained for panels aged in a desiccator at room temperature for 5-7 days. The panels treated in GPTS, DDS and PTMS exhibited significantly higher R_p and E_{corr} values relative to the blank. The remaining silanes performed poorly and did not provide satisfactory corrosion resistance. All R_p values obtained in this series were lower than those obtained in the cases of specimens prepared from the undiluted organosilanes.

Table VI

Initial and Two-Hour Polarization Resistances and Corrosion Potentials for 5%-Silanized Cold-Rolled Steel Specimens

Silane	Log $R_{p,i}$	$E_{corr,i}$	Log $R_{p,2h}$	$E_{corr,2h}$
PTS	3.35	-.233	2.97	-.712
MTS	3.35	-.644	3.24	-.680
GPTS	4.41	-.300	3.92	-.307
MPDS	2.89	-.722	3.22	-.756
DDS	4.03	-.296	3.83	-.316
PTMS	3.91	-.355	3.81	-.424
BLANK	3.13	-.624	3.11	-.699

Polarization Resistance in $V/A/cm^2$.
Corrosion Potential in Volts vs. SCE

Accelerated Rusting

Table VII summarizes the results obtained for the accelerated rusting tests. The silanes are listed in this table according to their performance in the polarization resistance experiments, thus allowing direct comparison of the relative behavior in these two types of tests. The tabulated performance of the DDS-, HMDS- and ETS-treated panels at 7 days is misleading. Steel panels treated with these silanes are not readily wet by methanol or methanol solutions and the result is a localization of the rusting solution on the surface and consequent localized rusting during accelerated testing. When the spreading problem is taken into account, these silanes exhibited poor corrosion resistance under accelerated rusting conditions. The best resistance to corrosion was exhibited by PTS, MTS and GPTS with the MTS-treated panel showing exceptional performance.

Table VII

Percentage of Silanized Steel Surface Covered by Rust
after 2, 7 and 21 Days Accelerated Rusting

Silane	2 Days	7 Days	21 Days
PTS	5	40 d	90 d
MTS	0	1	1
GPTS	5	40 d	100 d
MPDS	35	70	100 d
DDS	1	25 s	85 md
HMDS	0	5 s	40 vd
ETS	1	30 d	100 vd
TCS	100	100 d, f.	100 d, f
PTMS	10	70 d	90 d
BLANK	25	95	100 d
DCS	100	100 d, f	100 d, f

d-dense, md-medium dense, vd-very dense, f-flaky

AC Impedance

Bode plot representations of the impedance data obtained for 7 of the room temperature silanized steel are given in Figures 1 and 2. The MTS-, GPTS- and PTS-treated panels exhibited impedance behavior similar to an equivalent circuit comprised of a resistor in series with a resistor/capacitor in parallel. The most corrosion resistant surface (MTS) exhibited the largest value for the total impedance at the lowest frequency. Ideally, the polarization resistance is equivalent to the value of the total impedance at 0 Hz; therefore, one should be able to estimate the value of R_p from the low frequency intercept of the log Z vs. log f plots. The values of R_p estimated for MTS, GPTS and PTS are in reasonable agreement with those obtained by the polarization resistance technique. The Bode phase plots, along with the impedance plots, indicate capacitive behavior at intermediate frequencies.

Figure 2 gives the Bode plots for 4 silanes exhibiting pseudo-inductive behavior at low frequencies. The Bode magnitude plots reach a maximum about 10^{-1} Hz and the total impedance drops appreciably as the frequency is decreased below this value. The agreement with the R_p values obtained by the polarization technique is fair at the maximum value of the impedance.

Polarization Curves

The cathodic and anodic polarization curves obtained for the PTS-, GPTS- and MTS-treated steels and that for the blank in the borate-chloride medium are given in Figure 3 and 4. The MTS-treated steel exhibited

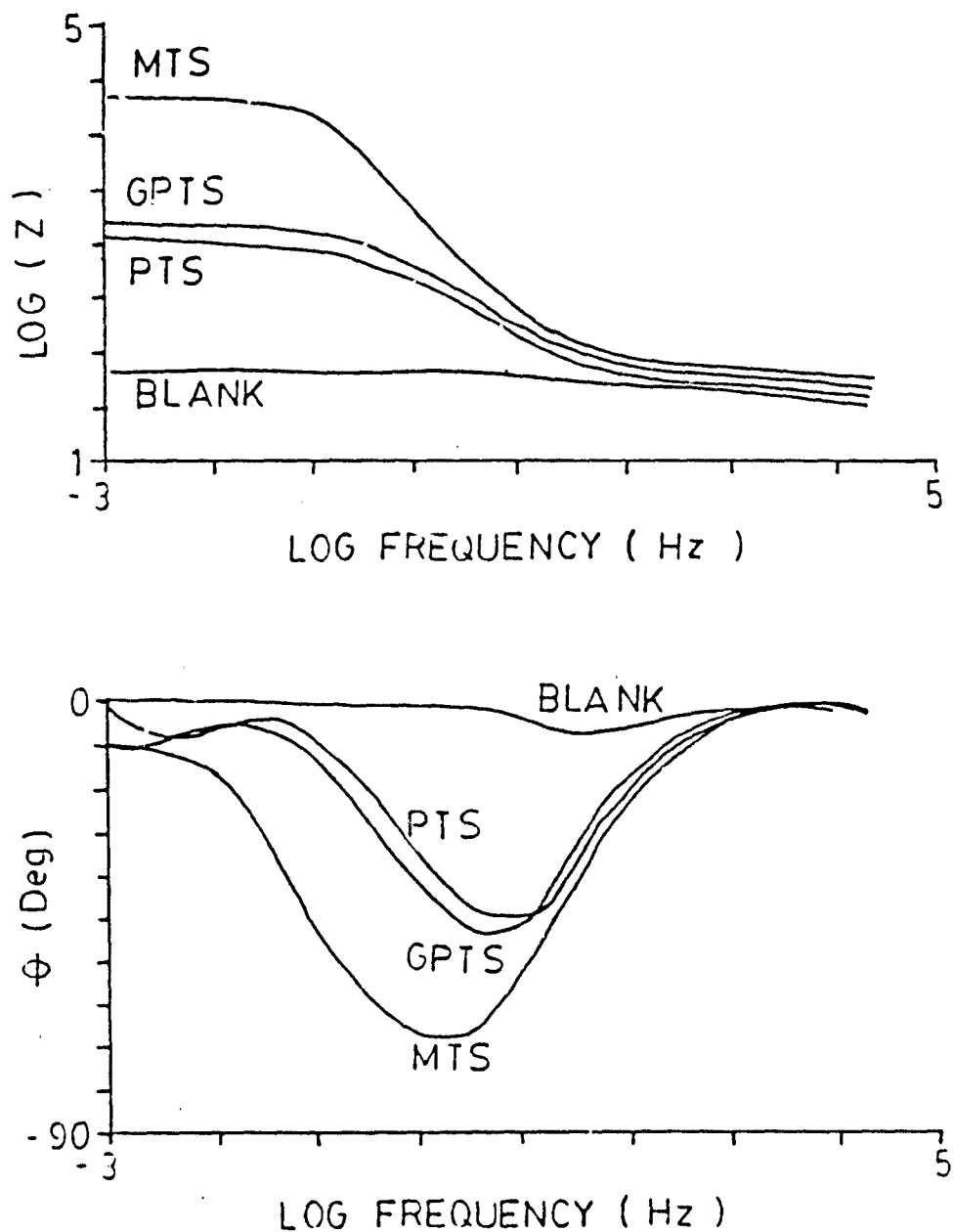


Figure 1. Bode plot representation of the impedance data obtained for room temperature cured non-, MTS-, GPTS- and PTS-treated steel panels in borate-chloride media. (a) Bode-Magnitude; (b) Bode-Phase.

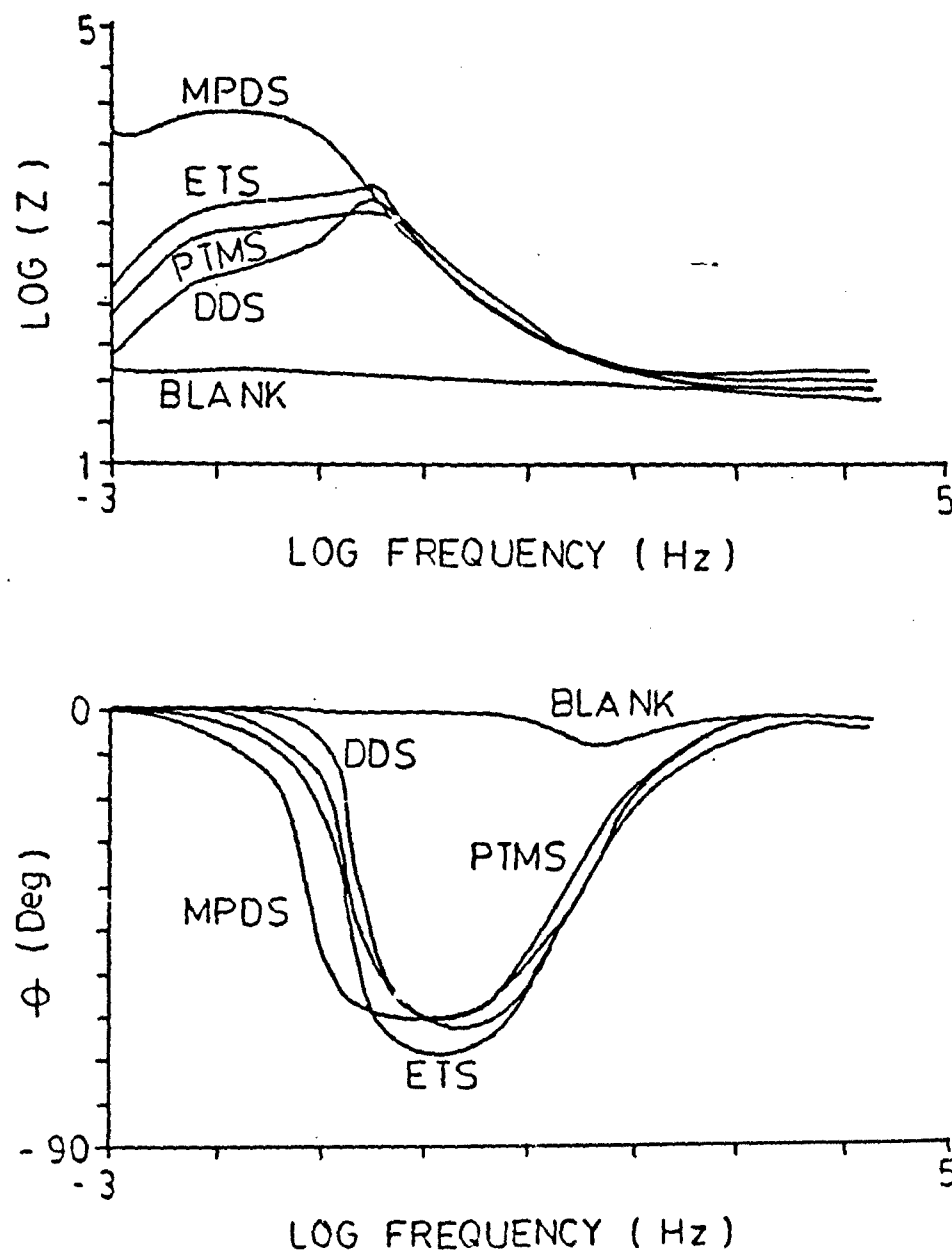


Figure 2. Bode plot representation of the impedance data obtained for room temperature cured non-, ETS-, MPDS-, DDS-, HMDS- and PTMS-treated steel panels in borate-chloride media. (a) Bode-Magnitude; (b) Bode-Phase.

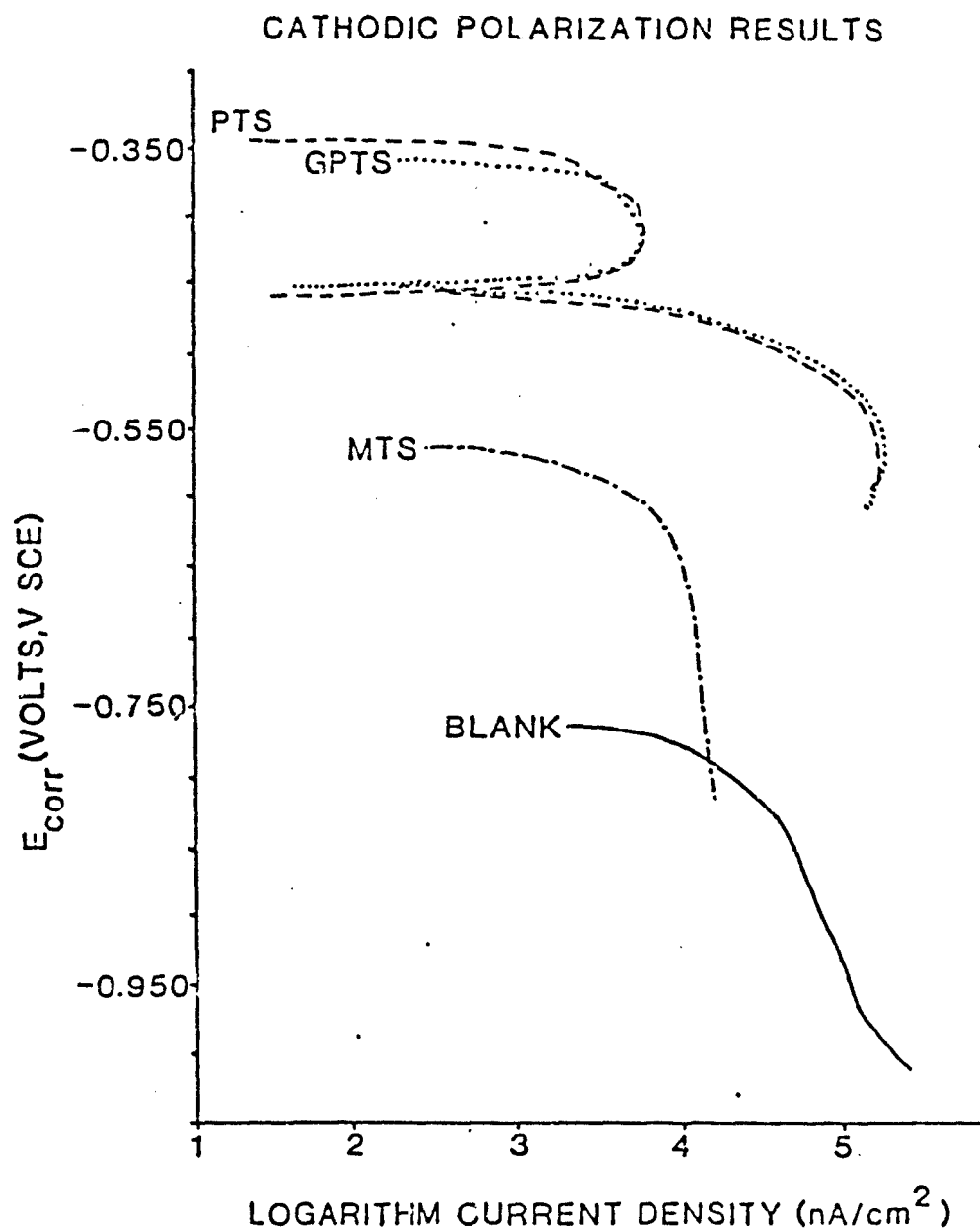


Figure 3. Cathodic polarization curves for MTS-, GPTS-, PTS- and non-silanized steel panels in borate-chloride media.

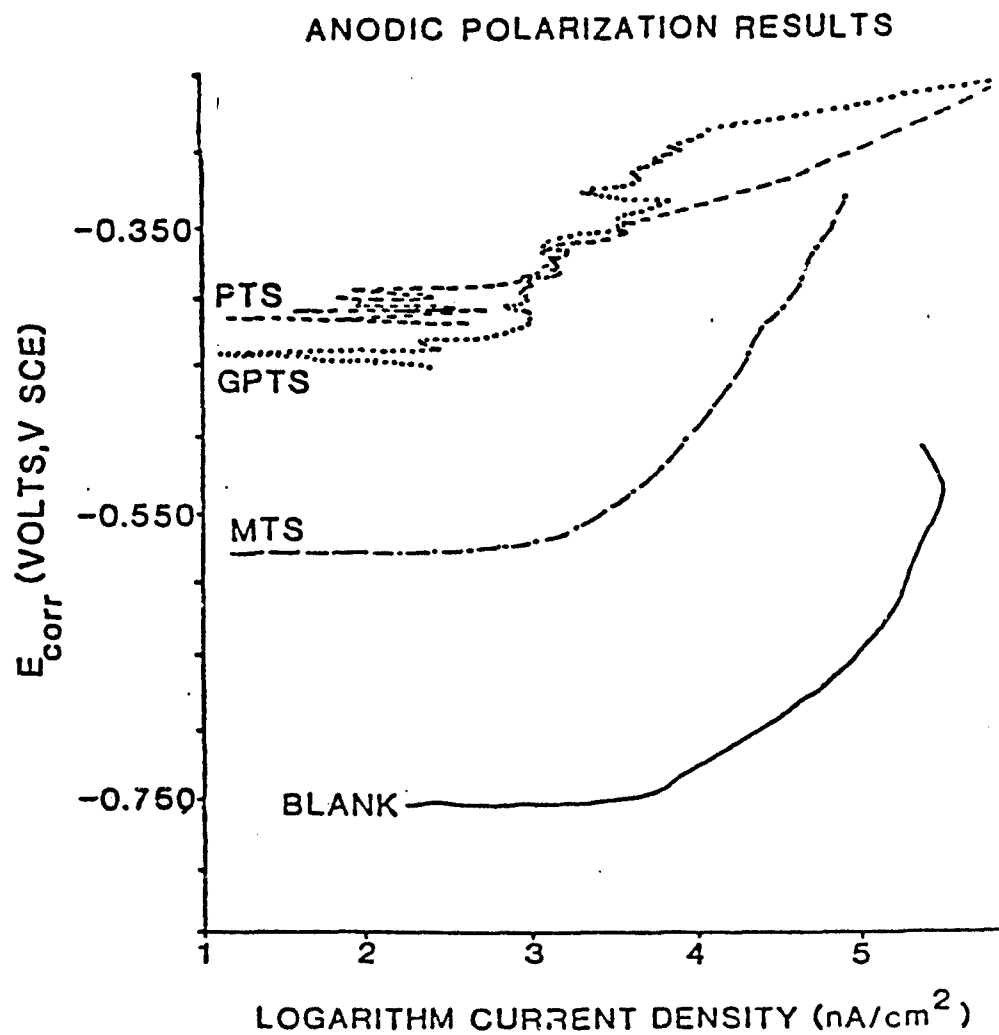


Figure 4. Anodic polarization curves for MTS-, GPTS-, PTS- and non-silanzed steel panels in borate-chloride media.

smooth cathodic and anodic curves with a cathodic current density in the plateau region significantly less than that of the blank.

Cathodic Delamination

Three silanized panels were examined for their ability to alter the cathodic delamination characteristics of polybutadiene-coated steel. Data are reported in Figure 5 for these materials relative to the blank. It will be noted in all three cases, the rates of delamination were slower than that of the blank. The MTS-coated panel was outstanding in that no delamination occurred in approximately 11 hours of exposure.

Surface Analysis

The surface concentrations of O, C, Si, Fe and Cl for the MTS-, GPTS- and PTS-treated and untreated steel, before and after exposure to the borate-chloride medium, as determined by XPS are listed in Table VIII. The concentration of each element was determined from the XPS spectra according to the equation.

$$C_x = [I_x/S_x]/[I_i/S_i] .$$

where C_x is the concentration of the element at the surface, I_x is the peak intensity as defined by the area beneath the peak and S_x is a sensitivity factor (0.63, 0.205, 0.17, 3.8 and 0.48 for O, C, Si, Fe and Cl, resp.). The atomic percentages of these elements in the pure silane are included for comparison purposes.

Inspection of Table VIII reveals that no iron was detected on any of the samples prior to exposure. The lack of an iron signal implies complete coverage by the silanes. After exposure, only the GPTS-treated panel exhibited an iron peak in the XPS spectrum, and the low intensity of the peak indicates that the majority of the surface was still covered. Therefore, all three silanes showed retention on the surface under the conditions used.

XPS spectra for DDS-, HMDS- and PTMS-treated panels yielded iron peaks indicative of the fact that the silane did not cover the entire surface of the steel.

The GPTS-treated panel was also examined by Auger spectroscopy. Complete coverage of the surface by GPTS was indicated by the lack of an iron signal and by a strong signal for silicon. Argon sputtering of the surface led to a decrease in the O, C and Si peaks with time and the development of a bare substrate free of O, C and Si after sputtering for 2.5 min. The sputter rate suggests a silane coating approximately 300 Å in thickness.

Specular reflectance FTIR was used to obtain absorbance spectra for the silanized steel substrates. Table IX gives the vibrational frequencies for the various silanized surfaces. These data, along with the XPS data, provide a basis for a qualitative characterization of the surface.

DELAMINATION OF POLYBUTADIENE
IN 0.5M NaCl AT -0.800v. vs. SCE

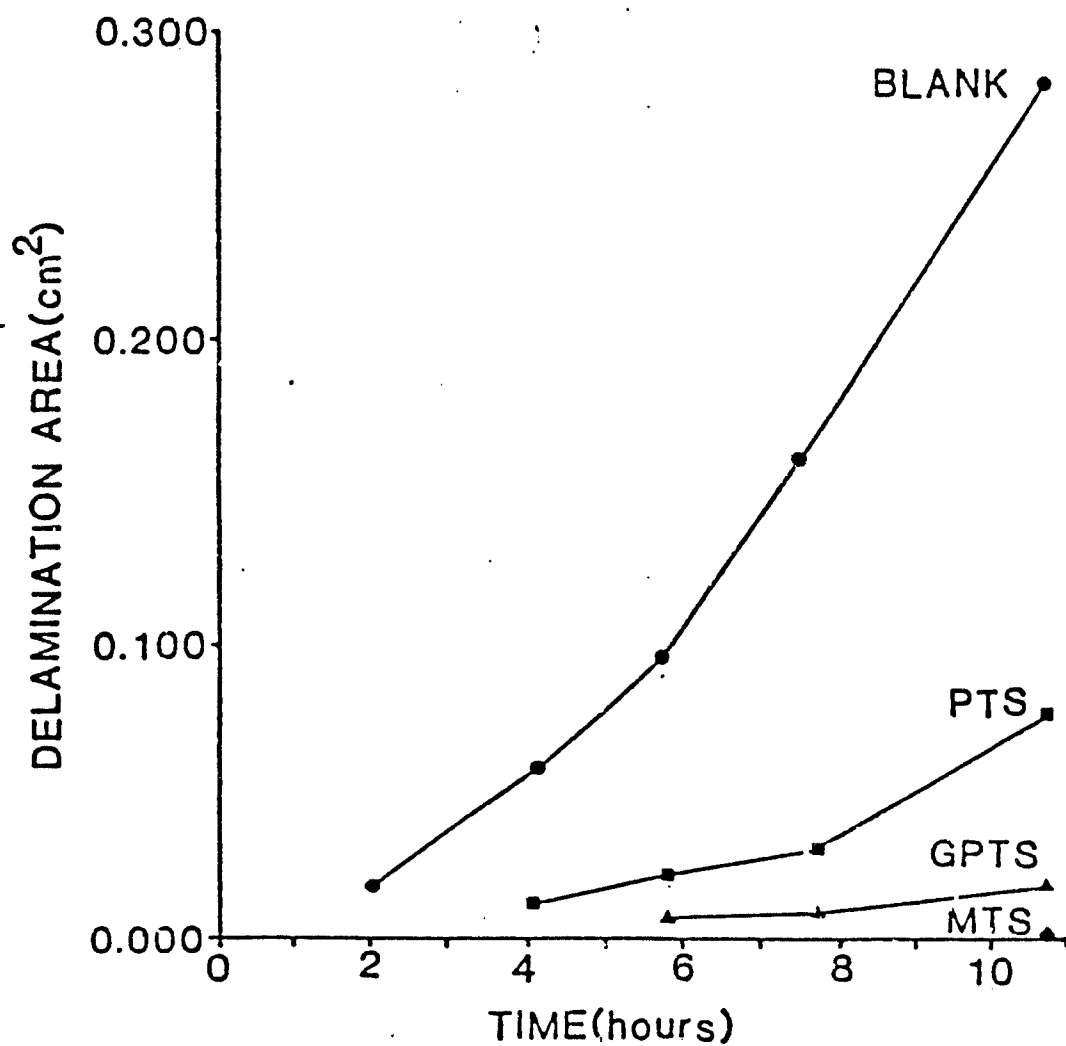


Figure 5. Plots of delaminated area vs. time for polybutadiene coated MTS-, GPTS-, PTS- and non-treated panels exposed to borate-chloride media.

Table VIII
Composition of Silanized and Blank Steel Surfaces as Determined
by XPS Spectroscopy

Specimen	Formula At%	Initial (%)	After 1 h* (%)
BLANK		68.9 C 29.7 O 1.4 Fe	66.7 C 27.0 O 4.7 Fe 1.6 Cl
MTS	43.6 C 50.0 O 6.4 Si	41.0 C 42.6 O 16.4 Si 0.0 Fe	56.1 C 31.8 O 12.1 Si 0.0 Fe 0.0 Cl
PTS	60.0 C 32.9 O 7.1 Si	65.7 C 28.6 O 5.7 Si 0.0 Fe	62.5 C 31.3 O 5.7 Si 0.5 Fe 0.0 Cl
PTS	74.3 C 18.9 O 6.8 Si	75.0 C 19.4 O 5.6 Si 0.0 Fe	70.6 C 16.2 O 13.2 Si 0.0 Fe 0.0 C

*After 1 h exposure to 0.15M borate/0.05M chloride solution.

Table IX

Specular Reflectance FTIR Determined Bonding for Silanized Rolled Steel Substrates

Silane	Bonds (Vibrational Stretch)
PTS	Aromatic C=C, CH ₂ , CH ₃ , SiCH ₂ , SiOSi, SiOC, Si(C ₆ H ₅), SiC, Si(OCH ₃), OH
MTS	OH, OOCCH ₃ , CH ₃ , SiCH ₃ , SiOC, SiC, SiOSi
GPTS	OH, CH ₂ , COC, SiOSi, CH ₃ O, SiOCH ₂ CH ₂ CH ₂ O
PTMS	OH, CH ₃ , C=C, Si(C ₆ H ₅), C ₆ H ₅ R, Si(CH ₃) ₃
MPDS	OH, CH ₃ , CH ₂ , CH ₃ O, SiCH ₃ , SiOCH ₃ , SiOSi, C ₆ H ₅ R, C ₆ H ₅ Si
DDS	OH, CH ₂ , CH ₃ , Si(OCH ₂ CH ₃) ₂ , OH—O
ETS	OH, CH ₃ , CH ₂ , OCH ₂ CH ₃ , SiOH
HMDS	OH, SiOH, CH ₃ , SiCH ₃ , SiOSi, OH—O

DISCUSSION

The data show that steel substrates treated with MTS, PTS and GPTS provide corrosion and cathodic delamination resistance. The surface analysis indicates that these compounds, or their products of reaction, are present on the surface and remain on the surface after a 1-h exposure to the borate-chloride electrolyte. The FTIR spectra for these systems show the presence of Si-O-Si bonding in addition to Si-R bonding. All the data support the concept that the silanes are uniformly distributed on the steel surface and that the silane layer consists of a cross-linked polymer network. The other silanes afforded the substrate moderate-to-poor corrosion protection and did not exhibit spectral features characteristic of polymerization. The XPS spectra for these silanized panels revealed the presence of iron, thus suggesting incomplete coverage. The FTIR spectra were relatively weak in further support of the idea that the silane was not present at the surface in significant amounts. The HMDS-treated panel did exhibit a weak Si-O-Si peak but this peak is probably characteristic of the parent silane and not to cross-linking. The poor performance of the latter group is directly related to inadequate coverage and the absence of cross-linking and polymerization of the silane.

The XPS and FTIR spectra of the MTS-, PTS- and GPTS-treated steel also provide information regarding the bonding mechanisms of the silanes with the substrate. Table VIII compares the atomic composition of the silane with the composition of the silanized surface prior to and after exposure to the electrolyte. The data suggest that the silanes are bound to the surface with a loss of single acetoxy and methoxy groups. Comparison of the atomic composition of the silane with the composition of the product on the surface after 1 h exposure to the electrolyte indicates a large increase in the concentration of Si. These data are supportive of the concept of polymerization with the development of Si-O-Si bonds.

The FTIR spectra exhibit peaks which may be associated with the presence of Si-O-X and R-O-X groups, where X may be Si, a halide or Fe. The determination of the nature of the X group is not readily made. If the peaks are representative of R-O-Fe groups, there is the likelihood that the silanes are both singly and doubly bound to the surface, with freed acetoxy and methoxy groups also binding to the surface. The net change in overall composition is probably the result of the loss of a single group though multiple silane bonds are present. Figure 6(a) gives our concept of the method of bonding of PTS, MTS and GPTS to the steel substrate; Figure 6(b) is a representation of bonding between PTS, MTS, and GPTS and polybutadiene.

One important aspect of the bonding of these silanes to the substrate is the possibility of direct interaction between organic moieties and surface hydroxyl groups on the iron. The oxygens of the acetoxy groups of MTS and the glycidoxypentyl chain of GPTS may hydrogen bond with the hydroxylated surface. The phenyl groups of PTS are also capable of undergoing interactions with surface oxygens [2]. Each of these interactions presumably helps to stabilize the silanized surface and to provide greater surface coverage and better corrosion protection.

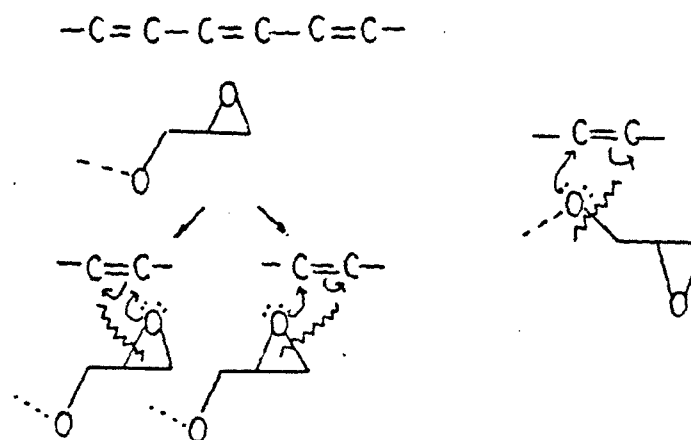
[illegible]

The diagram illustrates the cyclization of a linear siloxane chain. The top part shows a linear chain with a carboxylic acid group (HO-C(=O)-Me) and a carboxylate group (Me-C(=O)-O-Si-Me). The bottom part shows the resulting cyclic structure, a 6-membered ring containing two silicon atoms and two oxygen atoms, with two methyl groups and two acetoxy groups attached to the silicon atoms. A curved arrow indicates the nucleophilic attack of the hydroxyl group on the carbonyl carbon of the acetoxy group.

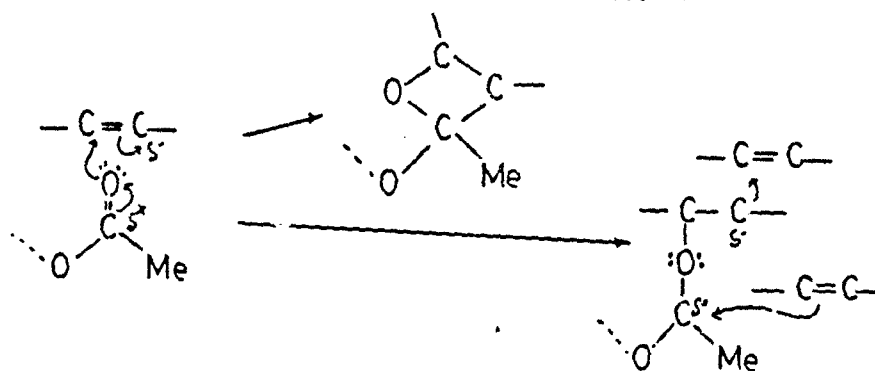
The top structure shows a poly(oxazoline) chain with pendant oxazoline rings. The chain is represented by a horizontal line with vertical bonds to oxygen atoms. The pendant oxazoline rings are shown as five-membered rings with an oxygen atom and a nitrogen atom. The nitrogen atom is bonded to a methyl group (Me) and a hydrogen atom (H). The oxygen atom is bonded to the chain and a hydrogen atom (H). The bottom structure shows a poly(oxazoline) chain with pendant oxazoline rings. The chain is represented by a horizontal line with vertical bonds to oxygen atoms. The pendant oxazoline rings are shown as five-membered rings with an oxygen atom and a nitrogen atom. The nitrogen atom is bonded to a methyl group (Me) and a hydrogen atom (H). The oxygen atom is bonded to the chain and a hydrogen atom (H).

-111-

A. GPTS / POLYBUTADIENE INTERACTIONS



B. MTS / POLYBUTADIENE INTERACTIONS



C. PTS / POLYBUTADIENE INTERACTIONS

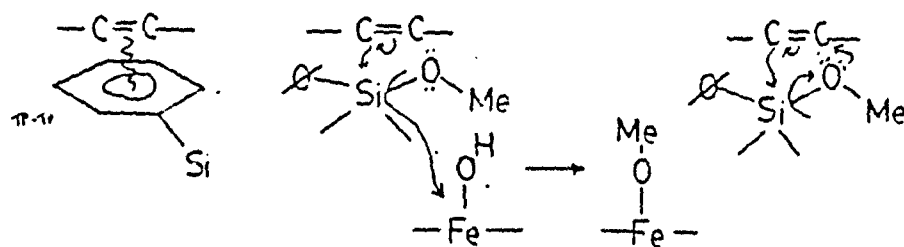


Figure 6(b). Schematic representation of bonding between PTS, MTS and GPTS and polybutadiene.

The effect of surface coverage and silane stability on the electrochemical behavior of silanized steel can be seen from the AC impedance and polarization resistance data. The Bode-magnitude plot for MTS, PTS and GPTS show a region of frequency-independent behavior at low frequencies and a linear region with a slope of about -1 at intermediate frequencies. The low frequency behavior can be represented by the sum of the resistances within the electrochemical system. The solution resistance is normally small relative to R_p ; therefore, the intercept of the curve at 0 Hz is approximately R_p . The second segment of the curve is represented by a resistor and capacitor in parallel. Therefore, the Bode plots show that the silanes impart capacitive components to the electrochemical responses of the systems. The magnitude of these capacitive components can be seen in the Bode-phase plots. A phase angle of 90° indicates capacitive behavior while a 0° phase angle implies the system is resistive in nature. GPTS- and PTS-treated samples showed nearly identical magnitude and phase responses while the MTS-panel exhibited a greater capacitive component and a larger value for R_p . The greater capacitance and larger R_p for MTS indicates more complete coverage and is consistent with a higher degree of corrosion resistance than GPTS and PTS.

The Bode plots for the remaining silanes exhibited decreasing values for $\log Z$ and positive values for the phase angle as the frequency falls below 1 Hz. This behavior is indicative of systems exhibiting a pseudo-inductance as a result of the development of an electromagnetic field on the surface. Pseudo-inductive behavior is commonly observed when the metal substrate is "seen" through a thin surface coating. These plots would therefore indicate that the substrate is "peaking-through" the silane layer as a result of incomplete coverage. These silanes do impart some capacitance to the surface but the effects are felt over a narrower frequency range than observed for MTS-, PTS- and GPTS-treated samples.

The polarization resistance and corrosion potential data for the test silanes confirm the AC impedance findings. Those systems which exhibited highly capacitive characteristics at intermediate frequencies and large values for the total impedance at low frequencies also exhibited the most noble corrosion potentials and the largest values for R_p . These findings are not unexpected, for a noble E_{corr} is often representative of a system in the passive state which, in turn, implies a relatively low corrosion current. The low corrosion current and highly capacitive nature of the silane layer indicates a high degree of protection and therefore a large value for R_p . Likewise, those systems exhibiting pseudo-inductive behavior would be expected to support a higher corrosion current, have more active corrosion potentials than the corrosion resistant systems and therefore lower R_p values. A comparison of the impedance and R_p data confirm these expectations.

The stability of the silanized surfaces was also shown as an outcome of the potentiodynamic measurements. The systems which had shown good corrosion resistance (GPTS, PTS and MTS) showed only minor changes in E_{corr} and in R_p after 2 h exposure to chloride. The systems showing only moderate degrees of corrosion resistance (MPDS, DDS and HMDS) exhibited negative shifts in E_{corr} approaching that of the substrate. This shift suggests rapid breakdown of the protective nature of the silane layer. No large shifts in R_p were observed for GPTS, MTS and PTS indicating that the silane layer had not significantly changed during exposure.

The polarization resistance studies also showed that dilute (5%) silane solutions, while reportedly providing optimum coupling characteristics, provide only transient improvement in the corrosion resistance of the substrate. The poor performance of these systems can be attributed to poor or incomplete surface coverage due to increased competition with water and methanol for surface sites and increased polymerization of the silane in the solution itself. PTMS and GPTS did afford some degree of protection due to the ability of the phenyl and glycidoxypentyl groups to "lay down" on the surface. DDS also showed transient improvement in corrosion performance due to the increased rate of ethoxy hydrolysis and, therefore, a higher rate of interaction with the surface [3].

The ability of a coupling agent to improve the adhesion of an organic coating to a metal is dependent upon the adhesive properties at both the substrate/agent and agent/coating interfaces. If there is any sign of instability at either interface, poor adhesion would be expected. The electrochemical and rusting data obtained for test silanes showed that only GPTS, MTS and PTS form stable, protective polymeric coatings on mild steel. Therefore, cathodic delamination studies were only carried out for these systems. The delamination data show that MTS afforded the greatest degree of delamination resistance. The good performance of MTS can be attributed to the corrosion resistance of the surface (MTS-treated steel exhibited large values for R_p and a low rate of oxygen reduction), the number of Fe-O-Si bonds formed during silanization (1 or 2 per molecule) and the formation of strong bonds between acetoxypentyl groups of the silane and the diene carbons of the coating. In addition, XPS and FTIR data suggest that presence of acetoxypentyl groups bound directly to the surface thereby increasing the number of coating/substrate linkages. Thus it is the ability of the MTS-treated system to inhibit the corrosion reaction combined with strong adhesion at both the substrate/silane and silane/coating interfaces which affords the system good delamination resistance.

GPTS and PTS were also observed to improve the delamination resistance of polybutadiene-coated steel; however, the degree of improvement was somewhat less than that for MTS. The differences in performance can be attributed to lower R_p values, a decrease in the number of silane/substrate bonds, and weaker silane/polymer interactions (methoxy rather than acetoxypentyl). GPTS can also form relatively stable bonds with the polymer through the interaction of the oxygens of the glycidoxypentyl chain with the carbons of the butadiene molecule. This second mode of direct bonding between substrate and coating probably accounts for the greater degree of delamination resistance observed for GPTS.

ACKNOWLEDGEMENT

We are grateful to Robert Hart for preparing some of the XPS spectra and to Gary W. Simmons for assistance in the interpretation of the spectra. We are also grateful to Thomas Lane for discussions relative to the properties of silanes.

REFERENCES

- [1] R. D. Granata, M. A. De Crosta, and H. Leidheiser, Jr., "Corrosion and Coating Delamination Properties of Steel Ion-Implanted with Aluminum and Titanium," Proceedings of the International Congress on Metallic Corrosion, Toronto, Canada, June 3-7, 1984, pp. 264-68.
- [2] Thomas Lane, private communication.
- [3] I. L. Singer, R. N. Bolster and J. A. Sprague, J. Appl. Phys. 58(3), 1255 (1985).

SECTION - #7

Ionic Migration through Organic Coatings and Its Consequences to Corrosion

Principal Investigator: Henry Leidheiser, Jr.
Associate: Jeffrey Parks (Ph.D. awarded)

ABSTRACT

The migration rates of sodium, chloride and cesium ions through an alkyd topcoat, an alkyd topcoat plus primer and polybutadiene on steel were determined. Coated samples of steel were exposed to 0.5M solutions of ions doped with trace amounts of ^{22}Na , ^{36}Cl and ^{137}Cs and the residual radiation in the coating was measured. Migration coefficients were calculated for open circuit and cathodic polarization (-0.80 v vs. Ag/AgCl) conditions for the coating with and without an intentionally scribed defect. Polarization resulted in a 3- to 28-fold increase in ion uptake. The major pathway for ionic motion under cathodic polarization conditions was through the coating. Lateral motion from the defect to the delamination front appeared to be the principal transport pathway at open circuit. The ion flux through the coating was sufficient to account for the observed delamination rate at -0.80 v when certain assumptions were made.

INTRODUCTION

Paints applied to metal surfaces provide corrosion protection by introducing a barrier to ionic transport and electrical conduction. When a painted metal is exposed to electrolyte, there is a gradual reduction in barrier protection as water, oxygen and electrolyte penetrate the coating. Defects within the coating introduce direct pathways for environmental species to reach the metal substrate resulting in the localized loss of barrier protection. The corrosion of the exposed metal can be prevented by cathodically polarizing the substrate. Under these conditions, however, many coating systems have been observed to separate from the substrate radially about the defect. This so-called "cathodic delamination" of a coating from a metal is accompanied by a further reduction in barrier protection. The loss of corrosion protection due to the onset of delamination is a widely recognized problem, particularly during the cathodic protection of damaged coated metal pipelines and the electroless plating of photoresist-coated metal substrates (Leidheiser et al., 1985).

Cathodic delamination has been the subject of a number of publications from this laboratory in recent years (Leidheiser, 1980, 1981; Leidheiser and Wang, 1981; Leidheiser et al., 1983), and a comprehensive mechanism for the disbondment process has been developed (Dickie et al., 1981; Koehler, 1984; Leidheiser et al., 1983; Watts and Castle, 1983). The

applied cathodic potential results in the activation of the cathodic reaction immediately at the defect and at the boundary between the coating and the metal. At moderate applied potentials in aerated electrolytes, the oxygen reduction reaction, $\text{H}_2\text{O} + 1/2\text{O}_2 + 2\text{e}^- = 2\text{OH}^-$, is the dominant reaction. In deaerated solutions or at more negative potentials, the hydrogen evolution reaction occurs, $2\text{H}^+ + 2\text{e}^- = \text{H}_2$. Both reactions lead to the development of a very alkaline environment at the boundary between the coating and the metal and the bond between the coating and the metal is broken. The pH at this site may be as high as 14 (McIntyre; Ritter and Kruger, 1980).

Two important questions remain unresolved. The first unresolved question relates to the mechanism by which the bond is broken and diverse views abound (Dickie et al., 1981; Koehler, 1984; Leidheiser et al., 1983; Watts and Castle, 1983). This question will not be treated in the present article. The second unresolved question relates to the route by which the charge-carrying cations reach the site where the OH^- ions are formed. It is this matter which the present study addresses.

The major purpose of this work is to determine the effect of an imposed defect and an applied potential on ionic transport through three types of organic coatings on steel. By correlating ionic transport with observed cathodic delamination rates, the question as to whether there is a sufficient number of cations penetrating the coating to support delamination is also addressed.

EXPERIMENTAL

Two cations, Na^+ and Cs^+ , and one anion, Cl^- , were selected for study since convenient radiotracers of these elements are readily available in the form of ^{22}Na , ^{137}Cs , and ^{36}Cl . Half molar solutions of NaCl , doped with both ^{22}Na and ^{36}Cl , and CsCl solutions doped with ^{137}Cs only were prepared and calibration curves correlating radiotracer counts with ion concentrations were constructed. A Nuclear Chicago Model 132A well scintillation counter was used to detect the gamma radiation from ^{22}Na and ^{137}Cs and a Nuclear Chicago Model 157 radiation detector was used to detect the beta radiation from ^{22}Na and ^{36}Cl .

The determination of ion uptake by the coated metal was carried out in the cell shown in Figure 1. A polyethylene cylinder, 1.4 cm in diameter, was secured to the flat test specimen using an epoxy cement. The doped electrolyte was introduced and the coating was exposed to the electrolyte for one hour. The electrolyte was removed, the cell was rinsed 10 times with distilled water and the surface of the coating was dried with a paper tissue. The radiation remaining in the cell was determined and the electrolyte was then returned to the cell and the procedure was repeated after each exposure period. The experiment was terminated when rust spots, blistering or severe de-adhesion was observed.

Three coating systems were selected for study on the basis of prior experience in cathodic delamination studies: (1) an alkyd topcoat (Rust-o-Leum #7791), (2) the #7791 topcoat in conjunction with a primer coat

(Rust-o-Leum #7773), and (3) polybutadiene. The coatings were spin coated onto degreased and abraded cold rolled steel panels and the coating thickness was measured with a magnetic thickness gauge after curing. The alkyd coatings were cured at room temperature for no less than 1 week prior to testing. For plates with a primer coat, the topcoat was applied 24 hours after the primer. Polybutadiene was oxidatively cured at 200°C for 20 minutes. Ion uptake was studied both on coatings which were presumed to be defect free and those into which a 3 mm diameter defect had been scribed. The delamination of the samples with the defect was monitored and the rate of delamination was determined.

The delaminated area could be seen visually without destroying the sample in the case of polybutadiene because this coating is transparent. The alkyd coatings, however, were opaque and the coating had to be destroyed in each test. The method for determining the delaminated area was as follows. After removing the specimen from the electrolyte, it was dried and then stored in a desiccator for 24 hours before touching adhesive tape to the surface and determining the area that disbonded. This procedure had to be followed with the alkyd coatings because the poor wet adhesion properties allowed the entire coating to be removed by the tape and the boundary of the cathodically delaminated region could not readily be measured.

Ion uptake and delamination rates were determined both on samples which were not polarized and those which were cathodically polarized to a potential of -0.80 v using the combination counter-reference electrode depicted in Figure 1. Constant potentials were maintained using the simple potentiostat designed by Baboian et al. (1979). All potentials are given with respect to the Ag/AgCl reference electrode. Since ionic uptake by the coating has been measured with and without an applied potential and with and without an intentional defect in the coating, the use of the term, "diffusion," appears inappropriate. We have adopted the terms, "migration" and "migration coefficient," in order to take account of the fact that the transport mechanism may involve factors other than simple diffusion.

In order that experiments carried out under different conditions can be compared, approximate values of the migration coefficient of the ions in the coating were determined. The flux M is defined by:

$$M = \frac{1}{A} \cdot \frac{d(\text{no. moles})}{dt}$$

and the migration coefficient M becomes

$$M = \frac{1}{A} \frac{d(\text{no. moles})}{dt} \cdot \frac{l}{C}$$

where A is the area exposed, l is the thickness of the coating, and C is the ion concentration in the bulk solution, 5.0×10^{-4} moles/cm³.

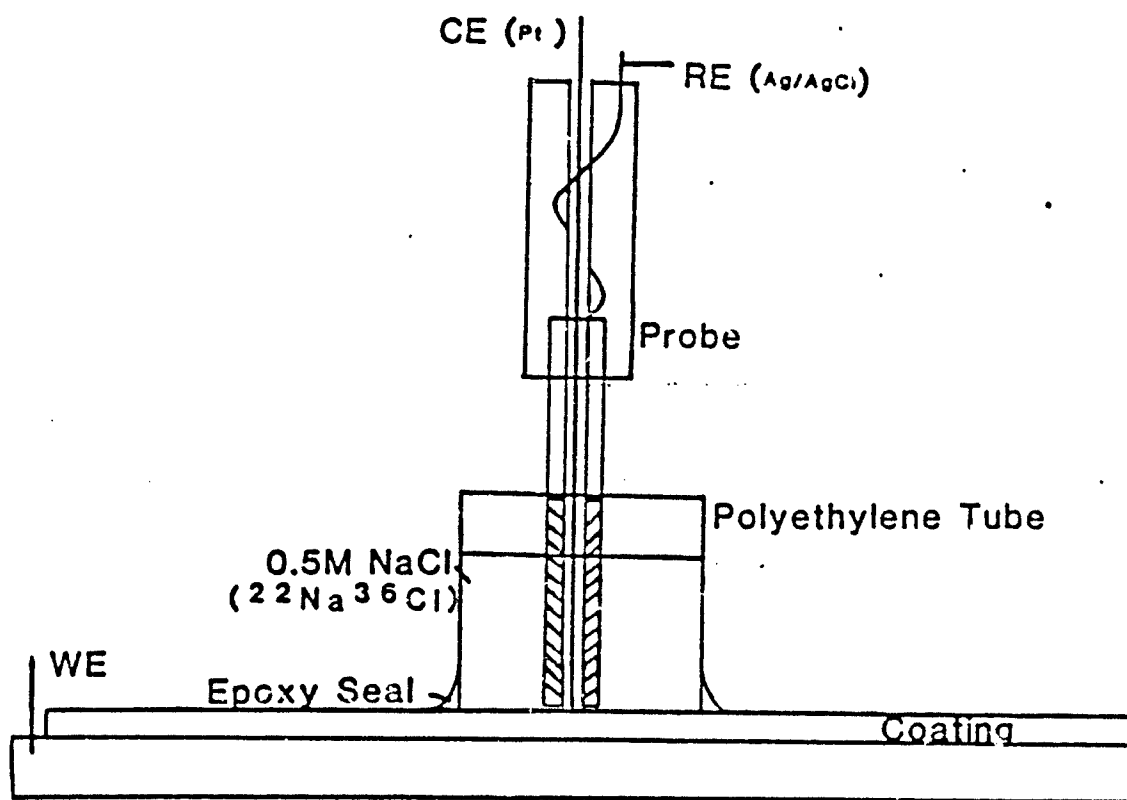


Figure 1. Cell used in the ion uptake measurements. The potential was applied between the counter electrode (CE) and the substrate working electrode (WE) and the potential was measured by means of a silver/silver chloride reference electrode (RE) compactly packaged within a probe.

RESULTS

Typical ion uptake rates for the alkyd coating systems are shown in Figures 2 and 3 and for polybutadiene in Figures 4 and 5.

The calculated migration coefficients for Na^+ , Cs^+ and Cl^- migration into the three coating systems are summarized in Table I for defect-free coatings. The migration coefficients have been normalized by dividing the calculated value by the thickness of the coating, in mils, in order to minimize differences resulting from differences in thickness. The data are thus comparative, but not absolute in value. This manner of presentation has been selected so as to be comparable with much diffusion data through free films as found in the literature. Table II summarizes similar data for the coatings into which the 3 mm defect was introduced.

The precision of the migration coefficients given in Tables I and II represents the standard deviation from the mean when the coefficient was determined for a large number of samples. These values ranged from 20 to 65% of the mean. When too few samples were used to obtain a standard deviation, no precision is given and the result is a simple average value.

Data showing the rates of delamination of the three coating systems while immersed in 0.5M CsCl , both with and without an applied cathodic potential, are summarized in Figures 6, 7 and 8. The lines drawn in Figures 6 and 8 have been drawn in a linear fashion and have been extended to the horizontal axis. This procedure has been followed to permit a comparison of the "delay times" as defined in previous work (Wang and Leidheiser, 1984). The non-linear behavior with the alkyd topcoat in Figure 7 may be a consequence of the fact that this coating exhibits poor wet adhesion.

The total cation uptake as a function of delaminated area for measurements made at open circuit and at -0.80 v is summarized for the three coating systems in Figures 9, 10 and 11. It is striking that the slopes of these curves are similar at both open circuit and at -0.80 v in all three coating systems.

DISCUSSION

It is apparent from the data summarized in Table I that all three ions, Na^+ , Cs^+ and Cl^- , migrate through the three coatings when the boundary condition is a 0.5M solution of the alkali metal chloride. The rates under open circuit conditions yield values of the migration coefficient in the range of 10^{-10} to 10^{-8} $\text{cm}^2/\text{hr}/\text{mil}$. These values are in the same range as values obtained for the diffusion of ions through free films. For example, representative values from the literature are summarized in Table III.

The effect of polarizing the substrate to -0.80 v, a value approximately 250 mV cathodic to the corrosion potential, on the calculated migration coefficient, is summarized in Table IV. It is apparent that the

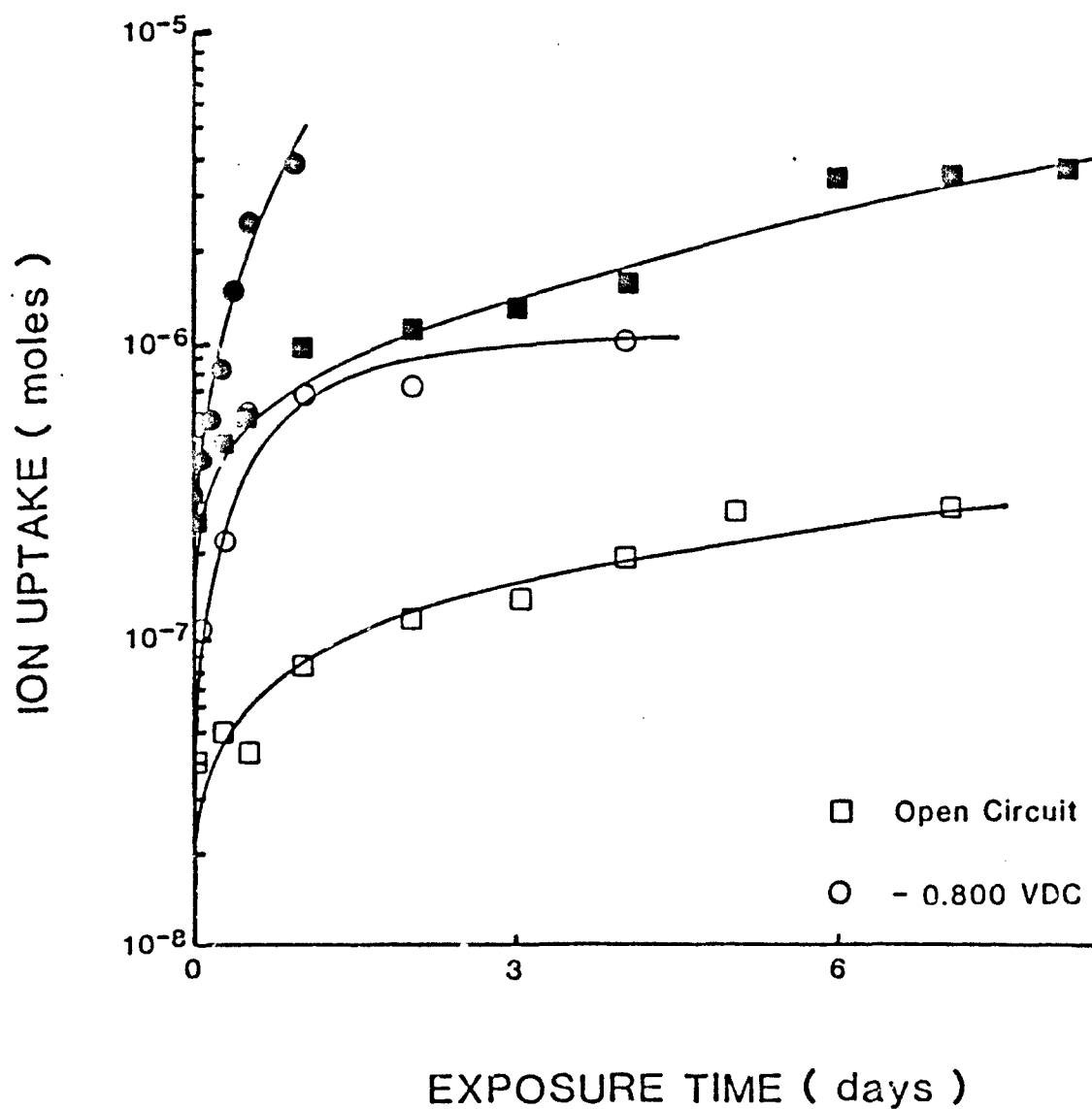


Figure 2. Representative measurements of $^{137}\text{Cs}^+$ uptake by an alkyd topcoat plus primer on a steel substrate during exposure to 0.5M CsCl solution. Coating thickness ranged from 57.7 to 65.9 μm . Open symbols represent defect-free coatings and solid symbols represent coatings into which a 3 mm defect was introduced. Data obtained under open circuit conditions and with an applied potential of -0.80 v are given.

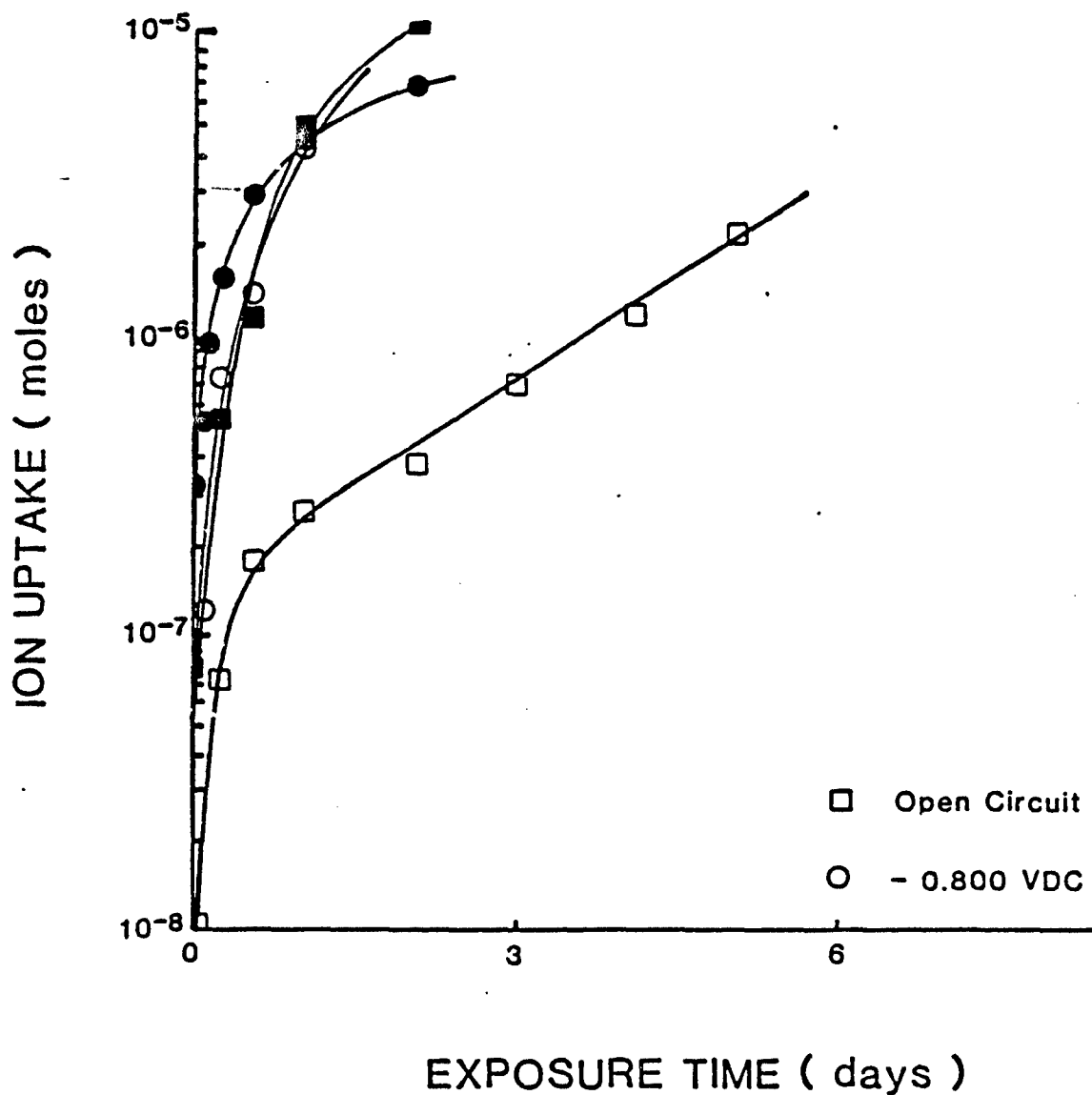


Figure 3. Representative measurements of $^{137}\text{Cs}^+$ uptake by an alkyd top-coat, 25.4–38.0 μm in thickness, during exposure to 0.5M CsCl solution. Open symbols represent defect-free coatings and solid symbols represent coatings into which a 3 mm defect was introduced. Data obtained under open circuit conditions and with an applied potential of -0.80 v are given.

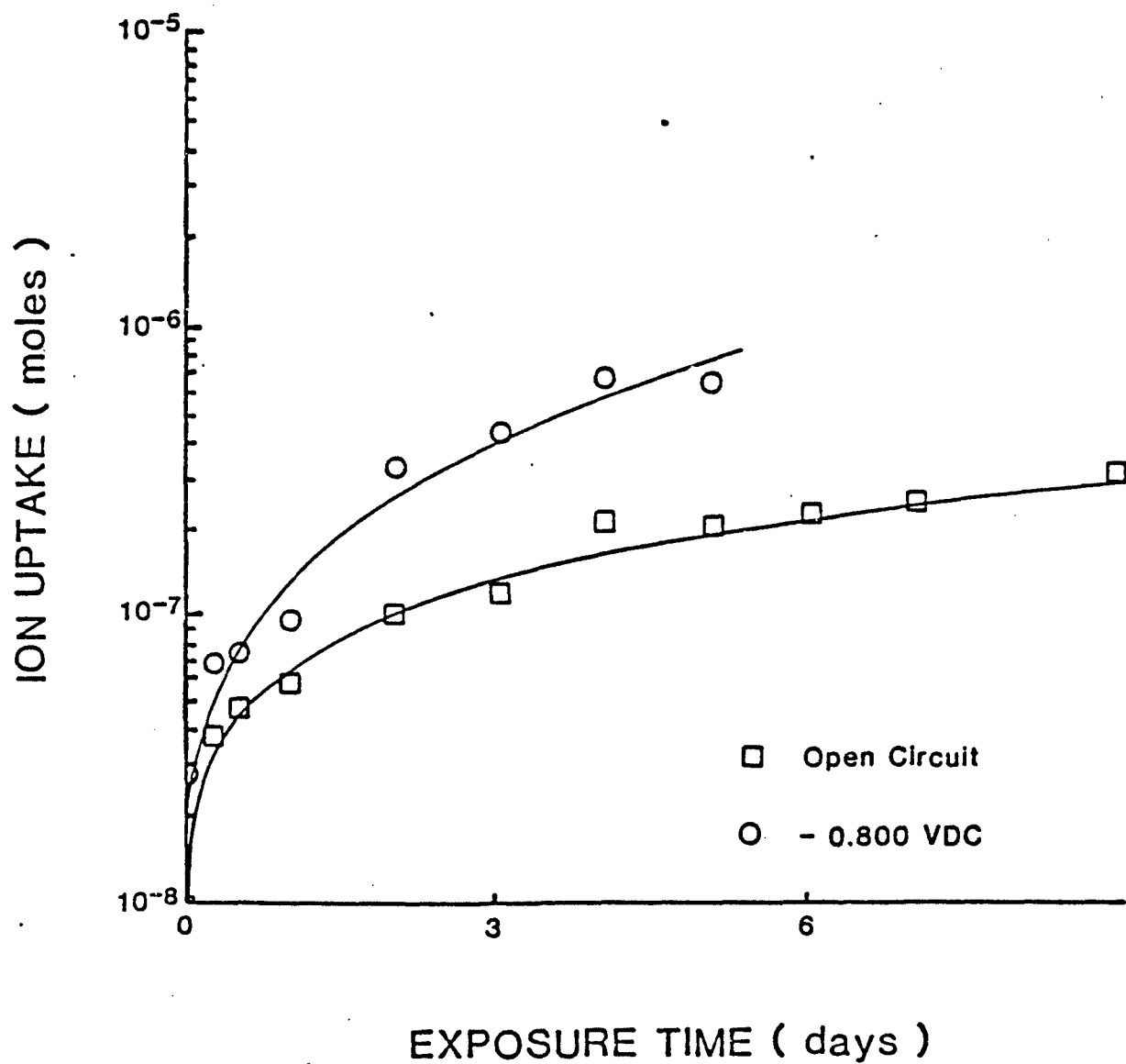


Figure 4. Representative measurements of ^{137}Cs uptake by a defect-free polybutadiene coating, 16.3 μm thick, on a steel substrate during exposure to a 0.5M CsCl solution. Data obtained under open circuit conditions and with an applied potential of -0.80 v are given.

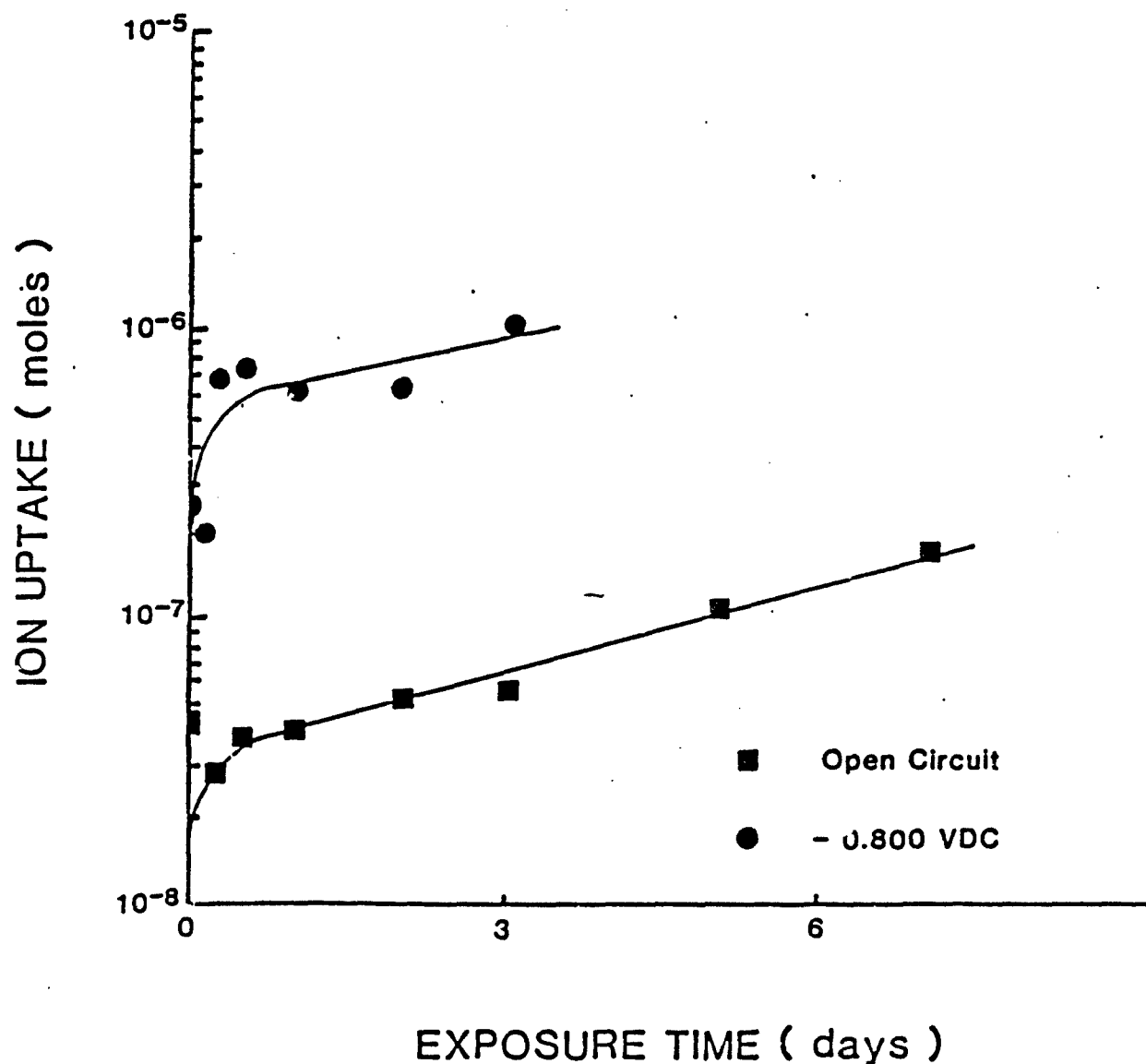


Figure 5. Representative measurements of ^{137}Cs uptake by a polybutadiene coating, 18.4–19.7 μm thick, on a steel substrate during exposure to a 0.5M CsCl solution under conditions where a 3 mm diameter defect was introduced into the coating. Data obtained under open circuit conditions and with an applied potential of -0.80 v are given.

Table I
Calculated Migration Coefficients for the Migration of Ions into
Defect-Free Coatings on Steel

<u>Coating System</u>	<u>Applied Potential</u>	Normalized Migration Coefficient ($\text{cm}^2/\text{hr}/\text{mil}$)		
		Na^+	Cs^+	Cl^-
Alkyd Topcoat	Open Circuit	$4.6 \pm 3.0 \times 10^{-8}$	$8.9 \pm 0.6 \times 10^{-8}$	$1.5 \pm 0.8 \times 10^{-8}$
	-0.80 v	$3.5 \pm 0.7 \times 10^{-7}$	5.7×10^{-7}	$4.4 \pm 0.9 \times 10^{-8}$
Alkyd Topcoat Plus Primer	Open Circuit	$3.2 \pm 0.9 \times 10^{-9}$	2.0×10^{-9}	$7.2 \pm 1.4 \times 10^{-10}$
	-0.80 v	$4.7 \pm 2.4 \times 10^{-8}$	$3.2 \pm 0.2 \times 10^{-8}$	$1.8 \pm 0.9 \times 10^{-8}$
Pclybutadiene	Open Circuit	1.8×10^{-9}	1.7×10^{-9}	5.4×10^{-10}
	-0.80 v	3.7×10^{-8}	2.0×10^{-8}	1.5×10^{-8}

Table II

Calculated Migration Coefficients for the Migration of Ions into
Coatings on Steel in which a 3 mm Defect Was Introduced

Coating System	Applied Potential	Normalized Migration Coefficient ($\text{cm}^2/\text{hr}/\text{mil}$)			
		Na^+	Cs^+	Cl^-	
Alkyd Topcoat	Open Circuit	4.5	$\times 10^{-7}$	7.6	$\times 10^{-7}$
	-0.80 v	3.3	$\times 10^{-7}$	4.6	$\times 10^{-7}$
Alkyd Topcoat Plus Primer	Open Circuit	$9.3 \pm 3.2 \times 10^{-8}$		$8.7 \pm 5.1 \times 10^{-8}$	3.1×10^{-8}
	-0.80 v	9.8	$\times 10^{-8}$	6.3	$\times 10^{-7}$
Polybutadiene	Open Circuit	9.0	$\times 10^{-9}$	4.4	$\times 10^{-9}$
	-0.80 v	6.6	$\times 10^{-8}$	3.0	$\times 10^{-8}$

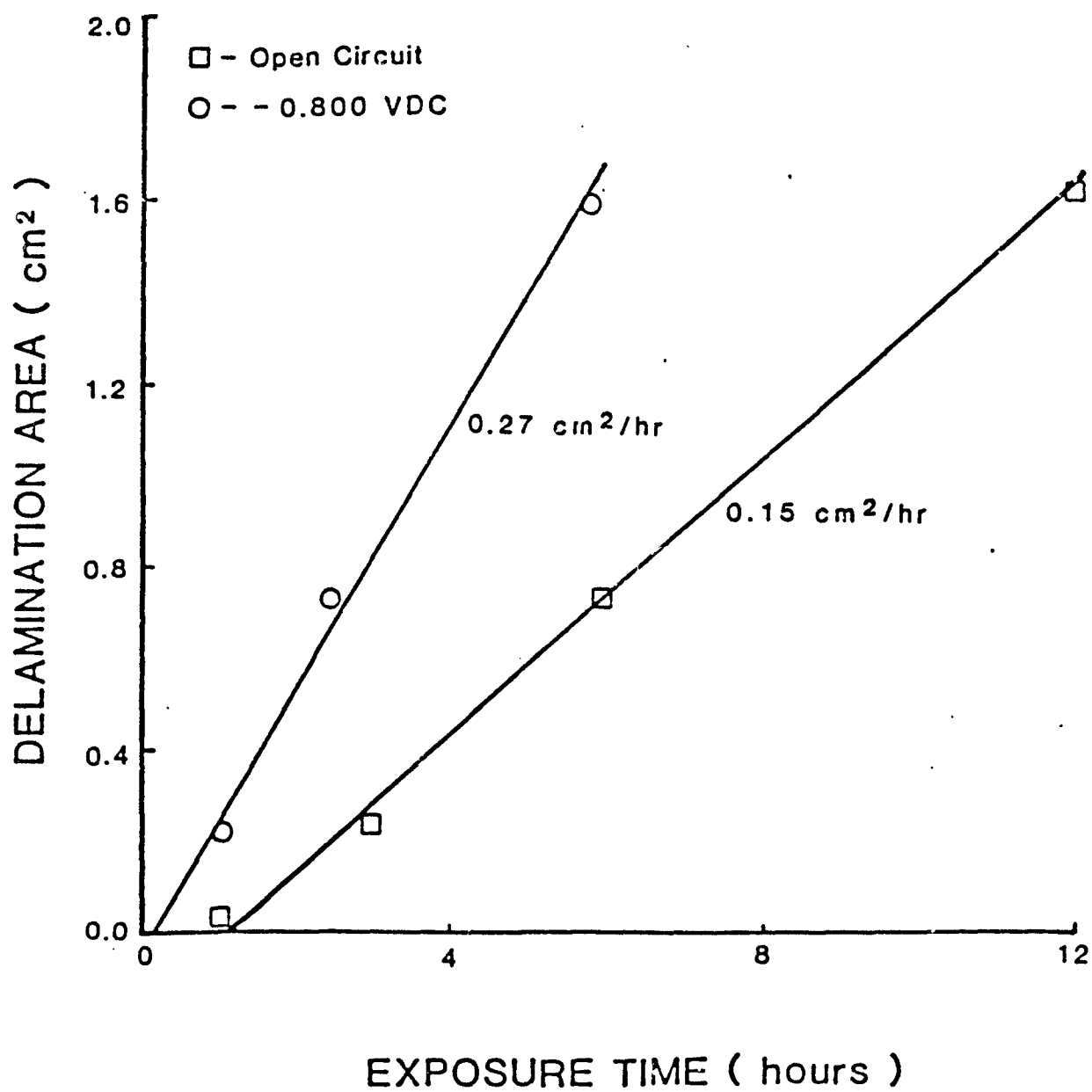


Figure 6. Delamination of an alkyd topcoat plus primer, 63.5-66 μm thick, under open circuit conditions and with an applied potential of -0.80 v while immersed in 0.5M CsCl solution.

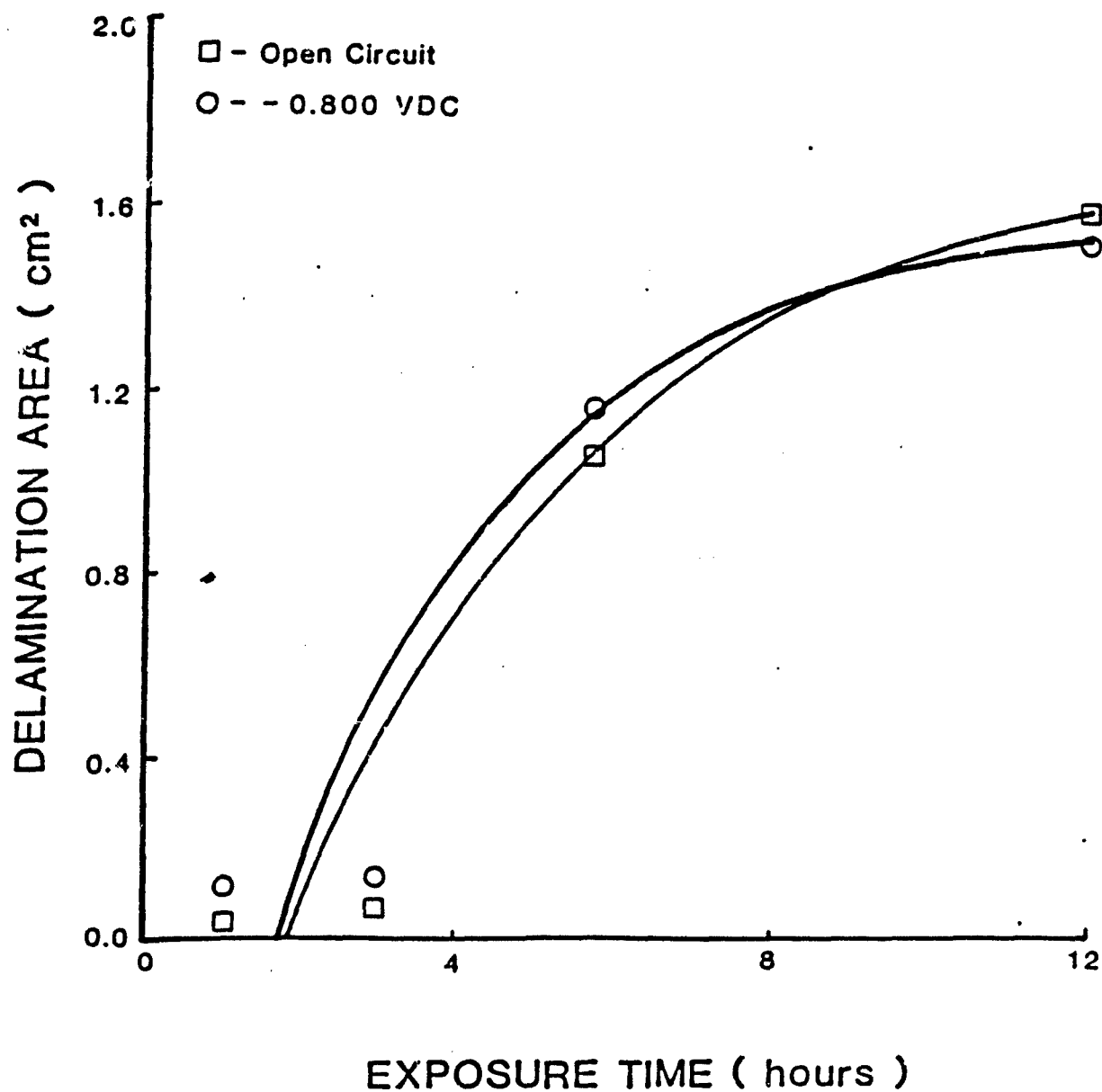


Figure 7. Delamination of the alkyd topcoat, 38.0-46.8 μm thick, under open circuit conditions and with an applied potential of -0.80 v while immersed in 0.5M CsCl solution.

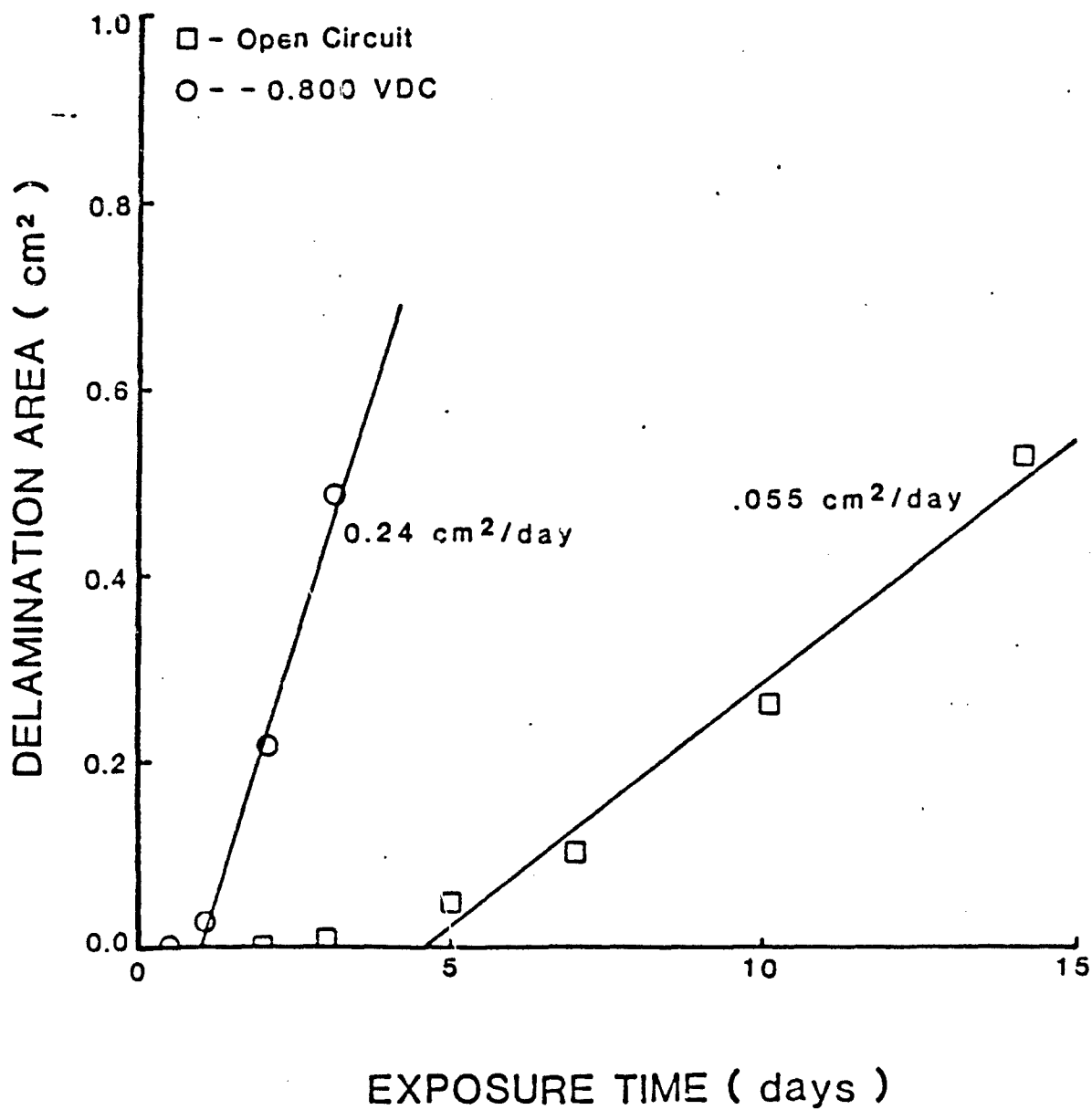


Figure 8. Delamination of a polybutadiene coating, 18.4 and 19.7 μm thick, under open circuit conditions and with an applied potential of -0.80 v while immersed in 0.5M CsCl solution.

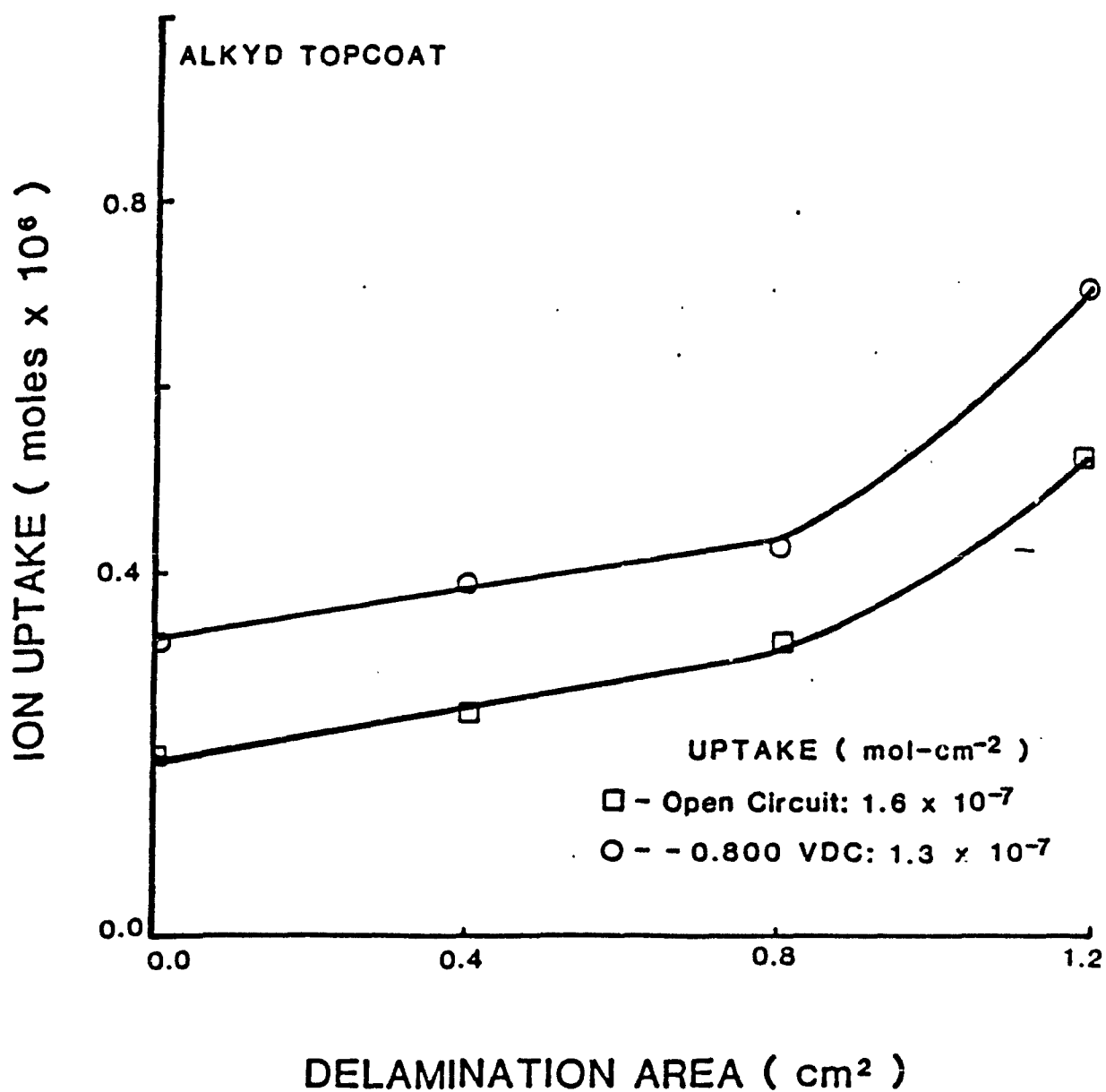


Figure 9. Total uptake of ^{137}Cs by the alkyd topcoat $38.0 \mu\text{m}$ thick, as a function of the delaminated area under both open circuit conditions and at a potential of -0.80 v .

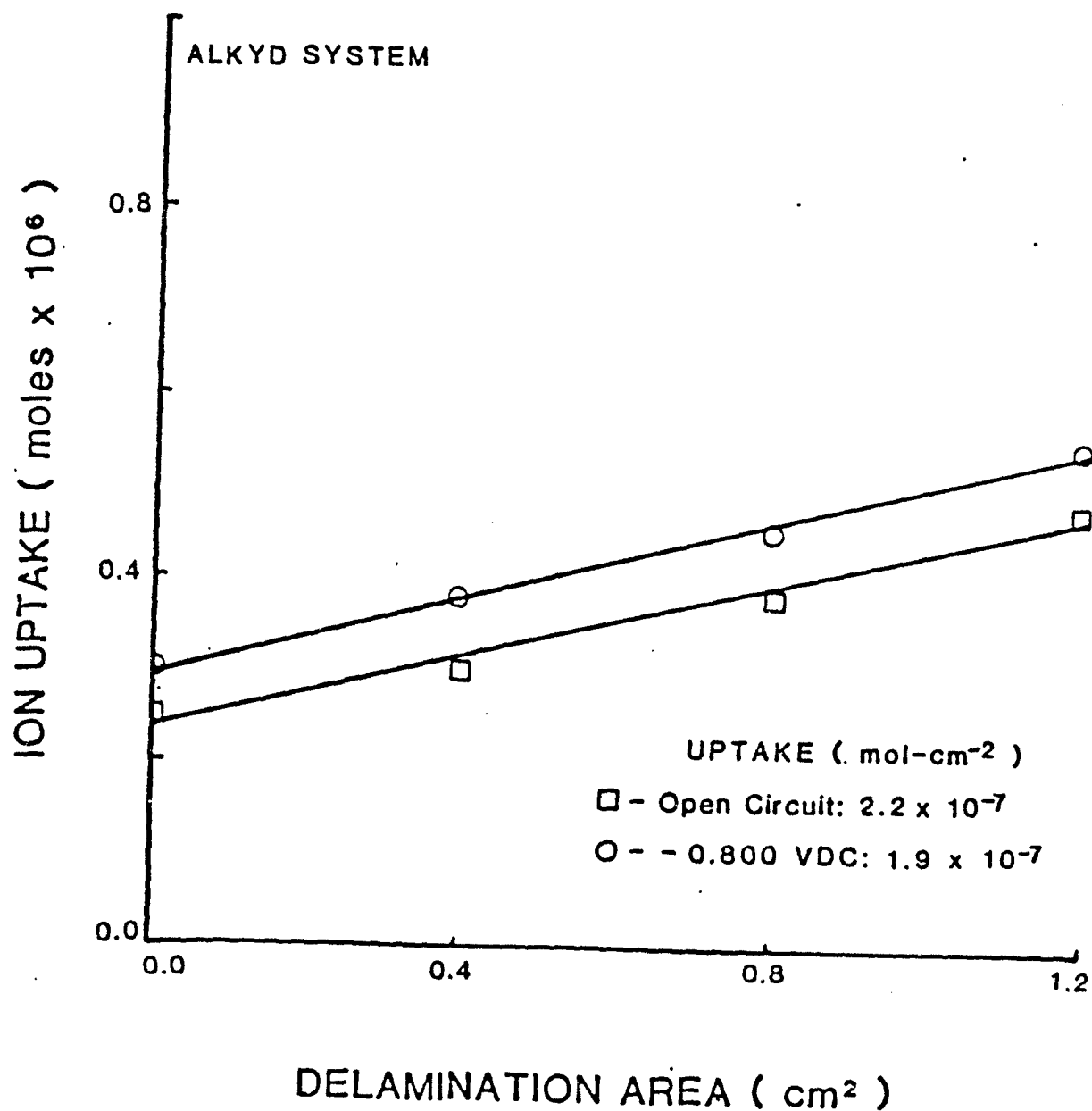


Figure 10. Total uptake of ^{137}Cs by the alkyd topcoat plus primer, $65.9 \mu\text{m}$ thick, as a function of the delaminated area under both open circuit conditions and at a potential of -0.80 v .

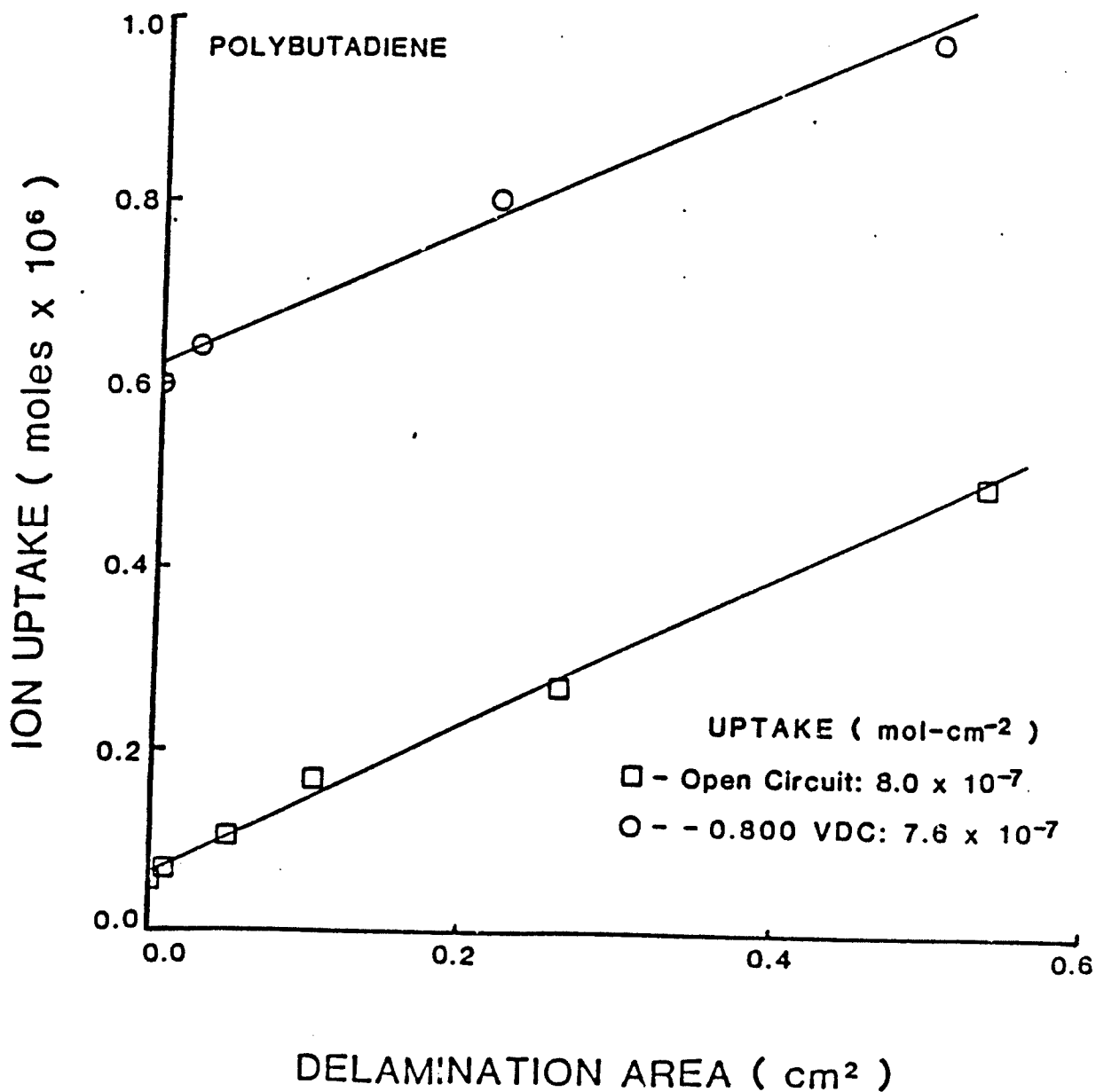


Figure 11. Total uptake of ^{137}Cs by the polybutadiene coating, 18.4-19.7 μm thick, as a function of the delaminated area under both open circuit conditions and at a potential of -0.80 v.

Table III
Representative Diffusion Coefficients for Na⁺ and Cl⁻
Ion Diffusion through Free Films

Film	Diffusion Coefficient in cm ² /hr		Reference
	Na ⁺	Cl ⁻	
Alkyd		7.6-40.3 x 10 ⁻¹⁰	Rao and Yaseen, 1978
Alkyd	8.3 x 10 ⁻¹⁰		Svoboda et al., 1971
Cellulose Acetate	2.6 x 10 ⁻⁶	6.3 x 10 ⁻⁷	Glass and Smith, 1966
Epoxy-Polyamide	1.1 x 10 ⁻⁷	1.7 x 10 ⁻⁸	Glass and Smith, 1967
Neoprene	1.6 x 10 ⁻⁸	2.4 x 10 ⁻⁹	Glass and Smith, 1966
Pigmented Epoxy	3.1 x 10 ⁻⁹	2.1 x 10 ⁻⁹	Glass and Smith, 1966

Table IV
Values of the Ionic Migration Coefficients under an Applied Potential
of -0.80 v Relative to Those Obtained under Open Circuit Conditions

Coating	Value of M under an Applied Potential of -0.80 v Relative to Open Circuit Conditions		
	Na ⁺	Cs ⁺	Cl ⁻
Alkyd Topcoat	8	6	3
Alkyd Topcoat Plus Primer	15	16	25
Polybutadiene	21	12	28

applied potential increased the rates of migration of both cations as well as the anion. The increase in the rate of cation migration is understandable in terms of the potential gradient, but the increase in the rate of Cl^- migration is a puzzle. Several possible explanations present themselves. First, the migration of the cations under the potential gradient in the absence of a cathodic reaction at the interface may result in a follow-on effect. The Cl^- may be attracted into the coating by virtue of the accumulation of a positive charge in the coating near the coating/metal interface. Second, the applied potential may enlarge the minute aqueous pathways that exist in the coating such that diffusion of all species is enhanced. Third, it is probable that both anions and cations diffuse through the coating as aquo complexes which react differently to the potential gradient than the unsolvated ion. It is known from other work based on impedance measurements (Parks) that an applied cathodic potential of -0.80 v increases the rate of diffusion of water through the same coatings used in the present study. The increase in diffusion rate of the Cl^- ion may thus be a result of the increased rate of diffusion of water under the applied potential.

A critical question which this study was designed to address is "What is the route by which the charge-carrying cations reach the site where the OH^- ions are formed?" A comparison of the data summarized in Tables I and II permits us to address this question. The data in these two tables are compared in Table V as the ratio of the migration coefficients obtained with and without a purposely formed defect in the coating. It is especially noteworthy that the relative migration coefficients are high under open circuit conditions for all three coatings, while under the influence of an applied cathodic potential the relative values of M are very low and, in seven of the nine cases, there is no major difference between the calculated migration coefficients with and without a defect. That the coatings with the defect take up ions much more rapidly than those in which there is no defect at open circuit is understandable in terms of the mechanism of the delamination process when there is no applied potential. Under such conditions, the cathode occurs under the coating and the anode occurs at the defect (Leidheiser and Kendig, 1976) during the corrosion process. The direction of migration of the ions is thus parallel to the surface from the defect. As the corrosion reactions occur, the delamination opens a crevice between the metal and the coating and there is free access of the solution to the interfacial zone. In the presence of an applied cathodic potential, our interpretation is that the diffusion path is largely through the coating when there is an applied cathodic potential whether or not there is a defect in the coating. We do not believe that all the ions diffuse through the coating, but we do believe that the ions which act as the counterions for the OH^- ions generated by the cathodic reaction at the delaminating front diffuse through the coating.

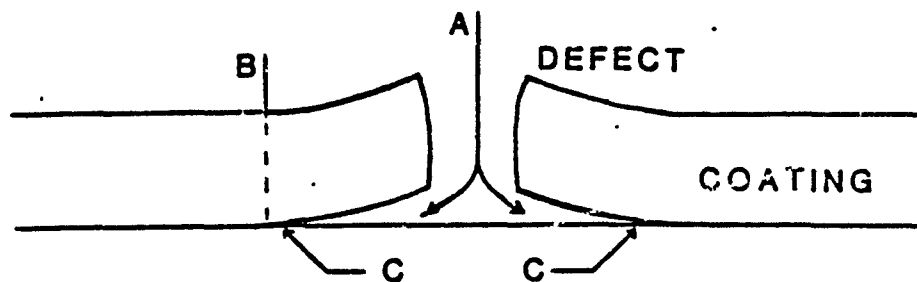
Table V

The Relative Migration Coefficients for the Ions, Na^+ , Cs^+ and Cl^- , as Calculated for Coatings Having a Purposely Formed Defect and Equivalent Coatings without a Defect

Coating	Relative Values of M for Coatings Having a Purposely Formed Defect and Equivalent Coatings without a Defect		
	<u>Na^+</u>	<u>Cs^+</u>	<u>Cl^-</u>
Alkyd Topcoat			
Open Circuit	10	9	7
-0.30 v	0.9	0.8	4
Alkyd Topcoat Plus Primer			
Open Circuit	29	43	43
-0.80 v	2	20	2
Polybutadiene			
Open Circuit	5	3	7
-0.80 v	2	1.5	1.7

The rationale for the migration of ions through the coating is elaborated on in Figure 12 which is a schematic of a defective coating on a metal substrate immersed in an electrolyte under cathodic polarization. The potential of the metal immediately under the defect is approximately equal to the applied potential, whereas the potential becomes less negative at distances on the metal away from the defect because of resistance effects. The possible ionic conductance paths to the sites where the OH^- ions are generated may be within the liquid phase beneath the coating or it may be through the coating. Intuitively, the liquid path appears to be the more logical route for the ions to follow but the potential distribution is such that the cations will be electrically attracted to the region immediately at the defect where the most negative potential exists. The pathway through the coating is also a logical route because it is possible to achieve a very high pH and high cation concentration at the disbonding front without having the cation migrate counter to the potential gradient at the metal surface. It is our conclusion based on the results summarized in Table V and the rationale above that the cations reach the disbonding site largely through the coating.

The data summarized in Figures 9-11 indicate that the number of Cs^+ cations in the coating and in the delaminated region at the interface is greater when there is an applied cathodic potential. The difference is slight in the case of the alkyd coatings but appreciable in the case of the polybutadiene coating. The similar slopes of ion uptake as a function of the delaminated area for both open circuit and an applied potential of -0.80 v suggest that the delamination mechanism is the same whether there

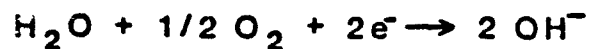


METAL

A: BULK ELECTROLYTE: M^+ , X^- , H_2O

B: M^+ , H_2O TRANSPORT THROUGH COATING

C: CATHODIC REACTION SITES:



REACTION LEADS TO DISBONDING

Figure 12. Schematic diagram of the two modes by which cations can reach the delaminating front.

is an applied potential or not. This conclusion is in accord with current thinking in that the delamination process is attributed to the fact that the oxygen reduction reaction occurs beneath the coating. These results also suggest that the cation transport is directly related to the disbondment progress, most likely as a counter ion to OH^- ion production or bond breakage.

The question, "Is the cation flux through the coating sufficient to support the observed delamination rate?" can easily be answered provided the following assumptions are made. First, it will be assumed as an extreme case that the surface roughness factor of the steel is 10 and that every surface atom is involved in the bonding between the metal and coating. This assumption leads to the conclusion that there are approximately 10^{16} bonds per apparent cm^2 of the metal surface. Second, it will be assumed that each OH^- ion that is formed has the capability of breaking one surface bond. Third, it will be assumed that for each OH^- ion generated, a cation will be available by diffusion through the coating. Let us now use these assumptions along with data generated for the diffusion of Cs^+ ions through a polybutadiene coating at an applied potential of -0.80 v. The delamination rate under these conditions is approximately 0.24 cm^2/day as given in Figure 8. The cation flux under these conditions is approximately 10^{-7} moles/day- cm^2 or approximately 6×10^{-8} moles/day- cm^2 for the geometry used in the measurements as calculated from the data in Figure 4.

A flux of 6×10^{-8} moles/day- cm^2 and a delaminated area of 0.24 cm^2 leads to a required flux of 1.5×10^{-8} moles/day or 9×10^{15} ions. The number of bonds between the metal and coating, under the assumptions outlined above, that are broken per day to yield a delaminated area of 0.24 cm^2 is 2.4×10^{15} . The cation flux through the coating under an applied potential of -0.80 v is thus sufficient to provide counterions for the OH^- ions generated by the cathodic reaction.

CONCLUSIONS

We have shown that the introduction of a defect into a coating on steel, or the cathodic polarization of the substrate, results in a significant increase in the rate of ionic transport into the coating. Under open circuit conditions, the cations appear to travel along the coating/substrate interface from the defect site as delamination progresses. When a cathodic potential is applied, the primary migration pathway appears to be through the coating. Chloride ion diffusion is observed to accelerate under the potential gradient, probably due to one of several possible carry-along mechanisms. The ion flux has been shown to support observed cathodic delamination rates, suggesting the disbondment mechanism. Ion uptake-delamination area profiles for the systems studied showed almost no potential dependence, suggesting the disbondment mechanism is the same under open circuit and cathodic polarization conditions.

REFERENCES

- Baboian, R.; McBride, L.; Langlais, R.; Haynes, G. Mater. Perf. 1979, 18(12), 40-44.
- Dickie, R. A.; Hammond, J. S.; Holubka, J. W. Ind Eng. Chem. Prod. Res. Dev. 1981, 20, 339-43.
- Glass, A. L.; Smith, J. J. Paint Technol. 1966, 38(495), 203-09.
- Glass, A. L.; Smith, J. J. Paint Technol. 1967, 39(511), 490-93.
- Koehler, E. L. Corrosion 1984, 40, 5-8.
- Leidheiser, H. Jr. Croat. Chem. Acta 1980, 53, 197-209.
- Leidheiser, H. Jr. Ind. Eng. Chem. Prod. Res. Dev. 1981, 20, 547-51.
- Leidheiser, H. Jr.; Kendig, M. W. Corrosion 1976, 32, 69-76.
- Leidheiser, H. Jr.; Wang, W. J. Coatings Technol. 1981, 53(672), 77-84.
- Leidheiser, H. Jr.; Wang, W. In "Corrosion Control by Organic Coatings"; Leidheiser, H. Jr., Ed.; National Association of Corrosion Engineers: Houston, TX, 1981; 70-77.
- Leidheiser, H. Jr.; Wang, W.; Igetoft, L. Prog. Org. Coatings 1983, 11, 19-40.
- Leidheiser, H. Jr.; Granata, R. D.; Atkinson, J. M.; McBride, D. G. IBM Journal of Research and Development 1985, 29(1), 27-36.
- McIntyre, J. Lehigh University, Bethlehem, PA, private communication, 1984.
- Parks, J. Lehigh University, Bethlehem, PA, unpublished measurements, 1984.
- Rao, R. V.; Yaseen, M. Pigment and Resin Technol. 1978, 7(2), 4-8.
- Ritter, J. J.; Kruger, J. Surface Science 1980, 96, 364-74.
- Svoboda, M.; Kuchynka, D.; Knappek, B. Farbe u. Lack 1971, 77(1), 11-15.
- Wang, W.; Leidheiser, H. Jr. "Proceedings - INTERFINISH '84, 11th World Congress on Metal Finishing"; Jerusalem, Israel, October 21-26, 1984, pp. 262-69.
- Watts, J. F.; Castle, J. E. J. Materials Sci. 1983, 18, 1987-3003.



SECTION - #8

The Effect of Alkali Metal Hydroxides on the Dissolution Behavior of a Zinc Phosphate Conversion Coating on Steel and Pertinence to Cathodic Delamination

Principal Investigator: Henry Leidheiser, Jr.
Associate: André J. Sommer (Ph.D. awarded)

ABSTRACT

Raman microprobe spectroscopy, scanning electron microscopy, energy dispersive spectroscopy and wet chemical methods of analysis were successfully employed to determine the effects of high pH environments on zinc phosphate conversion coatings. Results obtained from the latter three techniques showed that the selective removal of phosphate from the conversion coating was pH-dependent. At pH values associated with 0.1M NaOH, phosphate ion was selectively removed from the conversion coating, while at those pH values associated with 0.01M and 1.0M NaOH, zinc ion was preferentially removed from the coating. Raman spectra confirmed that selective removal of phosphate ion was a result of zinc oxide formation on the surface of the original phosphate conversion coating.

The cation of the alkali solution also proved to be an important factor in the dissolution of the phosphate conversion coating. Sodium hydroxide dissolved the phosphate coating to the greatest extent, followed by hydroxides of potassium, cesium and lithium. This reaction order was related to the number of precipitation products formed when the samples were exposed to each of the hydroxide solutions.

INTRODUCTION

A full understanding of cathodic delamination, i.e., the de-adherence of an organic coating around a defect when the substrate metal is made cathodic to the rest potential, has been an objective of this laboratory for the past several years. The majority of this work has dealt with model systems and unphosphated metal substrates [1-6] and only one paper has been concerned with phosphated surfaces representative of commercial practice [7]. The phosphate between the coating and the metal is attacked by the high pH generated by the cathodic reaction and the bond between the coating and the phosphate is lost. The process by which the phosphate is deteriorated during cathodic delamination is not well understood. It is the purpose of this paper to seek a better understanding of the deterioration of the phosphate.

Wiggle, Smith and Petrocelli [8] first reported that zinc phosphate corrosion coatings dissolve in the high pH environment formed under a coating when the metal surface serves as a cathode. Later studies by Roberts et al. [9] showed that phosphorus is selectively removed from the

coating when zinc phosphated steels were exposed to sodium hydroxide solutions. Uchida and Deguchi [10] and Van Ooij and De Vries [11] reported similar findings. Van Ooij interpreted XPS studies to show that hydroxide ions exchange with phosphate ions in the first few layers of the phosphate conversion coating. A number of questions still to be answered are: (1) Is the selective removal of phosphorus pH-dependent? (2) Why is phosphate ion selectively removed from the conversion coating? (3) What effect do cations have on the dissolution of the phosphate coating? and (4) What corrosion or dissolution products are formed? These questions are addressed in this paper.

The primary investigative technique used in this study is Laser Raman Microprobe Spectroscopy (LRMS). The instrument and the concomitant strengths and inadequacies of the technique have been discussed elsewhere [12,13]. The strengths of LRMS germane to this investigation are that the technique provides molecular information on a microscopic scale at ambient conditions. The inadequacies of the LRMS technique have been counteracted by measurements using energy dispersive spectroscopy (EDS), scanning electron microscopy (SEM), and wet chemical methods of analysis.

EXPERIMENTAL

The influence of two variables on the dissolution of zinc phosphate conversion coatings was investigated: the pH of the aqueous phase and the cation present in the aqueous phase. Zinc phosphated steel samples (Parker 210) were obtained from Parker Surface Treatment Products and cut into 2.5 cm squares. Only those squares cut from the center of the panel were used. The back side of the panels was marked prior to cutting so that the cut samples had the same side exposed to the different test solutions.

Three sets of six samples each were exposed to the different hydroxide solutions by clamping the panel as the base of an O-ring joint-type cell. At intervals of 10, 20, 30, 40, 50 and 60 min the samples were removed, rinsed lightly and allowed to dry. A small portion of the solution volume was then analyzed for orthophosphate and divalent zinc by a colorimetric method and atomic absorption spectroscopy, resp. The samples exposed to the hydroxide solutions for a total of one hr were analyzed by RMS, EDS, and SEM. The influence of pH was determined by exposing the phosphated steel samples to 0.01M, 0.1M, and 1.0M sodium hydroxide solutions. Hydroxide solutions (0.1M) of lithium, sodium, potassium, and cesium were used to determine the effect of the cation on the dissolution of the phosphate coating.

A model experiment conducted to determine the corrosion products generated employed a zinc phosphate tetrahydrate pellet exposed to 1.0M NaOH for 1 hr. Corrosion products were identified by comparing Raman spectra of known materials to those spectra recorded for the corrosion products. Corrosion products formed in the different alkali cation solutions were determined from samples exposed to 0.1M solutions for four days.

RESULTS AND DISCUSSION

Zinc Phosphate-Alkali Reaction Product

In order to determine what corrosion products are formed when a zinc phosphate coating is exposed to an alkaline environment, zinc phosphate tetrahydrate was exposed to 1.0M NaOH for 1 hr. The spectra shown in Figure 1 demonstrate that the primary corrosion products formed upon exposure of zinc phosphate tetrahydrate (hopeite) to an alkaline environment are zinc oxide, hydrozincite and hydroxyapatite. The reference spectra for zinc phosphate and zinc phosphated steel have been published previously [14]. The band appearing at 435 cm^{-1} shift is attributed to lattice modes or zinc-oxygen bonding modes within the zinc oxide crystal. Hydrozincite, whose formula is $2\text{ZnCO}_3 \cdot 3\text{Zn(OH)}_2$, gives rise to the band centered at 1060 cm^{-1} shift. This feature is characteristic of a symmetric stretching mode for the carbonate anion. The remaining band located at 980 cm^{-1} shift is assigned to the symmetric stretching mode of the phosphate anion in hydroxyapatite $(\text{Zn}_{10}(\text{OH})_2(\text{PO}_4)_6 \cdot n\text{H}_2\text{O})$. The broadness of the bands in each spectrum can be accounted for by the polycrystalline nature of the corrosion products.

Effects of pH

The results of exposing zinc phosphated steel to sodium hydroxide solutions of different pH are shown in Tables I and II. The rate at which the phosphate ion is removed from the conversion coating is given in $\mu\text{mole/l-min}$. Table I gives the measured rates for 0.01, 0.1 and 1M NaOH along with the rates normalized to 0.01M NaOH. The data show that the rate of phosphate removal is strongly dependent on the pH of the solution, a fact noted in previous studies [8].

Table I
Phosphate Ion Dissolution Rate ($\mu\text{mole/l-min}$)

Rate	NaOH 0.01M	NaOH 0.1M	NaOH 1.0M	LiOH 0.1M	KOH 0.1M	CsOH 0.1M
Measured	0.035	2.9	36.8	0.7	1.9	1.1
Normalized to 0.01M NaOH	1.0	100	1000	—	—	—
Normalized to 0.1M LiOH	—	4.8	—	1.0	3.2	1.8

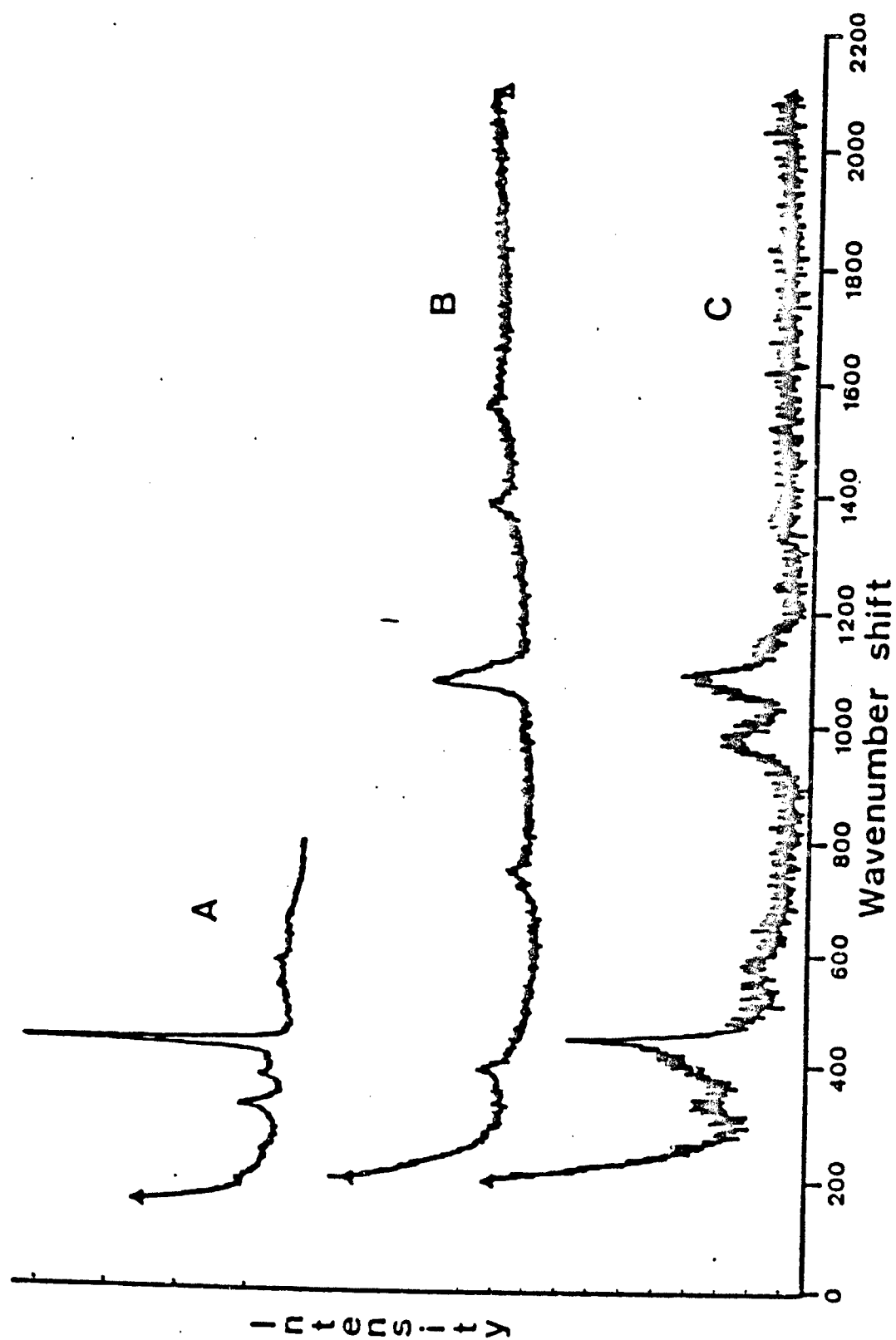


Figure 1. The Raman spectra of: A - zinc oxide; B - hydrozincite; C - a zinc phosphate tetrahydrate pellet exposed to 1.0M NaOH for 60 minutes.

Table II

Zinc/Phosphate Ion Ratio in Solution upon Dissolution of Zinc Phosphate

Time (min)	NaOH 0.01M	NaOH 0.1M	NaOH 1.0M	LiOH 0.1M	KOH 0.1M	CsOH 0.1M
10	2.60	1.45	3.07	3.98	1.89	1.66
20	3.31	0.86	3.13	2.57	1.19	1.45
30	2.70	0.72	2.94	2.40	1.20	1.36
40	3.25	0.55	3.00	2.24	1.10	1.45
50	2.95	0.40	3.03	1.94	0.91	1.12
60	2.94	0.36	2.95	1.62	0.84	1.22

The rapid dissolution of zinc phosphate in 0.1M hydroxide solutions is consistent with the experimental observation that the pH beneath an organic coating can exceed 13 when the system is made cathodic [14,15].

Table II gives the ratio of zinc ion to phosphate ion in solution as a function of time and pH. Earlier studies indicated that in 0.1M NaOH solutions, phosphate ion is selectively removed from the coating. Raman microprobe analysis of the samples used in this study showed that the surface was predominantly hopeite ($\text{Zn}_3(\text{PO}_4)_2 \cdot 4\text{H}_2\text{O}$) [16]. Selective removal of phosphate ion indicates that the ratio of zinc ion to phosphate ion in solution will be less than a value of 1.5 which is to be expected for uniform dissolution of the conversion coating. Preferential removal of phosphate ion is clearly evident for those samples exposed to 0.1M NaOH. However, the converse is true for those samples exposed to 0.01M and 1.0M NaOH. All (zinc ion)/(phosphate ion) ratios in solution for these latter samples are above 1.5. Another constituent which may be present in conversion coatings based on zinc is phosphophyllite $\text{Zn}_2\text{Fe}(\text{PO}_4)_2 \cdot 2\text{H}_2\text{O}$. If the conversion coating were to be predominantly phosphophyllite, uniform dissolution will yield a ratio of zinc ion to phosphate ion in solution of 1. In all cases, the ratio is either well below or above this value; thus the zinc ion or phosphate ion is being selectively removed from the coating dependent on the pH of the alkaline solution. To determine why ions were being selectively removed in solutions of differing pH, SEM, EDS, and RMS analyses were conducted on those samples exposed for one hr. The results of these analyses are summarized in Table III.

The results of SEM, EDS, and Raman analyses indicate that 0.01M NaOH solution had little effect on the surface composition over the time period of one hr. Each of these methods of analysis yielded results consistent with a normal zinc phosphate conversion coating. Samples exposed to 0.1M NaOH solution, however, changed in surface morphology and elemental composition.

Formation of a precipitate on the phosphate coating surface was clearly evident in the SEM photomicrographs of samples exposed to 0.1M NaOH. Elemental analysis by EDS indicated a loss of phosphorus from the conversion coating which corresponded to the loss of phosphate as seen by

wet chemical methods of analysis. Raman analysis, on the other hand, showed spectra consistent with the hopeite structure but with a lower signal-to-noise ratio. The lower signal to noise ratio could be attributed to a loss of the phosphate coating but is more likely due to the increased Rayleigh scattering by the precipitate on the coating surface. The precipitate is probably one of the compounds identified in the model experiments conducted with zinc phosphate tetrahydrate. The amount of precipitate on the coating was insufficient to make a clear identification. In order to increase the amount of precipitate, samples were exposed for a period of four days, after which the usual methods of analysis were applied. SEM photomicrographs of samples exposed for four days confirmed that a greater amount of precipitate had been deposited and subsequent Raman analysis identified the precipitate as zinc oxide.

Table III.

SEM, EDS, and Raman Analyses of Samples Exposed for 1 Hour

Analysis	NaOH 0.01M	NaOH 0.1M	NaOH 1.0M	LiOH 0.1M	KOH 0.1M	CsOH 0.1M
SEM	N.P.	ppt.	—	N.P.	ppt.	N.P.
EDS	N.P.	-P	-P,-Zn	N.P.	-P	-P
Raman	N.P.	N.P.*	—	N.P.	N.P.*	N.P.

N.P. = normal zinc phosphate
 * = loss of S/N in spectra

Exposure to 1.0M NaOH solution quickly dissolves the phosphate coating from the metal substrate. SEM photomicrographs exhibited a surface structure completely different from the original conversion coating. Elemental analysis indicated a dramatic decrease in the amount of phosphorus and zinc in the conversion coating which again paralleled the results obtained by wet chemical methods of analysis. No useful information could be obtained via Raman analysis.

The foregoing results show that the dissolution of phosphate conversion coatings is very dependent on the pH of the exposure solution. The low P/Zn ratio in the surface of zinc phosphate exposed to 0.1M NaOH observed in previous studies [9-11] was confirmed by Raman analysis performed in the present study. It is, however, a consequence of zinc oxide formation on the phosphate coating surface. Selective removal of phosphate and zinc was found to be pH dependent and can be explained as follows. In solutions with a pH close to that of 0.01M NaOH (11.6), the zinc phosphate conversion coating is slowly dissolved. Zinc ion is preferentially removed from the coating by the formation of soluble zincate ions. As the pH increases towards that associated with 0.1M NaOH (12.4),

the solubility product constant of zinc oxide is exceeded and zinc oxide is precipitated onto the surface. Since phosphate continuously dissolves, the precipitation of zinc oxide leads to a low P/Zn ratio on the surface. Increasing the pH further to that of 1.0M NaOH (13.4) solubilizes the zinc oxide precipitate and zincate complexes are present in solution.

Effects of Cations

Leidheiser and Wang [1] have shown that cations play an important role in cathodic delamination. The cations act as charge carriers and provide charge balance for the OH^- ions formed by the cathodic reaction. The combined effect of hydroxide anions and cations on phosphate coating dissolution had to be determined since future studies of cathodic delamination were to be conducted with zinc phosphated steel substrates.

Results presented in Table I show that cations also affect phosphate coating dissolution. The most surprising result is that sodium ion is 1.5, 3 and 5 times more effective in phosphate coating dissolution than potassium, cesium and lithium, respectively. Table II shows that phosphate ion is selectively removed from the conversion coating for sodium, cesium and potassium whereas zinc ion is selectively removed when the ion of the alkali solution is lithium. SEM, EDS, and Raman analyses were conducted on those samples exposed for one hr in an effort to explain these observations. The results of these analyses are given in Table III.

Raman spectra and SEM micrographs for samples treated with LiOH and CsOH were characteristic of a normal zinc phosphate coating. Similar studies for samples exposed to KOH and NaOH indicated that a precipitate was formed on the original phosphate coating. These results were discussed earlier for samples exposed to NaOH and similar remarks can be made for those sample exposed to KOH. Close examination of the SEM photomicrographs of samples exposed to KOH showed that the edges of the phosphate crystals were more rounded when compared to phosphate crystals exposed to NaOH. This observation suggests that KOH attacks the phosphate crystals more vigorously than NaOH. However, this inference conflicts with wet chemical results. A possible explanation for these observations is that the phosphate, once dissolved from the coating, may precipitate in another form. Elemental analysis of the coatings after exposure via EDS indicated that samples exposed to NaOH, KOH and CsOH all lost phosphorus while those samples exposed to LiOH exhibited EDS spectra with peak intensities characteristic of a normal zinc phosphate coating. Although these results confirmed those of wet chemical analysis, the order or effect of alkali cation on phosphate dissolution cannot be fully explained. Samples were again exposed for four days to 0.1M alkali solutions and subsequently analyzed by SEM, EDS, and LRMS. Results of these analyses are summarized in Table IV.

SEM and EDS analyses of these samples indicated that a precipitate had formed on the surface of each sample and that the surface lost phosphorus by exposure to each of the alkaline solutions. Observation of these surfaces under an optical microscope at 100X revealed differences consistent with the dissolution rate order seen on changing the cation of the alkaline exposure solution. Samples exposed to NaOH exhibited one phase which was later identified as zinc oxide by LRMS. Exposure of the

Table IV

SEM, EDS and Raman Analyses of Samples Exposed for Four Days

Analysis	LiOH 0.1M	NaOH 0.1M	KOH 0.1M	CsOH 0.1M
SEM	ppt.	ppt.	ppt.	ppt.
EDS	-P	-P	-P	-P
Optical Microscopy	3 phases	1 phase	2 phases	4 phases
Raman	vivianite, Fe_3O_4 , ZnO, hydrozincite	ZnO	ZnO, ortho- phosphate	vivianite, hydrozincite, orthophosphate $\text{FePO}_4 \cdot 2\text{H}_2\text{O}$

phosphated steel to KOH produced two phases identified by LRMS as zinc oxide and an orthophosphate of potassium, zinc and iron. Samples exposed to LiOH and CsOH exhibited three and four phases, resp., as concluded from optical microscopy. Subsequent Raman microanalysis of these phases confirmed the formation of vivianite, a ferric phosphate, Fe_3O_4 , zinc oxide and hydrozincite for samples exposed to LiOH and ferrous phosphate, vivianite, hydrozincite and an orthophosphate of cesium, zinc and iron for those samples exposed to CsOH.

Based on the foregoing results the effect of cations on phosphate coating dissolution seems to be related to the solubility of the precipitates formed after dissolution of the original zinc phosphate conversion coating. Generally the larger the cation, the more numerous are its insoluble salts, a fact that would account for the order of the dissolution rates on changing the cation from sodium to cesium but would not explain the dissolution rate observed in LiOH. In this case the dissolution rate may be related to the activities of the solvated ions or lie in the fact that weak acids of lithium salts are more insoluble than those of other alkali metal ions.

ACKNOWLEDGEMENTS

The authors are grateful to Dr. Karl Korinek of Parker Surface Treatments for supplying the phosphated steel samples. Dr. Fran Adar of Instruments SA is thanked for her invaluable knowledge and willingness to provide assistance in the interpretation of the Raman data.

REFERENCES

- [1] H. Leidheiser, Jr., and W. Wang, J. Coatings Technol. 53, No. 672, 77 (1981).
- [2] H. Leidheiser, Jr., W. Wang and L. Igetoft, Prog. Org. Coatings 11, 19 (1983).
- [3] H. Leidheiser, Jr., L. Igetoft, W. Wang and K. Weber, "Organic Coatings - Science and Technology," Vol. 5, G. D. Parfitt and A. V. Patsis, Eds., Marcel Dekker: New York, 1983, p. 307.
- [4] H. Leidheiser, Jr., W. Wang, R. D. Granata, H. Vedage and M. L. White, J. Coatings Technol. 56, No. 717, 55 (1984).
- [5] W. Wang and H. Leidheiser, Jr., Proc. Interfinish '84, 11th World Congr. Metal Finishing, Jerusalem, Israel, Oct. 1984, pp. 262-69.
- [6] J. M. Atkinson, R. D. Granata, H. Leidheiser, Jr., and D. G. McBride, IBM J. Res. Dev. 29, No. 1, 27 (1985).
- [7] R. A. Iezzi and H. Leidheiser, Jr., Corrosion 37, 28 (1981).
- [8] R. R. Wiggle, A. G. Smith and J. V. Petrocelli, J. Paint Technol. 40, 174 (1968).
- [9] T. Roberts, SAE Paper #800443 (1980).
- [10] K. Uchida and T. Deguchi, Nisshin Steel Co. Report #667.613 (1983), p. 32.
- [11] W. J. Van Ooij and O. T. De Vries, Tenth Internatl. Conf. Org. Coatings Sci. Technol., Athens, Greece, July 9, 1984.
- [12] G. J. Rosasco, "Raman Probe Spectroscopy," in Advances in Infrared and Raman Spectroscopy, R.J.H. Clark and R. E. Hester, Eds., Heydon, London, Vol. 7, p. 223 (1980).
- [13] R. J. Thibeau, C. W. Brown and R. H. Heidersbach, Appl. Spectro. 32, 532 (1978).
- [14] J. P. McIntyre, private communication, January 1984.
- [15] J. J. Ritter and J. Kruger, Corrosion Control by Organic Coatings, H. Leidheiser, Jr., Ed., Natl. Assoc. Corros. Engrs., Houston, TX (1981), p. 28.
- [16] A. J. Sommer and H. Leidheiser, Jr., Proc. 19th Annual Conf. Micro-beam Analysis Soc., A. D. Romig, Jr. and J. I. Goldstein, Eds., San Francisco Press, Inc., 1984, pp. 111-14.

SECTION - #9

Corrosion beneath Polymeric Coatings on Thin Metal Films as Studied Using Concurrent AC Impedance and Parallel DC Resistance Measurements

Principal Investigator: J. F. McIntyre
Associate: Henry Leidheiser, Jr.,
Prof. of Chemistry

ABSTRACT

A comparison is made between two electrical techniques for studying the deterioration of polymer coated metals. AC impedance measurements and parallel DC resistance measurements are concurrently made on the same sample exposed to a variety of aggressive environments. Thin metal films supported on glass and coated with polybutadiene are investigated. Together these two techniques provide complementary information on the state of a painted metal as a function of time. AC measurements integrate effects over the coating/metal interface, whereas the parallel DC measurements yield information about the electron conduction of the metallic substrate only.

INTRODUCTION

A number of techniques has been developed in recent years in an attempt to understand the nature of the processes responsible for polymeric coating failure in aggressive environments. The common objective of these studies is to predict successfully the useful lifetime of protective coatings in short times and, in addition, to aid in elucidating mechanistic information. Accurate assessment using conventional DC electrical and electrochemical techniques to predict the lifetime of a coating and/or determine quantitative corrosion rate data is often difficult because of the characteristic insulating properties of most paints. The large ohmic drop across the electrolyte/coating and coating/metal interfaces generally dominates the electrical response of the system and introduces large errors when attempting to calculate meaningful corrosion rate data. AC impedance techniques overcome this difficulty and a separation of the individual contributing factors related to coating breakdown and interfacial attack can be obtained, provided a large frequency range is tested and the relaxation times of the individual reactions are sufficiently different.

AC impedance techniques have been used with moderate success and some interesting information has been obtained by a number of groups [1-16]. More recently the authors have utilized a technique to measure the change in the parallel DC resistance of thin metal films coated with polymers [17]. The early stages of underfilm attack can be detected and,

in some situations, interfacial attack is evident in shorter times than indicated by AC impedance results.

The response of a coated metal to applied AC signals at early times of immersion is dominated by effects related to the electrical properties of the polymer, i.e., dielectric phenomena in which the impedance response is characterized by an ω^{-1} frequency dependence. Frequently, contributions to the overall AC impedance from interfacial reactions are minor and difficult to ascertain, particularly for thick coatings that retain their dielectric integrity. In those cases, the influence of interfacial reactions on the response to AC perturbations is often masked by the high impedance of the coating and noticeable effects only occur at later times when additional time constants appear. As a consequence, the initial stages of underfilm corrosion often go unnoticed.

The purpose of the work described herein is to compare the results obtained on similar samples using AC impedance measurements to study the system and parallel DC measurements to study the changes in the metallic substrate. Examples will be selected that illustrate the advantage of combining both types of measurements on a single sample. It should be emphasized that the AC measurements integrate effects over the coating, the coating/metal interface and the metal substrate, whereas the parallel DC measurements yield information about the electronic conduction of the metallic substrate only.

EXPERIMENTAL

Samples

Sample preparation involves the vapor deposition of iron or nickel onto clean glass slides. Metals of 99.99% purity in the form of wires are obtained from Alpha Products. A Denton Vapor Deposition Instrument, model DV-520, is used to deposit the metal of interest at a pressure of 10^{-5} - 10^{-6} torr, using resistive heating. The thin metal films are typically of the order of 400 Å in thickness. Subsequently, four lead wires, #32-7/40, are attached to the metal film using low resistance contact cement obtained from the Ernest Fullam Co.

Coatings

A polybutadiene coating is applied to metal films using a spin-coater. Polybutadiene coatings are cured at 195°C for 30 minutes in an air-forced oven. Coating thicknesses range from approximately 9 µm to 17 µm. All samples are stored in desiccators prior to testing, at which time samples are mounted in polyethylene cells and sealed with a commercial silicone caulking.

Parallel DC Resistance

A description of the experimental setup was given previously [17]. A variation of a four-point probe method is used to monitor the change in the parallel DC resistance of thin metal films coated with polybutadiene while exposed to a variety of aqueous environments.

AC Impedance

A Princeton Applied Research AC impedance system interfaced to an Apple IIe desk-top computer is used to make all AC measurements. A description of this system can be found in an earlier discussion [17]. The applied superimposed sinusoidal voltage is 15 mV in amplitude and data are acquired at the steady-state potential. Results are presented using the familiar Nyquist and Bode plots.

RESULTS AND DISCUSSION

Earlier work showed that the parallel DC resistance technique indicates changes at the interface in short times [15]. Samples in the previous work were exposed to mildly aggressive solutions, i.e., water or 3% NaCl. Research reported herein expands on this initial work and results for the polybutadiene system exposed to more aggressive environments are discussed. A definition of the electrical terms used throughout this paper can be found in Table I.

Table I

Definition of Electrical Terms

R_0	Parallel DC resistance of metal film at time zero
R_t	Parallel DC resistance of metal film at time t
ΔR_{DC}	Change in parallel DC resistance of metal film ($R_t - R_0$)
R_i	The resistance of the coating assuming a circuit of a capacitor and resistance in parallel
C_c	The capacitance of the coating assuming a circuit of a capacitor and resistance in parallel
Z'	The real portion of the total impedance
Z''	The imaginary portion of the total impedance

Example #1

Results typical of a nickel-polybutadiene system exposed to 3% NaCl pH = 6.6 for 40 days can be seen in Figure 1. The Bode plot indicates capacitive behavior at frequencies above about 1.0 Hz characterized by an ω^{-1} frequency dependence. A calculated initial value for the coating capacitance of 210 pF/cm², as indicated by this plot, changed slightly during the 40 days of immersion, reaching a final value of 230 pF/cm². A plot of phase angle, θ , against log frequency indicates only capacitive behavior at early times with values of θ approaching -90° at high frequencies and -75° at low frequencies. Phase angle values of -25° found at low frequencies at later times can be attributed to a short-circuiting of the polymer coating by an ionic resistance, R_i . This low frequency phase angle shift is often observed for systems exhibiting pseudo-Warburg behavior; however, a Randle plot of $\log Z'$ against ω^{-2} at low frequencies did not give the characteristic linear behavior for Warburg impedances.

Intuitively, a high R_i value of $4 \times 10^7 \Omega$ and a coating capacitance which changes only slightly during 40 days of exposure to 3% NaCl suggest that the coating has retained its integrity and continues to afford adequate protection; however, concurrent parallel DC resistance measurements indicate otherwise and a significant increase in the DC resistance is obtained as can be seen in Figure 2. Here a plot is made of a change in DC resistance versus the time of exposure. This increase in the parallel DC resistance occurs as a result of an interfacial corrosion reaction. A photograph of the interface at 25 days is shown in Figure 3. The development of interference fringes, first observed after 3 days, implies that water is present in significant amounts at the interface and the appearance of a few dark areas is indicative of localized corrosion. At the completion of this test, poor adhesion was observed when adhesive tape was applied to 1/2 of the coating surface and complete "pull-off" occurred. However, allowing the other half of the coating to dry in a desiccator overnight resulted in the deabsorption of water and a re-adherence of the coating. A subsequent parallel DC resistance measurement revealed that no change in ΔR_{DC} had occurred. Apparently the coating is able to rebond to the surface of the metal. No signs of water could be detected at the interface.

Example #2

Similar results to those obtained in Example #1 are found for an iron-polybutadiene system exposed to 3% NaCl pH = 6.6. Capacitive behavior is observed at early times as indicated by the shape of the Bode plot, Figure 4; however, at day 7, the capacitor-like coating is short-circuited by the ionic resistance of the coating and the system is represented by a

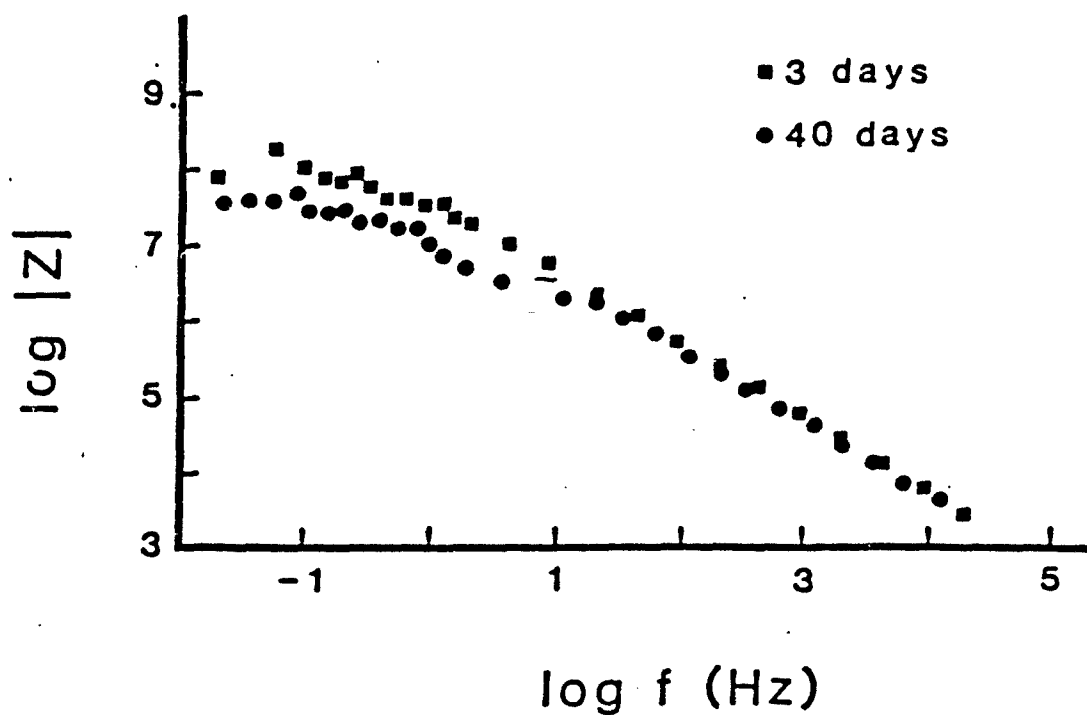


Figure 1. Bode plot for a 13 μm polybutadiene-coated nickel sample exposed to 3% NaCl at pH = 6.6. A slope of -1 is obtained at frequencies above about 0.5 Hz.

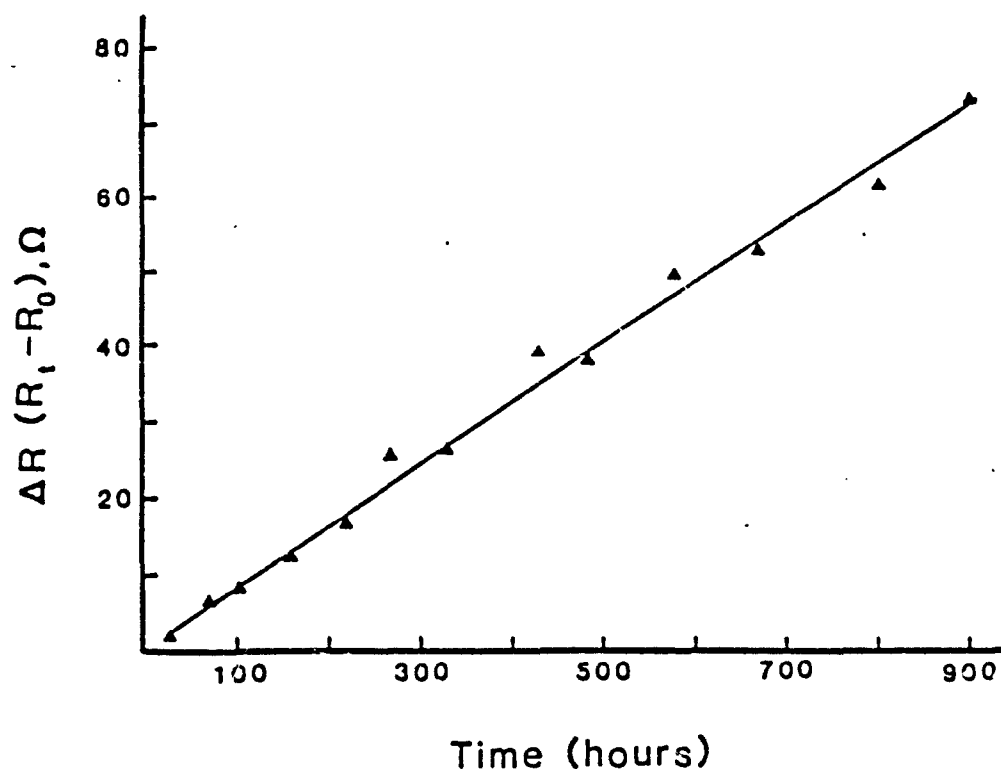


Figure 2. Plot of change in parallel DC resistance against time of exposure to 3% NaCl at pH = 6.6 for a 12 μ m polybutadiene-coated nickel sample.



Figure 3. Photograph (10X) of a nickel sample with a polybutadiene coating and exposed to 3% NaCl at pH = 5.6 for 25 days.

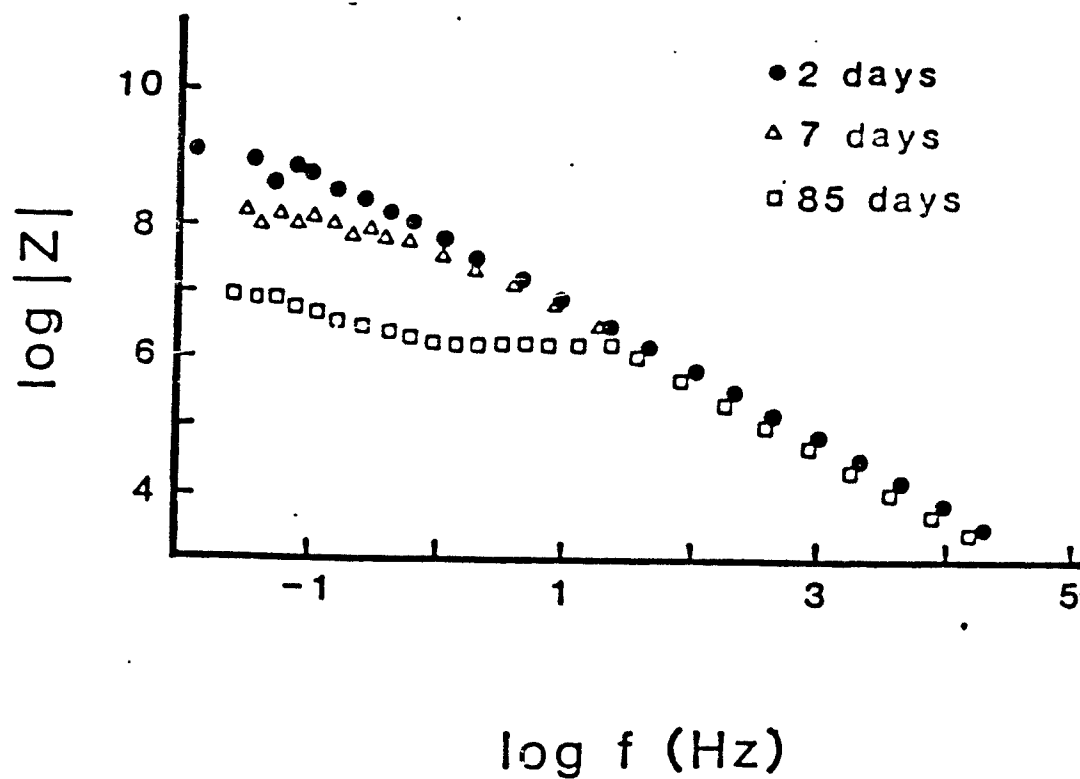


Figure 4. Bode plot of a 13 μm polybutadiene-coated iron sample exposed to 3% NaCl at pH = 6.6. A slope of -1 is obtained at high frequencies.

simple capacitor and resistor in parallel. A Warburg impedance is observed after 24 days below a frequency of 0.2 Hz.¹ This is a true Warburg impedance which is confirmed by a Randle plot giving nearly identical slopes for Z' vs. $\omega^{-1/2}$ and Z'' vs. $\omega^{-1/2}$.

Table II gives calculated values for the coating capacitance, C_c , and the resistance, R_i , of the coating. The capacitance values are calculated using the following equation:

$$|Z|_{\theta_{\max}} = \frac{1}{\omega C_c}$$

where, $|Z|$ is the total impedance, θ is the phase shift and ω is equal to $2\pi f$; these values are nearly identical to results obtained using a Nyquist plot. The R_i value is determined at θ_{\min} and is taken to be equivalent to the total impedance. Results obtained in this manner correspond to values obtained at the low frequency intercept of the Nyquist plot with the real axis. A decrease in the R_i values, Table II, from a high of 1.9×10^8 ohms to a low of 1.1×10^6 ohms suggests an increase in the conduction through the coating. Mansfield et al. [14] and others [15,16,18,19] have used the value of R_i to evaluate the effectiveness of a coating. According to Kendig et al. [15,16], for polybutadiene coated steel systems a large change in R_i is suggestive of a poorly protective coating, an indication of underfilm corrosion. Kendig et al. [15,16] attribute changes in the ionic resistance of the coating to an increase in solution penetration to the metal substrate caused by local film rupture(s) as a result of tensile stresses produced in the film by localized growth of corrosion products at the metal/coating interface. Our results may lend credence to their findings since a thin metal substrate limits the amount of corrosion product build-up and, hence, reduces the amount of induced stresses on the coating. This assumption that changes in R_i are principally a result of corrosion product growth may not be entirely accurate. The penetration of solution into a coating, hence a subsequent increase in the short-circuiting of a capacitor-like coating, can be influenced by other phenomena such as inhomogeneous coating thicknesses, coating defects, the nature of the coating, contaminants at the interface and other degradative processes, i.e., saponification. However, the authors do not dispute the important influence that interfacial corrosion reactions have on the AC impedance response of a system and agree that a rapid decrease in R_i values at early times may indeed be an indication of interfacial corrosion.

¹ Impedance behavior which results from a diffusion limited reaction, often termed the Warburg impedance, may have the same frequency dependence as an infinite RC transmission line. This is not to say that in a coating system an RC transmission line actually exists but behavior which is transmission-line-like may occur leading one to assume that a true Warburg impedance is responsible for the observed low frequency response. Randle plots of Z' vs. $\omega^{-1/2}$ and Z'' vs. $\omega^{-1/2}$ which exhibit linear responses of identical slopes confirm that a Warburg impedance can be ascribed to the observed low frequency behavior.

Table II

C_c (pF/cm ²)	r_i (Ω)	Time (days)
185	—	1
188	—	2
190	—	3
187	1.9×10^8	4
191	7.8×10^7	7
193	6.3×10^7	8
188	5.5×10^6	10
191	4.4×10^6	14
193	5.7×10^6	20
199	3.8×10^6	24
201	3.1×10^6	30
201	4.4×10^6	36
201	1.5×10^6	60
203	1.5×10^6	69
206	1.5×10^6	75
207	1.1×10^6	87

Capacitive behavior is observed during the first 3 days of immersion and, by the 4th day, a resistive component emerges; however, the ionic resistance, R_i , remains relatively large at 1.9×10^8 ohms, not indicative of coating degradation. A plot of ΔR_{DC} against time, Figure 5, shows a significant increase in resistance at times of less than 100 hours, thus indicating that a reaction is occurring on the metal surface. The final R_i value of 1.1×10^6 ohms is in the range where corrosion beneath an organic coating occurs at an appreciable rate [20] and is in accord with the DC results. Hubrecht et al. [13], in their recent work, obtained R_i values orders of magnitude lower than observed in our work. Their smaller R_i values were obtained in ten days or less for an 80 μ m thick styrene acrylic polymer on iron and, in addition, their impedance data showed a second time constant during this period at intermediate frequencies that they attributed to a Faradaic reaction occurring at the interface. This behavior is not observed in our work on a 13 μ m thick coating.

The metal/coating interface for this sample at 87 days can be seen in Figure 6; severe corrosion in several isolated areas is revealed in this photograph. The change in R_i during the course of this experiment cannot be solely attributed to an influence exerted by the interfacial corrosion reactions because the final R_i value remained high. This noticeably small change in R_i may be attributed to the limited amount of corrosion product build-up that occurs with thin metal substrates. Kendig's [15,16] concept of induced stresses in the coating caused by corrosion product growth will lead to an increase in the number of defects, hence giving rise to an increase in the penetration of the electrolyte. However, the thin metal films used in this experiment behaved similarly to the degreased and alkaline treated samples of Kendig's experiments [15]. The small change in R_i that occurred in these experiments might erroneously lead one to assume that interfacial corrosion is absent. The nature of the surface

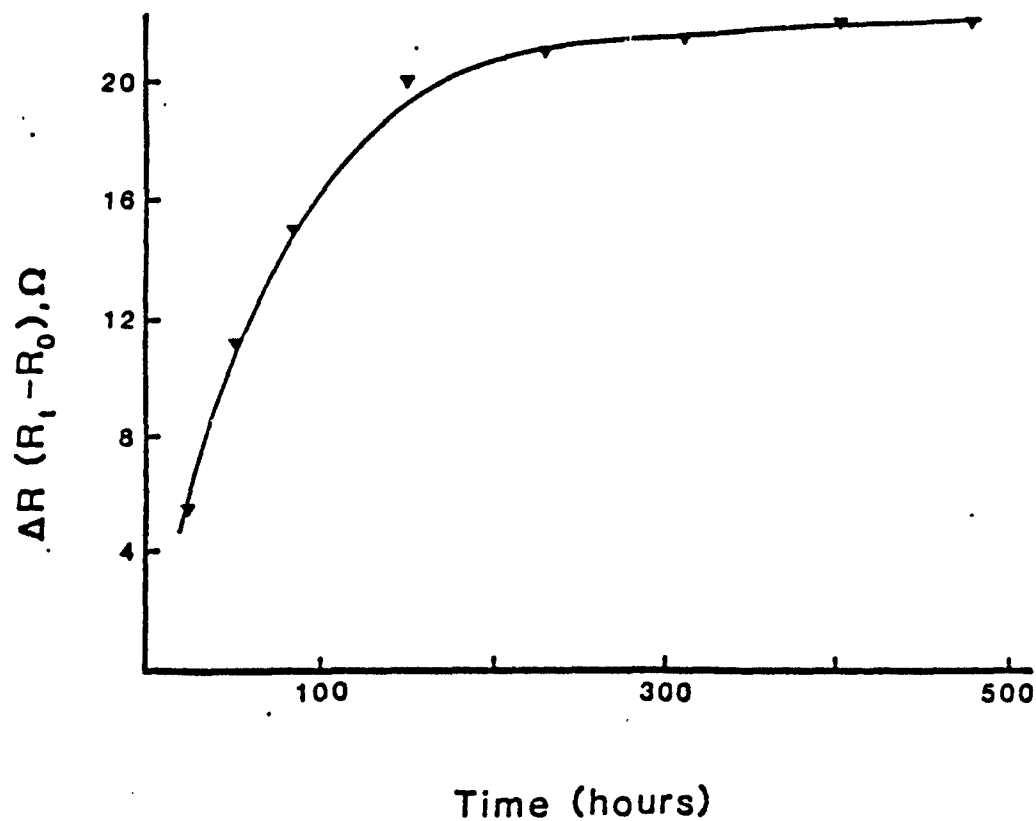


Figure 5. Plot of change in parallel DC resistance against time of exposure to 3% NaCl at pH = 6.6 for a 13 μm polybutadiene-coated iron sample.



Figure 6. Photograph (10X) of an iron sample with a polybutadiene coating and exposed to 3% NaCl at pH = 6.6 for 87 days.

should strongly influence the corrosion behavior of coated metals. A thin metal film may have a surface condition which promotes adhesion similar to several of Kendig's panels. The large decrease in R_i found by Kendig on many of the panels occurred on those samples with relatively rough surface profiles. A thin polymer coating of the order of 8 μm applied to a rough surface may lead to incomplete wetting of the surface thus creating voids or thinly coated regions and a consequent low value of R_i .

Values of R_i in the range of $10^3 - 10^4$ ohms might be expected for thin polymeric film systems which exhibit diminished protection, as a result of the interfacial corrosion process. This type of influence on the value of R_i has been reported by others [13-19] who observed significantly large decreases in R_i due to corrosion. The observed R_i values for this system are most likely a result of an increase in the solution penetration of the coating and not a result of significant contributions from the corrosion process.

Example #3

An iron-polybutadiene system exposed to 1% HCl exhibits coating failure in faster times than do similar samples exposed to 3% NaCl. Nyquist plots, Figure 7, indicate that a simple parallel capacitor-resistor scheme describes the behavior during the initial 48 hours; however, at later times, e.g. 124 hours, a second time constant is noticeable and can be attributed to the relative slowness of reactions occurring at the interface.² Indeed, a plot of ΔR_{DC} against time, Figure 8, confirms this assumption. No change in the parallel DC resistance is observed at times less than 100 hrs but an increase in resistance is obtained at times greater than 100 hrs at about the same time AC impedance results reveal the presence of a second time constant. A Nyquist plot, Figure 9, at 345 and 820 hrs shows the high frequency arc which is characteristic of coating behavior in this range. A decrease in the diameter of the semi-circle with time indicates a decrease in the coating's ionic resistance, i.e., probably an increase in the number of conductive pathways. The interfacial reaction occurring at earlier times, as indicated by a second time constant semi-circle at intermediate frequencies, is obscured by an intense Warburg-like impedance contribution at later times, the development of which can result from an increase in the number of time-constants due to the heterogeneity of a highly porous coating. A true Warburg impedance is only discernable at times between 124 and 340 hours which is confirmed

²Many complex impedance responses may occur for which a simple parallel capacitor-resistor model provides an inappropriate description for a system's behavior; however, at early times of exposure, a polymer coating/metal system can be accurately represented by a simple parallel capacitor-resistor model because the system's AC impedance response is determined by the dielectric properties of the polymer system. It only becomes more difficult to use such a model at later times, particularly when interfacial reactions make contributions to the overall impedance response. Indeed at these later times, an impedance curve cannot be adequately described in terms of simple lumped circuits of individual time constants but representation must be described in terms of a model that changes with frequency.

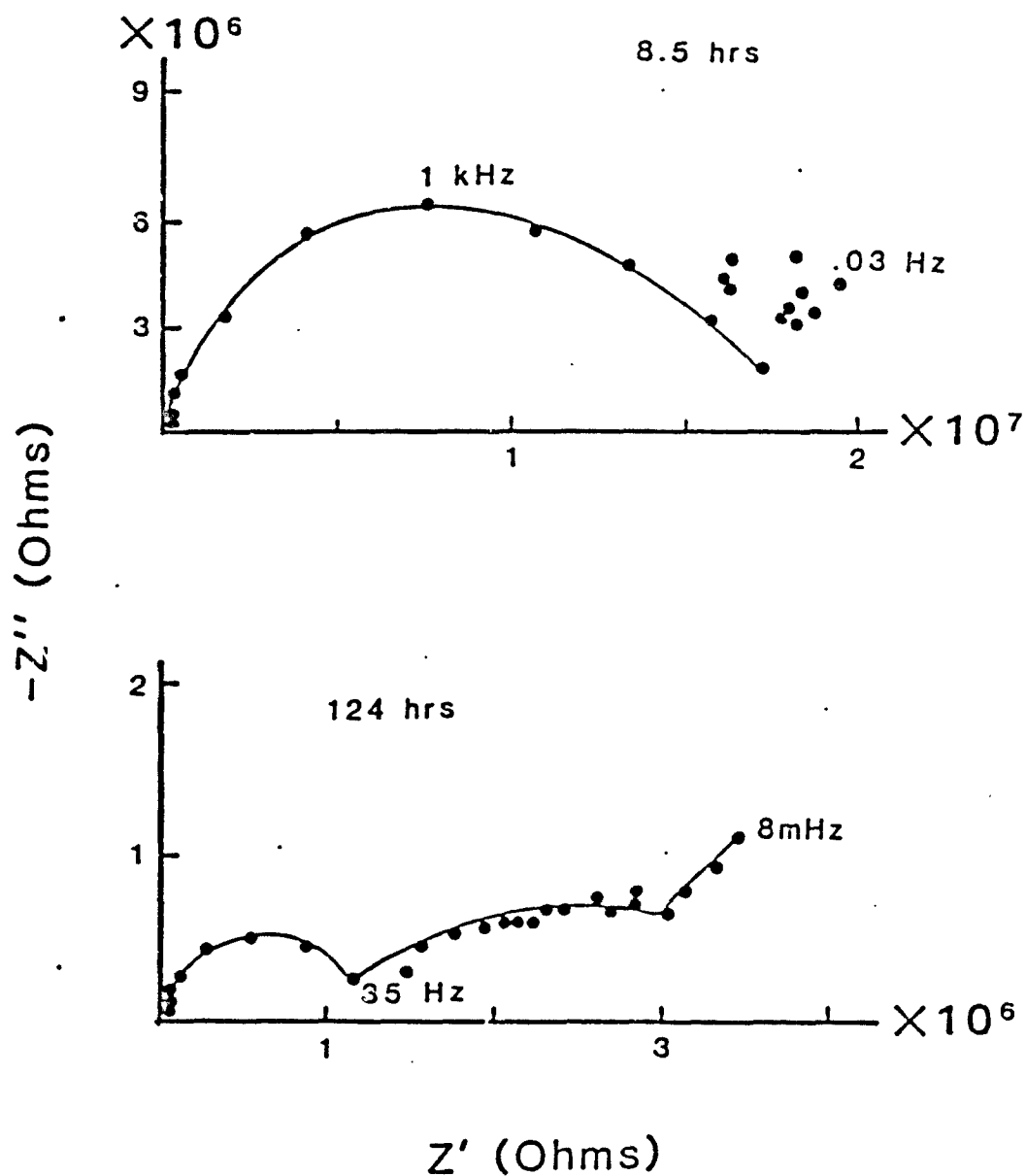


Figure 7. Nyquist plots for a 13 μ m polybutadiene-coated iron sample exposed to 1% HCl for 8.5 and 124 hrs.

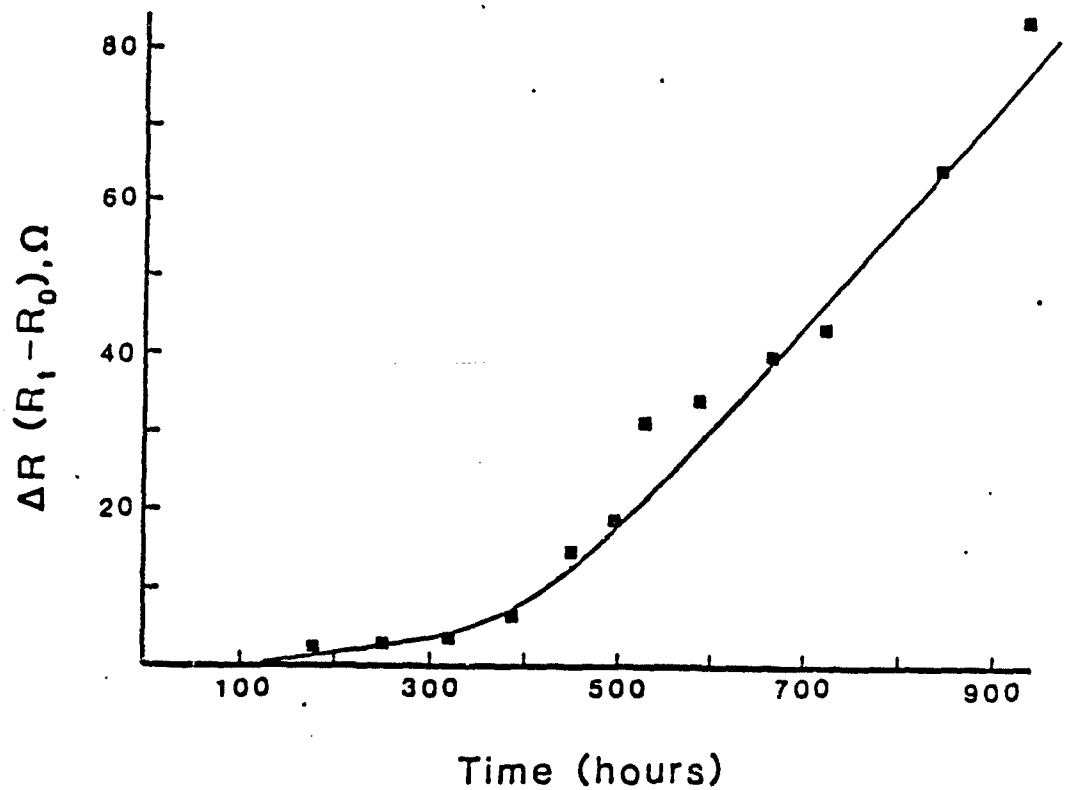


Figure 8. Plot of change in parallel DC resistance against time of exposure to 1% HCl for a 13 μm polybutadiene-coated iron sample.

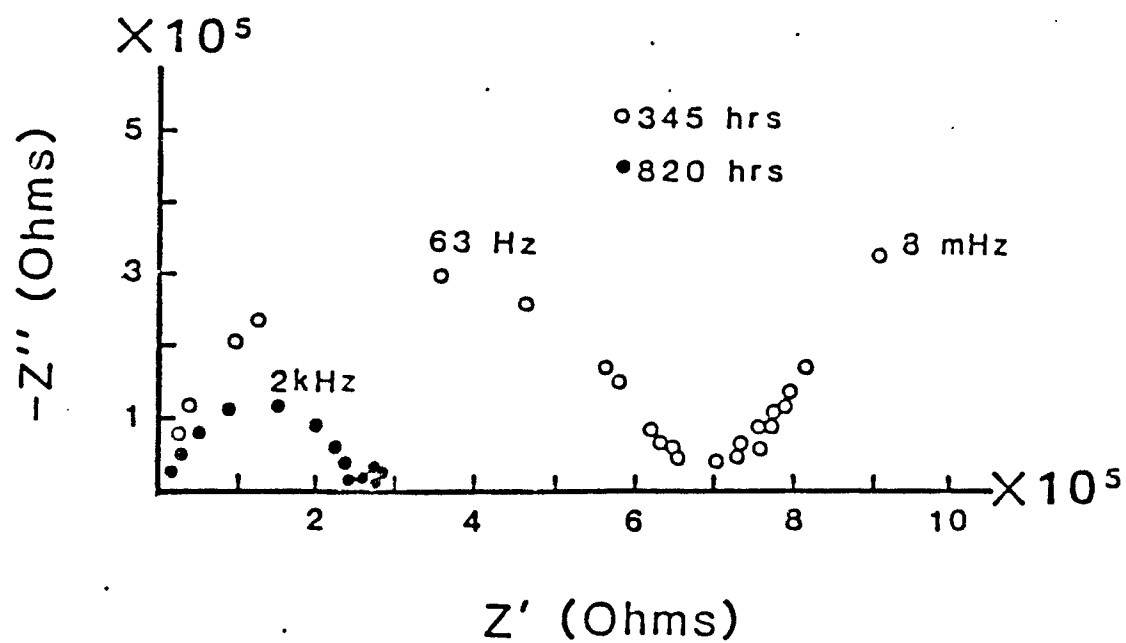


Figure 9. Nyquist plots for a 13 μm polybutadiene-coated iron sample exposed to 1% HCl for 345 and 820 hrs.

by Randle plots giving nearly identical slopes for Z' vs. $\omega^{-1/2}$ and Z'' vs. $\omega^{-1/2}$. Nonetheless, the dominance of a Warburg-like impedance at later times prevents an accurate assessment (at least, at the low frequency limits of this experiment) of the progress of interfacial attack and, according to the results plotted in Figure 8, a rapid increase in R_{DC} is noticed at times greater than 350 hrs, a period dominated by a Warburg-like diffusion.

Hubrecht et al. [13] discovered that the size of the semi-circle response attributable to Faradaic processes may increase with time under certain conditions where passivation of active sites occurs—this behavior would be difficult to monitor when the absence of a second semi-circle occurs because of diffusional control. Our results for the iron-polybutadiene sample exposed to 1% HCl reveal that interfacial corrosion accelerated at times when the Warburg-like impedance dominated the mid- to low-frequency response, thus effectively eliminating direct evidence from the AC measurements for changes in the corrosion rate or corrosion process.

Example #4

A thin polybutadiene-coated iron sample exposed to 1% NaOH gave a variety of responses to applied AC signals that were found to change with time and, as a consequence, this complex behavior is difficult to interpret based solely on AC impedance results. The situation is made more understandable when the change in the parallel DC resistance is followed as a function of time. Several Nyquist plots at various times are shown in Figure 10. The initial behavior, Figure 10A, can be described as follows: At 24 hrs, a short-circuiting of the dielectric by the penetration of solution into the coating occurs. The low-frequency response indicates a small Warburg diffusion contribution to the overall system impedance, a straight line with a positive slope of less than one which bends back towards the real axis. Nyquist plots from 48 - 143 hrs are similar in shape to that shown in Figure 10A for 24 hrs, except a second semi-circle at intermediate frequencies is noticeable but not fully formed and difficult to resolve. Apparently this deformation of the second semi-circle is caused by the strong influence of the Warburg impedance [4]. At times between 150 - 345 hrs the Warburg impedance dominates the low frequency response and the second semi-circle disappears, as shown in Figure 10A for 170 hrs. At times greater than 345 hrs, the electrical behavior of this system changes, an increase in R_i is noticed along with a concurrent decrease in C_c and a reappearance of the second semi-circle with its center located below the real axis. An increase in R_i can be seen in Figure 10B where a comparison is made between the high frequency arcs at 24 hrs and 490 hrs. The change in R_i and C_c versus time is plotted in Figure 11. The decrease in C_c begins at times greater than 280 hrs and at about the same time the R_i values begin to increase. Some insight into this complex behavior is obtained by examining a plot of ΔR_{DC} versus time, Figure 12. An increase in R_{DC} is obtained at initial times, 0-180 hrs. Since the initial R_i values are extremely small, e.g. 1.5×10^4 ohms, a second semi-circle representative of interfacial contributions to the overall impedance is detectable. During the period between 150 - 345 hrs the DC resistance of the metal remains nearly constant, a period where the diffusion of reactive species is rate-controlling as indicated by the strong Warburg contribution. However, at times greater than 345 hrs, the

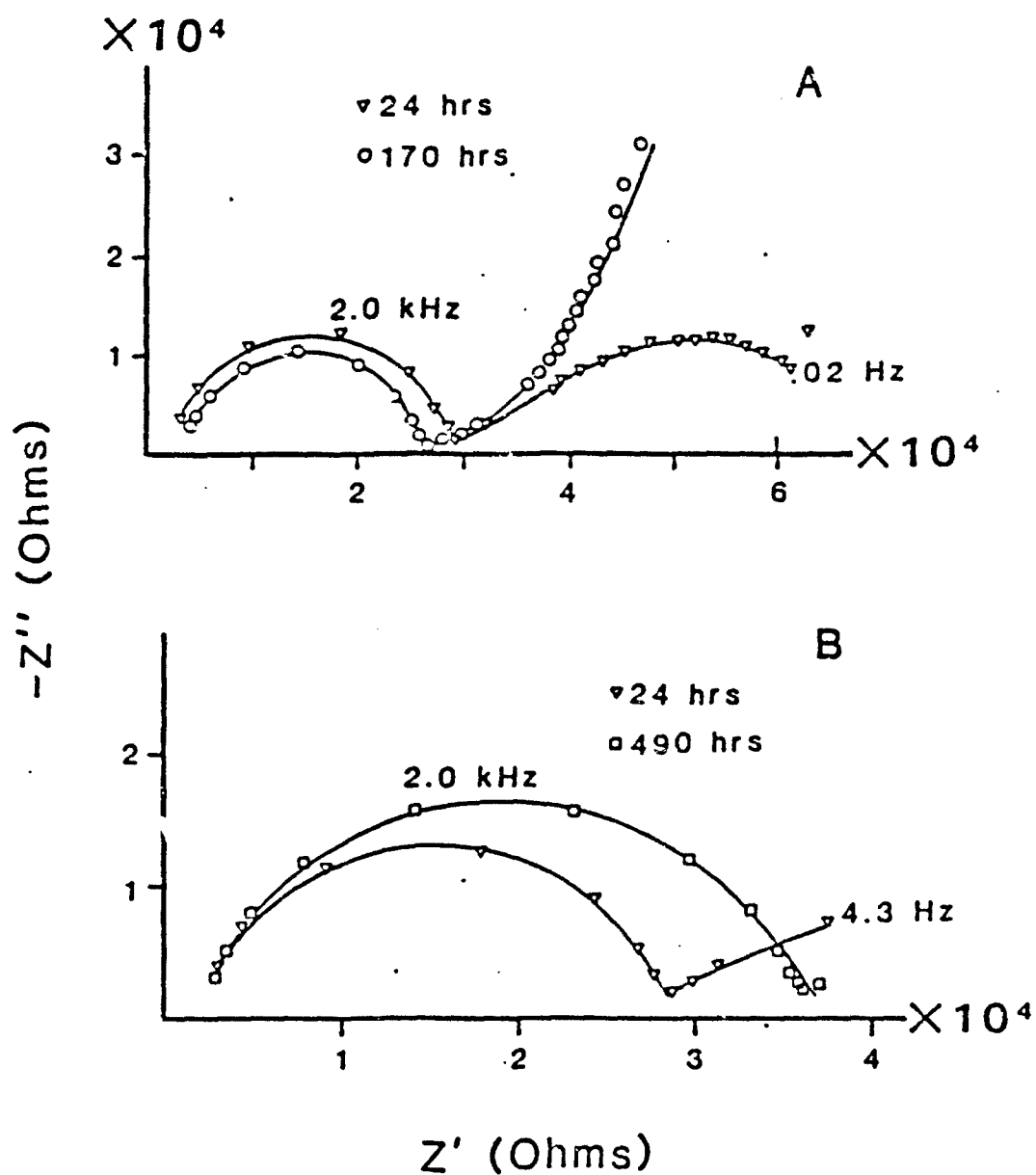


Figure 10. Nyquist plots for a 12 μm polybutadiene-coated iron sample exposed to 1% NaOH for various times.

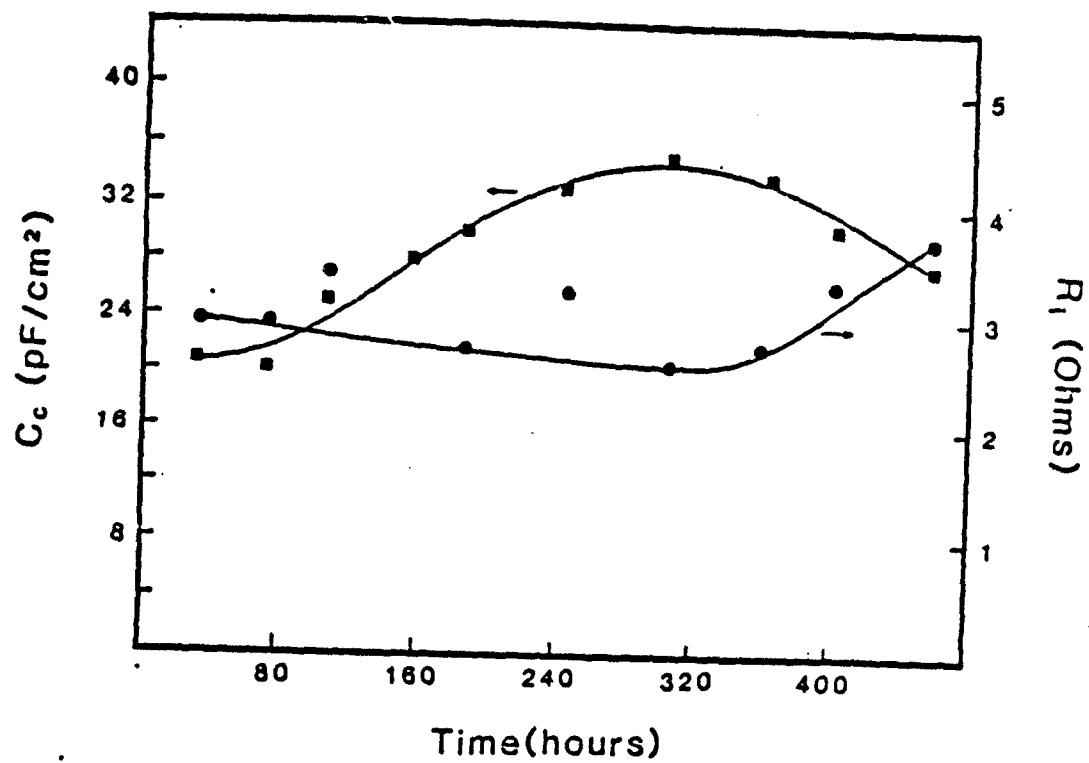


Figure 11. A plot of the change in parallel DC resistance and AC capacitance against time of exposure to 1% NaOH. Data presented here are for the sample sample as described by Figure 10.

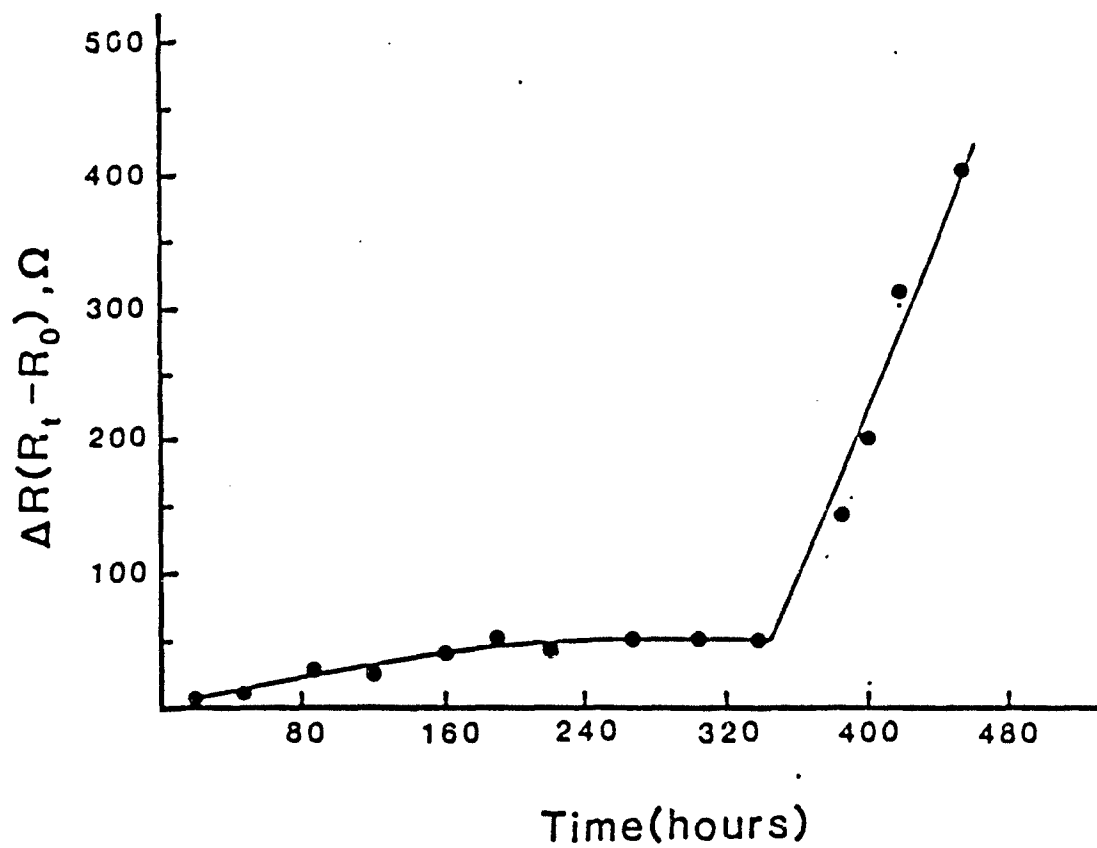


Figure 12. Plot of change in parallel DC resistance against time of exposure to 1% NaOH for a 12 μm polybutadiene-coated iron sample.

corrosion rate begins to increase rapidly, i.e. large increase in R_{DC} . At this point, R_i of the coating begins to increase and coating capacitance begins to decrease. The simultaneous increase in the corrosion rate provides evidence to support the idea that interfacial reactions can affect the electrical response of the coating. The ionic resistance of the coating increases because defects in the coating become blocked with corrosion products and, thus, fewer conductive pathways are present. A reaction in the volume % of solution in the coating pores explains the consequential decrease in the capacitance.

Mansfeld et al. [14] observed that R_i continuously decreased with time in the case of polybutadiene on iron immersed in 0.5M NaCl solution. They concluded that the corrosion process at the interface enhanced the conduction through defects in the coating. In the present study carried out in NaOH the value of R_i increased with time, probably as a result of pore or defect blockage by corrosion products. Both of these results provide support for the view that the corrosion process itself has an effect on the electrical properties of the coating.

The observed increase in R_{DC} during a period of strong diffusional influence is most likely a result of localized corrosion areas growing together which may go unnoticed when AC impedance measurements are the only criteria used to interpret corrosion behavior. The corrosion behavior for this system can be explained as follows: an initial period of coating breakdown and incipient localized corrosion at pore bases occurs followed by a period of strong diffusion control where the corrosion rate remains low; at later times, the corrosion rate accelerates as adjacent areas grow together causing the defects or pores to become blocked with corrosion products leading to an increase in R_i and a decrease in C_c .

CONCLUSION

Metal-paint systems exposed to corrosive environments produce a variety of electrical and electrochemical responses that are dependent on the nature of the processes occurring at the metal/coating interface, in the coating matrix, and at the coating/solution boundary. For intact paint films, the inherently large ohmic drop associated with high impedance values complicates the interpretation of data collected using AC impedance techniques. Representative examples have been provided in order to establish the fact that a number of problems may develop when attempting to describe fully the corrosion behavior of a coating/metal system. Many studies have proven the usefulness of AC impedance techniques and a number has warned of the potential difficulties that one may encounter.

Frequently the individual contributions to the overall impedance of a metal/paint system only appear when the protective coating has deteriorated during ageing as noticed by a significant reduction in the coating's ionic resistance and the appearance of distinct regions of corrosion. However, in such situations the detrimental effects related to underfilm corrosion remain obscured at early times by the high impedance of the coating. The possibility exists that localized underfilm corrosion may initiate and propagate without prior coating breakdown, and detection

becomes difficult when AC impedance techniques are used.

At present, the use of parallel DC resistance techniques can detect early signs of underfilm attack. This technique has shown that interfacial processes often go unnoticed and assumptions may be incorrect when attempting to assign specific significance to observations obtained using AC impedance methods. Also, the parallel DC resistance technique has proved that reactions occurring at the interface, in many situations, will affect the electrical response of the coating.

The benefits provided by the use of thin metal films can be summarized as follows: Deposition of pure metals onto glass substrates provides a means to observe the interface through the reverse side; the metal film resistance can be monitored as a function of time; and AC impedance techniques can be successfully utilized. Thus, several complementary techniques can be applied to one sample.

The important advantage of AC techniques is that they can be applied in the field to real systems whereas thin film techniques will probably be limited to laboratory studies. It is hoped that the thin film technique, when used in the laboratory in conjunction with impedance measurements, will provide clues as to possible improved interpretation of impedance data.

REFERENCES

- [1] R. E. Touhsaent and Henry Leidheiser, Jr., Corrosion 28(12), 435 (1972).
- [2] M. W. Kendig and H. Leidheiser, Jr., J. Electrochem. Soc. 123, 982 (1976).
- [3] L. Beaunier, I. Epelboin, J. C. Lestrade, and H. Takenouti, Surface Tech. 4, 237 (1976).
- [4] M. Piens and R. Verbist, FATIPEC Congress, 15th, III-273 (1980).
- [5] M. Piens and R. Verbist, in "Corrosion Control by Organic Coatings," H. Leidheiser, Jr., Ed.; NACE: Houston (1981), p.32.
- [6] I. Epelboin, G. Babrielli, M. Keddam, and H. Takenouti, in "Electrochemical and Corrosion Testing - ASTM," F. Mansfeld and U. Bertocci, Eds.; ASTM: Philadelphia (1981), p.150.
- [7] J. D. Scantlebury and K. N. Ho, J.O.C.C.A. 62(3), 89 (1979).
- [8] J. D. Scantlebury and Graham A. Sussex, in "Corrosion Control by Organic Coatings," H. Leidheiser, Jr., Ed.; NACE: Houston (1981), p.51.
- [9] L. M. Callow and J. D. Scantlebury, J.O.C.C.A. 64(2), 83 (1981).
- [10] L. M. Callow and J. D. Scantlebury, J.O.C.C.A. 64(2), 119 (1981).
- [11] L. M. Callow and J. D. Scantlebury, J.O.C.C.A. 54(2), 140 (1981).
- [12] F. Mansfeld, Corrosion 36(5), 301 (1981).
- [13] J. Hubrecht, J. Vereecken, and M. Piens, J. Electrochem. Soc. 131(9), 2010 (1984).
- [14] F. Mansfeld, M. W. Kendig and S. Tsai, Corrosion 38(9), 478 (1982).
- [15] M. Kendig, F. Mansfeld, and S. Tsai, Corr. Sci. 23(4), 317 (1983).
- [16] M. Kendig, F. Mansfeld, and A. Arora, Proc. 9th Int. Cong. on Metallic Corrosion, Toronto, Canada, June 3-7, 1984, pp.73ff.
- [17] J. F. McIntyre and Henry Leidheiser, Jr., Ind. Eng. Chem. Prod. Res. Dev. 24, 348 (1985).
- [18] M. W. Kendig, S. Tsai, and F. Mansfeld, Maters. Perf. 23(6), 37 (1984).
- [19] Henry Leidheiser, Jr., and M. W. Kendig, Corrosion 32(2), 69 (1976).
- [20] H. Leidheiser, Jr., Prog. Org. Coatings 7, 79 (1979).

DTIC

FILMED

4-86

END